SOLID STATE NMR BASED STRUCTURAL BIOLOGY ENHANCED BY DYNAMIC NUCLEAR POLARIZATION

DE IMPLEMENTATIE VAN DYNAMISCHE KERNSPINPOLARISATIE IN VASTE STOF NMR TEN BEHOEVE VAN STRUCTUURBIOLOGISCH ONDERZOEK

(met een samenvatting in het Nederlands)

PROEFSCHRIFT

ter verkrijging van de graad van doctor aan de Universiteit Utrecht op gezag van de rector magnificus, prof.dr. G.J. van der Zwaan, ingevolge het besluit van het college voor promoties in het openbaar te verdedigen op dinsdag 2 september 2014 des middags te 12.45 uur

door

Elisabeth Johanna Koers

geboren op 26 oktober 1987 te IJsselmuiden

PROMOTOR:
Prof. Dr. M. Baldus

"Unless you try to do something beyond what you have already mastered, you will never grow."

— Ralph Waldo Emerson

CONTENTS

1

GENERAL INTRODUCTION

1.1 SOLID-STATE NMR

Solid-state NMR (ssNMR) is a versatile analytical method used in a variety of scientific fields. In materials, it has been used for investigations of catalysts, Li batteries, zeolites, pharmaceuticals, paintings or bio-inorganic materials. Applications towards quantum technology include the excitation and reading of ^{31}P quantum bits in silica[1,2] or nitrogen vacancies (NV) defects in diamonds.[3] In structural biology, the technique has been used to tackle fundamental questions concerning the function and dynamics of membrane proteins, the structure of amyloid fibrils and recently also for studies of cellular membrane protein complexes.

The two main limitations of ssNMR are sensitivity and resolution. In contrast to solution state NMR, interactions like chemical shift anisotropy and dipolar interactions are not fully time-averaged. In practice, this leads to so-called "powder spectra" in which different molecular orientations give rise to different NMR signals, thereby complicating the spectral analysis. For studying complex biological samples, tailored isotope labeling schemes[4–7] and fast magic angle spinning (MAS)[8] are required to resolve the peaks of interest. The sensitivity issue stems from the small energy gap between the two spin states (in case of spin $\frac{1}{2}$).

The energy of the two spin states α and β is given by:

$$\varepsilon_\alpha = \mu_Z \cdot B_0 \tag{1.1.1}$$

and

$$\varepsilon_\beta = -\mu_Z \cdot B_0 \tag{1.1.2}$$

with B_0 as the external field and μ the component of the magnetic moment (of the nucleus) along the external field:

$$\mu_Z = -m\gamma\hbar. \tag{1.1.3}$$

m stands for the magnetic quantum number and γ represents the gyromagnetic ratio. For ^1H and ^{13}C nuclei, $m = \frac{1}{2}$. Combining these energy terms with Boltzmann statistics, leads to an equilibrium population difference of

$$P_{eq} = \frac{n_\alpha - n_\beta}{N} = \tanh\left(\frac{\gamma\hbar B_0}{2kT}\right) \tag{1.1.4}$$

in which n_α and n_β are the population of spins in the α or β state, respectively, N stands for the total number of spins, k is the Boltzmann constant and T represents the absolute temperature in Kelvin. When $2kT \gg \gamma\hbar B_0$, (at high temperature), the following approximation can be made:

$$P_{eq} = \frac{\gamma\hbar B_0}{2kT}. \tag{1.1.5}$$

According to equation 1.1.5, one way to increase the population difference and therefore the sensitivity of the NMR experiments, is to increase the B_0 field. Doubling the field will lead to a polarization increase of 2. The dependency of the signal-to-noise ratio on the B_0 field is different: $B_0^{3/2}$ [9] leading to a factor of 2.8. This is due to additional factors scaling with B_0: the radiofrequency power and electronic noise. Lowering the temperature from 273 K to 100 K adds up to a sizable polarization increase of a factor 2.7.

Another way to achieve high polarization, is to use high γ-nuclei (e.g. ^{1}H). Transferring polarization from high-γ nuclei to low-γ nuclei through magnetic dipole-dipole couplings[10] is common practice in ssNMR. In combination with magic angle spinning, this cross polarization method (CP-MAS[11]) provides a means to combine the sensitivity of one nucleus (and fast relaxation) with the spectral dispersion of another (for example ^{1}H with ^{13}C). Transfer can also be achieved from a specific chemical shift range specifically to another nucleus (SPECIFIC-CP)[12] enabling elaborate transfer schemes.

Even with the techniques mentioned above, sensitivity in ssNMR is often still an issue. A great potential though lies in the polarization transfer from unpaired electrons to nuclei, since electrons have a 2-3 orders of magnitude greater polarization (see Figure 1.1).

This has led to the discovery of Dynamic Nuclear Polarization, as is described in the next section.

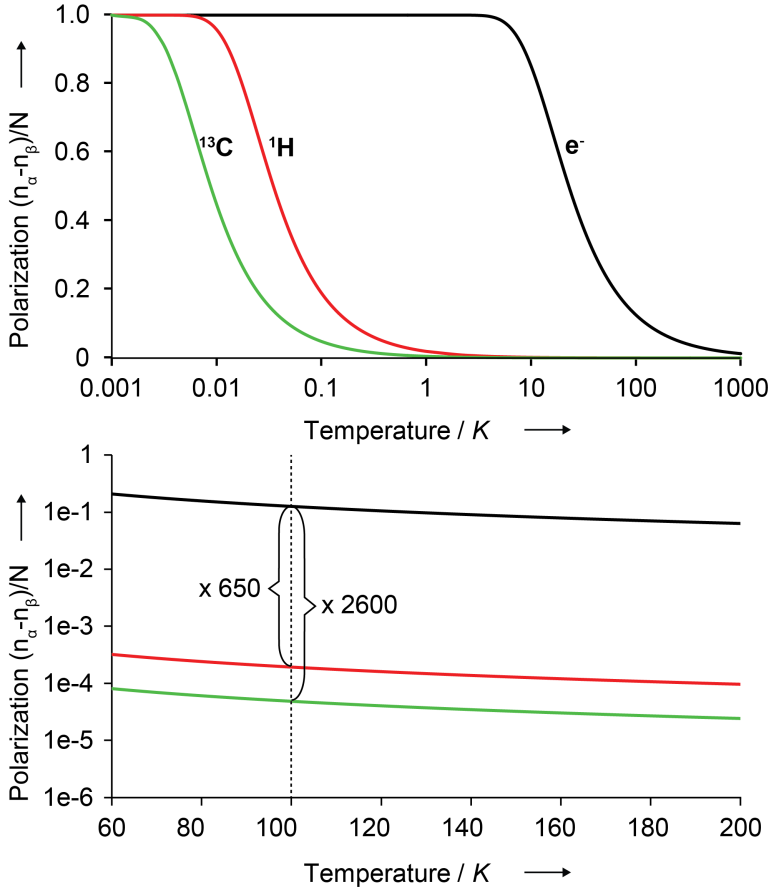

Figure 1.1: Difference in probability of state alpha and beta in equilibrium according to Boltzmann statistics. At 100 K and 18.8 T, free electrons have a 650 times higher probability ratio than ^{1}H and 2600 times higher than ^{13}C.

1.2 DYNAMIC NUCLEAR POLARIZATION

History

Polarization transfer from electrons to nuclei has been discovered early in the history of NMR. In 1953, Carver and Schlichter[13] confirmed Overhauser's theory[14] and they report:

"We have verified Overhauser's theory by observing the enhancement of the nuclear resonance in metallic lithium produced by electron saturation."

Carver and Slichter measured an increase in intensity corresponding to a 100 times higher population difference when they irradiated on the electron Larmor frequency. This relaxation phenomenon was later coined the Overhauser Effect. For this effect to take place, $\omega_{0S}\tau < 1$, in which ω_{0S} is the electron Larmor frequency and τ is the correlation time for the electron-nuclear interaction.[15] For higher fields, this condition is difficult to fulfill. Overhauser DNP is still used to polarize nuclei in solution state NMR[16], shuttle DNP[17,18] and in the form of Overhauser enhanced Magnetic Resonance Imaging (OMRI)[19–23].

A few years after the Overhauser Effect was discovered, Abragam and Proctor[24] and Erb[25]described a different DNP mechanism: the Solid Effect (SE). While the Overhauser Effect depends on irradiation of allowed transitions, the SE employs forbidden zero and double quantum transitions.

In the '60s an additional mechanism involving two electrons spins, called the Cross Effect (CE)[26–30], was added to the repertoire. This was followed soon after by a multi-electron spin mechanism Thermal Mixing (TM).[31,32] CE is currently the most used mechanism for measurements at ~ 100 K, while SE is the mechanism of choice for 25 K or lower.[33]

In the '80s, Magic angle spinning (MAS)[8,34] was implemented in DNP setups.[32,35,36] Please note that the applica-

tion of MAS has implications for the workings of the DNP mechanisms (see section 1.2). The development of superconducting magnets enabled scientist to work at higher magnetic fields. The klystron, used as the microwave source for DNP in these experiments, is not able to generate sufficient microwave power[37]at higher frequencies (> 95 GHz) necessary for matching the magnetic fields used in modern biomolecular NMR. With the introduction of gyrotrons to DNP setups, higher frequencies became accessible,[38,39] up to 527 GHz commercially available today. Other efforts include electron-nuclear cross polarization using pulsed DNP[40–42] and temperature-jump DNP.[43]

With DNP systems becoming more widely available, the use of DNP has found several applications. DNP has proven its usefulness in areas ranging from catalysts[44] to studies of whole cells.[45,46]

Polarization transfer mechanisms

From the four transfer mechanisms introduced above, two are relevant for this thesis: the solid effect and the cross effect. These mechanisms are discussed in more detail below and are summarized in figure 1.2.

Solid Effect

The SE is a polarization transfer mechanism between a (narrow line) radical and a nucleus. It involves the excitation of forbidden zero or double quantum transitions microwave frequencies $\Omega = \omega_S \pm \omega_I$ (see figure 1.2a). Due to a non-secular component of the hyperfine interaction, which mixes electronic and nuclear spin states, the nuclear relaxation process becomes allowed. If the microwave is strong enough to cause flip-flops faster than the nuclear longitudinal spin relaxation T_{1n}, the spins will be forced in the higher energy spin state. Usually, the amount of electrons is much lower than the nuclei to be polarized, hence the process has to be repeated to

reach full nuclear polarization. Couplings with other electrons or nuclei cause relaxation leakage of the polarization leading to a lower final nuclear polarization.[47] Radicals used for SE have a small homogeneous and inhomogeneous EPR line width compared to the nuclear Larmor frequency ω_n. If this is not the case, DQ and ZQ transition will be irradiated simultaneously, resulting in very little net effect. The SE scales with B_0^{-2} due to its dependence on forbidden transitions.[48]

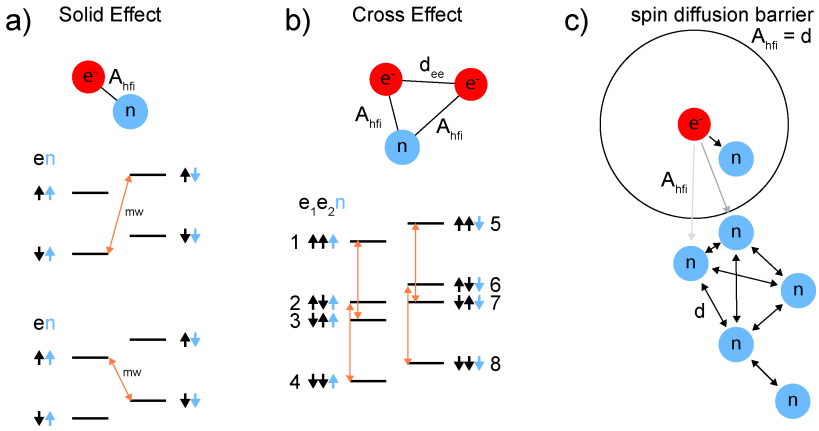

Figure 1.2: Interactions important for the discussed DNP transfer mechanisms and spin diffusion. a) Solid effect induced by 0Q (middle) or 2Q (bottom) microwave irradiation requires hyperfine interaction (A_{hfi}) between the nucleus and the electron. b) Interactions important for CE include a dipolar coupling between the two electrons (d_{ee}). The energy level diagram shows the CE by means of irradiation of e_1. Mixing of states 2,3, 6 and 7 are important for the polarization transfer of electrons to nuclei c) After the initial polarization transfer to the nuclei, spin diffusion between dipolar coupled nuclei causes equalization of the polarization throughout de sample. Nuclei within the spin diffusion barrier are strongly hyperfine coupled to the electron(s) and cannot transfer the hyperpolarization to the bulk nuclei.

Cross Effect

The cross effect (two electrons and one nucleus, see figure 1.2b) can be described with the following interactions. The Zeeman effect: the interaction of the nucleus I or the electron S with the z-component of the external magnetic field:

$$H_z = \omega_{e1} S_{1z} + \omega_{e2} S_{2z} + \omega_n I_z$$

leading to Larmor frequencies ω_e (with $i = 1$ and 2) and ω_n for the electron and nucleus. The second effect is the dipolar interaction between electron spin and the nuclear spin: hyperfine interaction (A_{hfi}).

$$H_{Ahfi} = A_{zz}2I_zS_{iz} + A_{xz}2I_xS_{iz} + A_{yz}2I_yS_{iz}$$

The dipolar interaction between the two electrons is also essential for the CE:

$$H_{dd} = d(2S_{1z}S_{2z} - S_{1x}S_{2x} - S_{1y}S_{2y})$$

A similar expression can be obtained for the interaction between two nuclei, which will be important for the discussion of nuclear spin diffusion (see below). The interaction between the electrons and the microwaves used in the experiments can be described as follows:

$$H_{mw} = \omega_1[(S_{1x} + S_{2x})cos(\omega_{mw}t) + (S_{1y} + S_{2y})sin(\omega_{mw}t)]$$

in which ω_1 is the microwave field strength and ω_{mw} the frequency.

In contrast to the SE, the CE makes use of allowed transitions. Continuous wave irradiation is then applied on one of the electron frequencies. When the matching condition $\omega_{0I} = \omega_{0S1} - \omega_{0S2}$, is met, the saturation of the electron transition of one of the electrons leads to a simultaneous spin flip of the other electron and the nucleus. Depending on what electron is irradiated, either positive or negative DNP enhancement is obtained. The electrons need to be sufficiently dipolar coupled to allow mixing of states. Also, the inhomogeneous width of the EPR powder line shape needs to exceed the nuclear Larmor frequency. As in the SE, the homogeneous breadth should remain small. Biradicals, two radicals tethered together via an organic linker, have been synthesized to meet these conditions (see section 1.2). The electron line width scales with the magnetic field, thus the matching condition is

obtained less frequently at higher fields. This leads to a (theoretical) dependence of the CE of B_0^{-1}.[48–50]

Cross Effect under MAS

Most theoretical descriptions of CE are those under static conditions.[51,52] Magic angle spinning can change the energy levels of electron spins with large g-anisotropy rapidly. Furthermore, the DNP effect is found to be dependent on the MAS speed.[53] A quantum mechanical description for the CE under MAS conditions has been given by Thurber *et al.*[54] In the three-spin model proposed in this work, irradiation, at either ω_{0S1} or ω_{0S2}, and the matching condition $\omega_{0I} = \omega_{0S1} - \omega_{0S2}$ occur at different time points during the MAS cycle. During avoided level-crossings, mixing of states 2,3,6 and 7 occurs (see figure 1.2b). In the first instance, polarization difference between the two electrons is created, while during the matching condition, some of this polarization difference is transferred to the nucleus. A third level crossing, between the energy levels of ω_{0S1} and ω_{0S2} concludes the sequence. The level crossings have to be adiabatic in order to exchange spin states. In case of non-adiabatic level crossings, the polarization of the two electrons will equalize. This is one of the reasons why the CE is expected to drop off at higher MAS speeds.

Spin diffusion of nuclear polarization

After the initial step of nuclear polarization through DNP, the polarization becomes spread through the sample up to a distance in the range of micrometers through the process of nuclear spin diffusion (see figure 1.2c).[55–57] It has been suggested that nuclei closest to the paramagnet will not take part in this process since the NMR line of the nuclei is shifted due to the proximity of the unpaired electron: the so-called nuclear spin diffusion barrier: $A_{hfi} = d$.[51,58,59] The nuclei within this sphere cannot undergo spin-spin transitions with bulk nuclei. Instead, bulk nuclei residing just outside this the spin diffusion barrier are polarized via CE and this polariza-

tion is spread through the sample leading to the observed DNP enhancement.

For the SE, it has been found that the kinetics of the whole DNP process are limited by the initial polarization transfer from electron to nucleus in case of Trityl, while for Gd-DOTA, the spin diffusion is the rate limiting step.[59] Although such studies have not been published for the CE, the good performance of highly deuterated solvents suggests that spin diffusion is probably not rate limiting for CE.[54,60]

Radicals

Although there are examples in the literature of the use of non-organic radicals like Gd^{3+}-DOTA,[61] most are stable free organic radicals. The stability of organic radicals comes usually from steric hindrance and the existence of resonance structures.[62] The most commonly used radicals are nitroxide-based (or more correctly: aminoxyl). The nitroxide radical 2,2,6,6-Tetramethylpiperidin-1-oxyl (TEMPO) possesses a delocalized unpaired electron which contributes to the stability of this compound. The resonance structure can be found in Figure 1.3. An advantage of these nitroxide radicals is that they have a relatively long T_{1e} (10^{-7}s at RT[63]) compared to for example Cu^{2+} and a very small anisotropic magnetic susceptibility tensor.[64,65] Due to its resonance structure, the radical is partially charged and neither very hydrophobic nor hydrophilic. Depending on the groups attached to the radical, the properties can be modulated. For example, TOTAPOL is relatively hydrophilic while bTbK is very hydrophobic[66] (see figure 1.4). Although nitroxide radicals are relatively stable, they can be reduced (lifetime of TEMPO in a cell is at the order of minutes) or broken down at low pH.[67]

For inital high-field DNP experiments, BDPA,[35,36,38,40] trityl radical[68] and 4-amino-TEMPO[69] were used. While these are all monoradicals, in the quest for higher DNP enhancements, biradicals were designed to establish the CE.

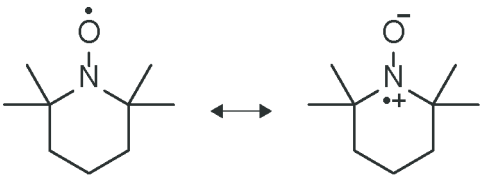

Figure 1.3: Resonance structure of the nitroxide radical. The resonance structure contributes to the stability of the radical. Another stabilizing factor is the steric hindrance caused by the methyls located on both sites of te aminoxyl group.

CE radical design

A plethora of biradicals have been designed in the past years in search of higher enhancements or to extend the application range of DNP. A few of these molecules can be found in figure 1.4 (right side). The first biradicals, the BTnE series, were designed to determine the optimal inter-electron distance for the CE.[70] The authors concluded that the best distance is probably shorter than what the BT2E linker provides (they did not succeed in synthesizing BT1E). The group did successfully synthesize TOTAPOL which has a short hydrophilic linker.[60] This strategy indeed yielded considerable DNP enhancements. Both BTnE and TOTAPOL can rotate around their linker bonds, which reduces the probability on a frequency match compared to a fixed orientation. A radical designed with the latter strategy in mind, bTbK[71], does have this rigid linker with perpendicular orientation of the radicals. The resulting DNP enhancement is about 1.4 times higher. However, such parameters are hard to compare due to different hydrophobicity and therefore different ideal solvent conditions. Due to its hydrophobic nature, bTbK is not compatible with a water/glycerol solvent. Yet, the radical has been successfully used in structural biology.[72]

In recent years, the attention has turned to the relaxation properties of the radicals leading to the synthesis of radicals such as PyPol and AMUPol.[79] In these biradicals, methyl groups next to the radicals are replaced with spirohexyl-groups. This greatly increases their T_{2e}. Also, AMUPol pos-

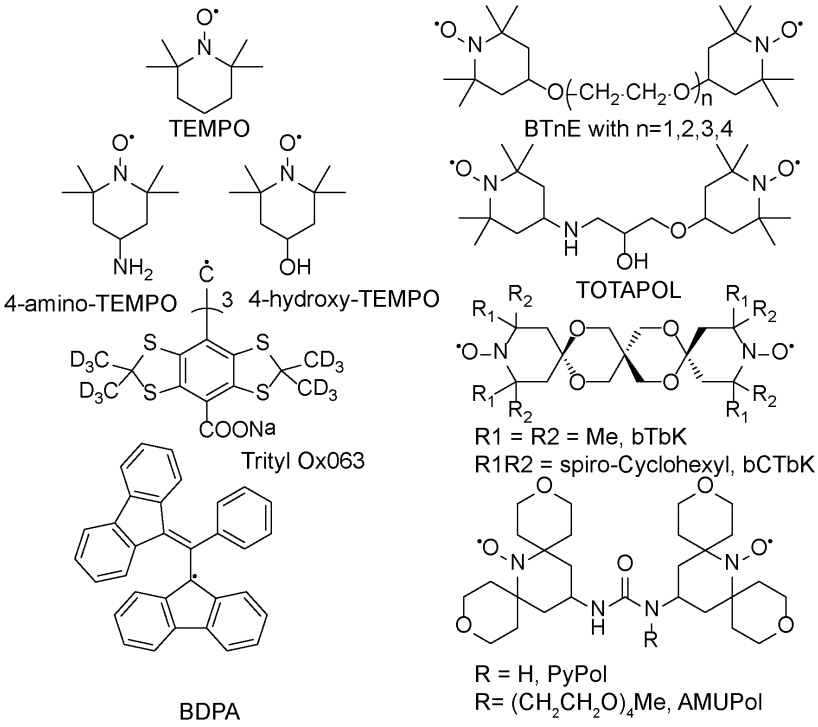

Figure 1.4: Persistent radicals used for ssNMR DNP include TEMPO and its monoradical derivatives and several biradicals including hydrophobic radicals like bTbK, bCTbK and PyPol as well as more water-soluble variants like bTUrea, TOTAPOL, and AMUPol. The Trityl OX063[68] radical is used in combination with TEMPO.[15] The biradical SPIROPOL[73] and the triradical DOTPOPA-TEMPO[74] are also used in DNP experiments. Other non-nitroxide radicals (not shown) used are BDPA[38], SA-BDPA[75], Gd-DOTA[76], Galvinoxyl and DPPH[77] and the endogeneous readical FMN (flavomononucleotide)[78].

sesses a longer electron T_{1e} due to the molecular size due to an additional polyethylene glycol tail. Longer T_{1e} and T_{2e} allow for better saturation of the EPR transitions. Additionaly these radicals have a stronger e-e dipole coupling due to their shorter linker (34 MHz vs 23 MHz of TOTAPOL). Furthermore, the linker is more rigid than for example TOTAPOL. Together, this combination leads to a 3.5 - 4 fold higher DNP enhancement. One other advantage of AMUPol above TOTAPOL is the more advantageous temperature dependency enabling experiments at higher temperatures.[79]

Optimization of DNP conditions

The main advantage of DNP compared to conventional ssNMR experiments is the significant sensitivity increase obtained with the technique. Traditionally, only the DNP enhancement is reported as a measure for the efficiency of the DNP process. The DNP enhancement is defined as the ratio between the signal intensities of the NMR spectra recorded with and without microwaves under otherwise similar conditions (low temperature, radicals present). In practice, it is not always the sample with the highest enhancement that gives the best sensitivity improvement compared to conventional ssNMR. This has been demonstrated for example by Lange *et al.*[80] At high paramagnet concentration, the sensitivity of the NMR experiment drops due to paramagnetic quenching of the signal. In fact, the sensitivity, usually expressed as signal-to-noise (S/N) per unit of time, is determined by multiple factors including temperature, the DNP build-up time, efficiency of cross polarization, magic angle spinning speed, magnetic field strength, saturation of the electron transition, the signal line width and the performance of the probe.[61,81,82]

Paramagnetic Relaxation

The addition of radicals greatly influences the relaxation properties of the nuclei. At 100 K, the ^1H T_1 in a non-deuterated environment is ~ 10 s. Due to the addition of radicals, the T_1 is reduced to 0.5 - 4 s depending on the radial concentration. Less advantageous is the reduction of the nuclear $T_{1\rho}$ and T_2 due to the paramagnetic centers. The efficiency of the nuclear cross polarization process becomes reduced. For experiments with multiple cross polarization steps, this aspect can lead to significant signal loss. Also, the signal line width is influenced by the vicinity of the radicals. As discussed in chapter 2 , this is only a minor contribution when 5-10 mM of TOTAPOL is used.[61]

Temperature

Several factors influencing the S/N-ratio depend on temperature. First of all, the electronic circuitry produces less thermal noise at lower temperature. Secondly, the DNP transfer mechanism become more efficient at lower temperature.[79] At lower temperature, spin relaxation becomes slower. The lengthening of the T_{1e}/T_{2e} improves the saturation of the electron transition. This leads to a steep increase in DNP enhancement with lower temperature. A third source of sensitivity increase can be deduced from figure 1.1. The equilibrium polarization is higher at lower temperatures (a factor of 2.7 between 273 K and 100 K). Lower temperatures also cause longer polarization build-up times. Therefore the question arises what temperature is most efficient per unit of time. According to Thurber *et al.*,[33] DNP methods applied at 25 K are more sensitive per unit of time than those used at 100 K. A disadvantage of working at these temperatures is the consumption of helium neccessary to work at these temperatures.

Conformational Heterogeneity

As can be read in detail in chapter 2, the presence of conformational heterogeneity can greatly influence the intensity of the ssNMR signals. At the experimental temperatures, almost all motion is frozen out. Conformational exchange that is too fast at ambient temperatures compared to the NMR time-scale, appears as individual signals for each conformation at low temperature conditions used for DNP.

1.3 DNP AS A TOOL FOR STRUCTURAL BIOLOGY

Membrane proteins have been a common research topic in ssNMR due to the inherent difficulty to study these systems with other structural biology tools including X-ray crystallography. Due to its exposure to the environment, membrane proteins are wide-spread drug targets. The sensitivity of conven-

tional ssNMR requires for overexpression and subsequent purification of the protein of interest. The aim of NMR scientists to investigate protein structures in their native environment is therefore often not reached. Moreover, not all membrane proteins can be easily purified and/or reconstituted. Recent progress on both the sample preparation side in combination with the sensitivity of DNP makes this kind of studies more feasible. Instead of overexpression, purification and reconstitution of the protein in artificial liposomes, cellular envelopes of bacteria with the protein of interest overexpressed can now be measured directly.[45,83]

DNP studies in the literature

Since the early 2000's, several DNP studies have been published on the topic of membrane proteins and peptides. Starting from labeled retinal in bR (bacteriorhodopsin), a handful of other biological systems have been the subject of DNP experiments. Depending on the sample preparation, the measurements of the Griffin group showed promising DNP enhancements ranging from 40-90.[84–87] For other membrane proteins, DNP enhancements between 8 and 32 at 400 MHz have been published up to date. These can be found in figure 1.5. The bR DNP enhancements are not included in the figure, since they were measured at 211 MHz or at 80 K and 380 MHz while all other samples were measured at 100 K using commercial Bruker Biospin 400 MHz/ 263 GHz systems. Data recorded in Utrecht at the 800 MHz/ 527 GHz DNP system are added for comparison. As can be expected, the enhancements are lower at 800 MHz than at 400 MHz (see section 1.2). Thanks to the use more efficient biradicals (section 1.2), the enhancements are still sizeable.

While the majority of structural biology studies involve membrane proteins, or membrane-associated proteins, also crystalline samples have been studied. For example, the PI3-SH3 domain[53] yielded an enhancement of 46 at 8 kHz spin-

ning. The fibrillar GNNQQNY7-13 from the yeast prion protein Sup35p yielded an enhancement of 120 (211 MHz, 90 K) and 20 (400 MHz, 100 K).[56,88] Another example is the elucidation of the structural organization of an amyloidogenic protein. Transthyretin (TTR105-115) was investigated using ssNMR and, additionally, with DNP enhanced ssNMR.[89]

In the following paragraphs, the biological systems, shown in figure1.5 on the left side, will be discussed in more detail. These systems can be divided into three categories: membrane (associated) peptides, reconstituted membrane proteins and cellular preparations and native membranes.

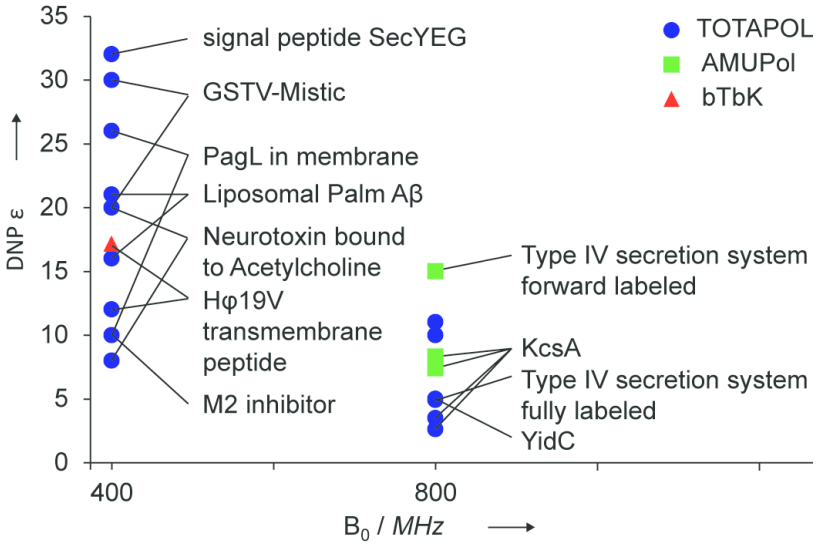

Figure 1.5: Published DNP enhancements on transmembrane proteins and peptides measured at 400 MHz / 263 GHz and 100 K compared to in-house measured enhancements on proteins at 800 MHz / 527 GHz and 100 K.

Membrane (associated) peptides

The transmembrane model peptide hΦ17W was investigated in oriented membranes.[66] In both oriented and non-oriented membranes several strategies were tested, including different concentrations of hydrophobic and hydrophilic biradicals.[72]

bTbK gave better DNP enhancements of the peptide than preparations using TOTAPOL.

The lipid-anchored N-terminal tail of protein Aβ, which is used in a liposomal vaccine against Alzheimer's disease was investigated using DNP. Details can be found in chapter 4.[90]

Reconstituted membrane proteins

In one study involving membrane proteins, SecYEG was reconstituted in *E. coli* with 40 nmol of a 25 amino acid signal peptide LamB.[91] The signal peptide contained 4 ^{13}C-labeled amino acids. In order to distinguish these from the natural abundance signal, double quantum filtering was utilized. The secondary chemical shift from the DQSQ experiment indicated an α-helical conformation of the signal peptide.

In the Griffin group, the binding sites of rimantidine to the influenza proton channel M2 were investigated using DNP.[92] A structural model of the rimantidine binding the M2 was designed based on distance measurements under DNP conditions.

Cellular preparations and native membranes

Three different cellular preparations have been reported in the literature up till now: PagL, NTII/nAChR and Mistic.

Mistic, an *E. coli* protein hypothesized to act as a chaperone, was subjected to 3D NCOCX and NCACX experiments in native membranes with the help of DNP. It is not known whether it is a transmembrane protein or membrane associated. Assignments were made in a specifically labeled sample. These experiments confirmed the α-helical structure of this particular stretch.[93]

The NTII/nAChR complex, a neurotoxin bound to an acetylcholine receptor, was measured in native membranes. The line width of the [2-^{13}C]-glycerol labeled neurotoxin depended heavily on sample storage conditions. While initially a strongly broadened diagonal was observed, a 4 week storage period in a freezer greatly reduced the resolution. At the

same time, half of the DNP enhancement was lost. The authors hypothesize that storage of the sample at -20 °C caused a reduction of the radicals in the hydration shell of the protein, which induced broadening through paramagnetic relaxation effects in their first experiment. As potential reducing agent, the cysteine residue's thiol group was suggested.[94]

The cellular envelope and whole cell preparations of PagL overexpressed in *E. coli* yielded DNP enhancements of 26 and 10, respectively. Apart from PagL, major components of the membrane could be distinguished: phospholipids, peptidoglycan, phospatidylethanolamine, lipopolysaccharide and also a small lipoprotein Lpp.[45] Interestingly, a recent study focused on the enhancement of cell wall materials and found an affinity of TOTAPOL for peptidoglycan.[46]

Factors influencing sample quality

Since LT-DNP experiments are performed far below glass transition temperature of proteins, cryoprotection is often needed. The formation of ice crystals could destroy the structural integrity of the protein. Up to date, glycerol or DMSO have been used to prevent the formation of ice crystals upon freezing. The efficiency of the DNP process, both the initial transfer step as well as the subsequent spread of polarization, is also influenced by the state of the solvent. Without glass formation, radicals are pushed out of the solvent during freezing. The subsequent uneven distribution of radicals leads to unfavorably fast relaxation close to the concentrated biradicals. This process then results in an efficiency decrease of the polarization transfer.[71,79,95] Also, it has been hypothesized[56,96] that the boundaries produced by crystal formation hinder the spin diffusion process which is essential for spread of the polarization throughout the sample.

For some biological samples, the lack of sufficient cryprotectant influences the DNP efficiency less. This is the case when the radical is either covalently attached to a protein (see chap-

ter 3) or the radical is enriched at the protein surface (see chapter 2 and Ravera *et al.*[96]).

1.4 SCOPE OF THE THESIS

This thesis is organized as follows. Chapters two and three comprise *methodological investigations* of solid-state DNP at both 400 MHz / 263 GHz and 800 MHz/ 527 GHz. Local DNP enhancements at specific protein residues are observed for the first time. MTSL-labeling, a widely used spin labeling technique in EPR, is shown to produce sizable DNP enhancements when placed on a well chosen position. In the last two chapters, *applications* of DNP on two different biological problems are described. In both cases, the molecules of interest are low abundant, precluding the use of conventional ssNMR experiments.

In *chapter 2*, experiments with the membrane embedded K^+ channel KcsA at a 800 MHz / 263 GHz DNP system are described. A four fold decrease in DNP enhancement compared to the 400 MHz system is observed. This number does not confirm the theoretical prediction for the field dependency of the CE, but is consistent with observations at 600 MHz.[79] The resolution of parts of the spectra did not change compared to ambient temperatures, while others parts became broadened. This is likely due to conformational heterogeneity, which reflects local dynamics at ambient temperatures. Furthermore, it was observed for the first time that DNP enhancements can fluctuate in the vicinity of the radical.

Chapter 3 describes the employment of MTS spin labels for DNP. For this study cysteine mutants of the tetrameric KcsA were used. Labels on both sites of the membrane were tested. The label position at the intracellular site (G116C), showed the highest enhancement, rivaling the enhancements observed for a similar concentration of the biradical TOTAPOL.

Chapter 4 describes the observation of multiple conformations of the N-terminal part of the Aβ protein in a liposomal Alzheimer's vaccine. The fifteen-residue, palmitoyl-anchored peptide contained three ^{13}C-^{15}N labeled amino acids. The measured secondary chemical shifts of these residues revealed several peptide conformations depending on the lipid composition of the liposome. These data agree with random coil conformations and conformations with less or more β-strand character.

In *chapter 5*, experiments on biominerals extracted from the marine unicellular eukaryote *Stephanopyxis turris* are presented. The location and character of the relatively low amount of organic material in the pores of the silica-based cell wall (frustule) is investigated with DNP. The ^{29}Si labeled frustules revealed a wide variety of chemically non-equivalent sites. Additional ^{15}N labeling of the culture revealed signals of the proteinacious components of the frustules as well as polyamines.

The last chapter of this thesis is *chapter 6* which encompasses conclusions and future perspectives.

1.5 REFERENCES

[1] Kane B E, A silicon-based nuclear spin quantum computer **1998**, 393, 133–137.

[2] Pla J J, Tan K Y, Dehollain J P, Lim W H, Morton J J L, Zwanenburg F A, Jamieson D N, Dzurak A S, and Morello A, High-fidelity readout and control of a nuclear spin qubit in silicon, *Nature* **2013**, 496, 334–8.

[3] Waldherr G, Wang Y, Zaiser S, Jamali M, Schulte-Herbrüggen T, Abe H, Ohshima T, Isoya J, Du J F, Neumann P, and Wrachtrup J, Quantum error correction in a solid-state hybrid spin register, *Nature* **2014**, 506, 204–7.

[4] Markley J L, Putter I, and Jardetzky O, High-resolution nuclear magnetic resonance spectra of selectively deuterated staphylococcal nuclease, *Science* **1968**, 161, 1249–51.

[5] LeMaster D M and Kushlan D M, Dynamical mapping of E. coli thioredoxin via 13 C NMR relaxation analysis, *J Am Chem Soc* **1996**, 118, 9255–9264.

[6] McIntosh L P and Dahlquist F W, Biosynthetic Incorporation of 15N and 13C for Assignment and Interpretation of Nuclear Magnetic Resonance Spectra of Proteins, *Q Rev Biophys* **2009**, 23, 1.

[7] Nand D, Cukkemane A, Becker S, and Baldus M, Fractional deuteration applied to biomolecular solid-state NMR spectroscopy, *J Biomol NMR* **2012**, 52, 91–101.

[8] Andrew E R, Bradbury A, and Eades R G, Nuclear magnetic resonance spectra from a crystal rotated at high speed, *Nature* **1958**, 182, 1659–1659.

[9] Abragam A, *Principles of nuclear magnetism*, **1961**.

[10] Hartmann S and Hahn E, Nuclear Double Resonance in the Rotating Frame, *Phys Rev* **1962**, 128, 2042–2053.

[11] Schaefer J and Stejskal E O, Carbon-13 nuclear magnetic resonance of polymers spinning at the magic angle, *J Am Chem Soc* **1976**, 98, 1031–1032.

[12] Baldus M, Petkova A T, Herzfeld J, and Griffin R G, Cross polarization in the tilted frame: assignment and spectral simplification in heteronuclear spin systems, *Mol Phys* **1998**, 95, 1197–1207.

[13] Carver T and Slichter C, Polarization of nuclear spins in metals, *Physcial Rev* **1953**, 92, 212–213.

[14] Overhauser A W, Polarization of nuclei in metals, *Phys Rev* **1953**, 92, 411–415.

[15] Hu K N N, Bajaj V S, Rosay M, and Griffin R G, High-frequency dynamic nuclear polarization using mixtures of TEMPO and trityl radicals, *J Chem Phys* **2007**, 126, 044512.

[16] Pavlova A, McCarney E R, Peterson D W, Dahlquist F W, Lew J, and Han S, Site-specific dynamic nuclear polarization of hydration water as a generally applicable approach to monitor protein aggregation, *Phys Chem Chem Phys* **2009**, 11, 6833–9.

[17] Reese M, Türke M T, Tkach I, Parigi G, Luchinat C, Marquardsen T, Tavernier A, Höfer P, Engelke F, Griesinger C, and Bennati M, (1)H and (13)C dynamic nuclear polarization in aqueous solution with a two-field (0.35 T/14 T) shuttle DNP spectrometer, *J Am Chem Soc* **2009**, 131, 15086–7.

[18] Krahn A, Lottmann P, Marquardsen T, Tavernier A, Türke M T, Reese M, Leonov A, Bennati M, Hoefer P, Engelke F, and Griesinger C, Shuttle DNP spectrometer with a two-center magnet, *Phys Chem Chem Phys* **2010**, 12, 5830–40.

[19] Lurie D J, Bussell D M, Bell L H, and Mallard J R, Proton-electron double magnetic resonance imaging of free radical solutions, *J Magn Reson* **1988**, 76, 366–370.

[20] Golman K, Petersson J S, Ardenkjaer-Larsen J H, Leunbach I, Wistrand L G, Ehnholm G, and Liu K, Dynamic in vivo oxymetry using overhauser enhanced MR imaging, *J Magn Reson Imaging* **2000**, 12, 929–38.

[21] Krishna M C, English S, Yamada K, Yoo J, Murugesan R, Devasahayam N, Cook J A, Golman K, Ardenkjaer-Larsen J H, Subramanian S, and Mitchell J B, Overhauser enhanced magnetic resonance imaging for tumor oximetry: coregistration of tumor anatomy and tissue oxygen concentration, *Proc Natl Acad Sci U S A* **2002**, 99, 2216–21.

[22] Benial A M F, Ichikawa K, Murugesan R, Yamada K i, and Utsumi H, Dynamic nuclear polarization properties of nitroxyl radicals used in Overhauser-enhanced MRI for simultaneous molecular imaging, *J Magn Reson* **2006**, 182, 273–82.

[23] Lingwood M D, Siaw T A, Sailasuta N, Abulseoud O A, Chan H R, Ross B D, Bhattacharya P, and Han S, Hyperpolarized water as an MR imaging contrast agent: feasibility of in vivo imaging in a rat model, *Radiology* **2012**, 265, 418–25.

[24] Abragam A and Proctor W G, Une nouvelle methode de polarisation dynamique des noyaux atomiques dans les solides, *C R Hebd Seances Acad Sci* **1958**, 246, 2253–2256.

[25] Erb E, Motchane J L, and Uebersfeld J, Effet de polarisation nucleaire dans les liquides et les gaz adsorbes sur les charbons, *C R Hebd Seances Acad Sci* **1958**, 246, 2121–2123.

[26] Kessenikh A, Lushchikov V, Manenkov A, and Taran Y, Proton polarization in irradiated polyethylenes, *Sov Physics, Solid State* **1963**, 5, 321–329.

[27] Kessenikh A, Manenkov A, and Pyatnitskii G, On explanation of experimental data on dynamic polarization of proton in irradiated polyehtylenes, *Sov Physics, Solid State* **1964**, 6, 641–643.

[28] Hwang C and Hill D, New effect in dynamic polarization, *Phys Rev Lett* **1967**, 18, 110–112.

[29] Hwang C and Hill D, Phenomenological model for the new effect in dynamic polarization, *Phys Rev Lett* **1967**, 19, 1011–1014.

[30] Wollan D, Dynamic nuclear polarization with an inhomogeneously broadened ESR line. I. Theory, *Phys Rev B* **1976**, 13, 3671–3685.

[31] Atsarkin V, Dynamic polarization of nuclei in solid dielectrics, *Sov Physics, Uspekhi* **1978**, 21, 725–744.

[32] Wind R, Duijvestijn M, van der Lugt C, Manenschijn A, and Vriend J, Applications of dynamic nuclear polarization in 13C NMR in solids, *Prog Nucl Magn Reson Spectrosc* **1985**, 17, 33–67.

[33] Thurber K R, Yau W M, and Tycko R, Low-temperature dynamic nuclear polarization at 9.4T with a 30mW microwave source, *J Magn Reson* **2010**, 204, 303–313.

[34] Lowe I, Free induction decays of rotating solids, *Phys Rev Lett* **1959**, 2, 285–287.

[35] Singel D, Seidel H, Kendrick R, and Yannoni C, A spectrometer for EPR, DNP, and multinuclear high-resolution NMR, *J Magn Reson* **1989**, 81, 145–161.

[36] Afeworki M, McKay R A, and Schaefer J, Selective observation of the interface of heterogeneous polycarbonate/polystyrene blends by dynamic nuclear polarization carbon-13 NMR spectroscopy, *Macromolecules* **1992**, 25, 4084–4091.

[37] Granatstein V, Parker R, and Armstrong C, Vacuum electronics at the dawn of the twenty-first century, *Proc IEEE* **1999**, 87, 702–716.

[38] Becerra L, Gerfen G, Temkin R, Singel D, and Griffin R, Dynamic nuclear polarization with a cyclotron resonance maser at 5 T, *Phys Rev Lett* **1993**, 71, 3561–3564.

[39] Bajaj V, Farrar C, Hornstein M, Mastovsky I, Vieregg J, Bryant J, Eléna B, Kreischer K, Temkin R, and Griffin R, Dynamic nuclear polarization at 9T using a novel 250GHz gyrotron microwave source, *J Magn Reson* **2003**, 160, 85–90.

[40] Weis V, Bennati M, Rosay M, and Griffin R G, Solid effect in the electron spin dressed state: A new approach for dynamic nuclear polarization, *J Chem Phys* **2000**, 113, 6795–6802.

[41] Weis V and Griffin R G, Electron-nuclear cross polarization, *Solid State Nucl Magn Reson* **2006**, 29, 66–78.

[42] Smith A A, Corzilius B, Bryant J A, DeRocher R, Woskov P P, Temkin R J, and Griffin R G, A 140 GHz pulsed EPR/212 MHz NMR spectrometer for DNP studies, *J Magn Reson* **2012**, 223, 170–9.

[43] Joo C G, Hu K N, Bryant J A, and Griffin R G, In situ temperature jump high-frequency dynamic nuclear polarization experiments: enhanced sensitivity in liquid-state NMR spectroscopy, *J Am Chem Soc* **2006**, 128, 9428–32.

[44] Lesage A, Lelli M, Gajan D, Caporini M a, Vitzthum V, Miéville P, Alauzun J, Roussey A, Thieuleux C, Mehdi A, Bodenhausen G, Copéret C, and Emsley L, Surface enhanced NMR spectroscopy by dynamic nuclear polarization, *J Am Chem Soc* **2010**, 132, 15459–61.

[45] Renault M, Pawsey S, Bos M P, Koers E J, Nand D, Tommassen-van Boxtel R, Rosay M, Tommassen J, Maas W E, and Baldus M, Solid-state NMR spectroscopy on cellular preparations enhanced by dynamic nuclear polarization, *Angew Chemie Int Ed* **2012**, 51, 2998–3001.

[46] Takahashi H, Ayala I, Bardet M, De Paëpe G, Simorre J P, and Hediger S, Solid-state NMR on bacterial cells: selective cell wall signal enhancement and resolution improvement using dynamic nuclear polarization, *J Am Chem Soc* **2013**, 135, 5105–5110.

[47] Abragam A and Goldman M, Principles of dynamic nuclear polarisation, *Reports Prog Phys* **1978**, 41, 395–467.

[48] Barnes A B, Paëpe G D, van der Wel P C A, Hu K N, Joo C G, Bajaj V S, Mak-Jurkauskas M L, Sirigiri J R, Herzfeld J, Temkin R J, and Griffin R G, High-field dynamic nuclear polarization for solid and solution biological NMR, *Appl Magn Reson* **2008**,

34, 237–263.

[49] Hu K N, Debelouchina G T, Smith A A, and Griffin R G, Quantum mechanical theory of dynamic nuclear polarization in solid dielectrics, *J Chem Phys* **2011**, 134, 125105.

[50] Hu K N N, Polarizing agents and mechanisms for high-field dynamic nuclear polarization of frozen dielectric solids, *Solid State Nucl Magn Reson* **2011**, 40, 31–41.

[51] Hu K N, Debelouchina G T, Smith A A, and Griffin R G, Quantum mechanical theory of dynamic nuclear polarization in solid dielectrics, *J Chem Phys* **2011**, 134, 125105+.

[52] Hovav Y, Feintuch A, and Vega S, Theoretical aspects of dynamic nuclear polarization in the solid state - the cross effect, *J Magn Reson* **2012**, 214, 29–41.

[53] Mentink-Vigier F, Akbey U, Hovav Y, Vega S, Oschkinat H, and Feintuch A, Fast passage dynamic nuclear polarization on rotating solids, *J Magn Reson* **2012**, 224, 13–21.

[54] Thurber K R and Tycko R, Theory for cross effect dynamic nuclear polarization under magic-angle spinning in solid state nuclear magnetic resonance: the importance of level crossings, *J Chem Phys* **2012**, 137, 084508.

[55] Bloembergen N, Purcell E, and Pound R, Relaxation effects in nuclear magnetic resonance absorption, *Phys Rev* **1948**, 73, 679–715.

[56] van der Wel P C A, Hu K N, Lewandowski J, and Griffin R G, Dynamic nuclear polarization of amyloidogenic peptide nanocrystals: GNNQQNY, a core segment of the yeast prion protein Sup35p, *J Am Chem Soc* **2006**, 128, 10840–10846.

[57] Rossini A J, Zagdoun A, Hegner F, Schwarzwälder M, Gajan D, Copéret C, Lesage A, and Emsley L, Dynamic nuclear polarization NMR spectroscopy of microcrystalline solids, *J Am Chem Soc* **2012**, 134, 16899–908.

[58] Blumberg W, Nuclear Spin-Lattice Relaxation Caused by Paramagnetic Impurities, *Phys Rev* **1960**, 119, 79–84.

[59] Smith A A, Corzilius B, Barnes A B, Maly T, and Griffin R G, Solid effect dynamic nuclear polarization and polarization pathways, *J Chem Phys* **2012**, 136, 015101.

[60] Song C, Hu K N, Joo C G, Swager T M, and Griffin R G, TOTAPOL: A biradical polarizing agent for dynamic nuclear polarization experiments in aqueous media, *J Am Chem Soc* **2006**, 128, 11385–11390.

[61] Corzilius B, Andreas L B, Smith A A, Ni Q Z, and Griffin R G, Paramagnet induced signal quenching in MAS-DNP experiments in frozen homogeneous solutions, *J Magn Reson* **2013**.

[62] Forrester A R and Thomson R H, Stable nitroxide radicals, *Nature* **1964**, 203, 74–75.

[63] Bertini I, Luchinat C, and Parigi G, *Solution NMR of paramagnetic molecules*, Elsevier B.V., Amsterdam, **2001**.

[64] Sengupta I, Nadaud P S, and Jaroniec C P, Protein structure determination with paramagnetic solid-state NMR spectroscopy, *Acc Chem Res* **2013**, 46, 2117–26.

[65] Jaroniec C P, Solid-state nuclear magnetic resonance structural studies of proteins using paramagnetic probes, *Solid State Nucl Magn Reson* **2012**, 43, 1–13.

[66] Salnikov E, Rosay M, Pawsey S, Ouari O, Tordo P, and Bechinger B, Solid-state NMR spectroscopy of oriented membrane polypeptides at 100 K with signal enhancement by dynamic nuclear polarization, *J Am Chem Soc* **2010**, 132, 5940–5941.

[67] Ma Y, Loyns C, Price P, and Chechik V, Thermal decay of TEMPO in acidic media via an N-oxoammonium salt intermediate, *Org Biomol Chem* **2011**, 9, 5573–8.

[68] Ardenkjaer-Larsen J H, Laursen I, Leunbach I, Ehnholm G, Wistrand L G, Petersson J S, and Golman K, EPR and DNP properties of certain novel single electron contrast agents intended for oximetric imaging, *J Magn Reson* **1998**, 133, 1–12.

[69] Rosay M, Zeri A C, Astrof N S, Opella S J, Herzfeld J, and Griffin R G, Sensitivity-enhanced NMR of biological solids: dynamic nuclear polarization of Y21M fd bacteriophage and purple membrane, *J Am Chem Soc* **2001**, 123, 1010–1011.

[70] Hu K N, Yu H h, Swager T M, and Griffin R G, Dynamic nuclear polarization with biradicals, *J Am Chem Soc* **2004**, 126, 10844–10845.

[71] Matsuki Y, Maly T, Ouari O, Karoui H, Le Moigne F, Rizzato E, Lyubenova S, Herzfeld J, Prisner T, Tordo P, and Griffin R G, Dynamic nuclear polarization with a rigid biradical, *Angew Chemie Int Ed* **2009**, 48, 4996–5000.

[72] Salnikov E S, Ouari O, Koers E, Sarrouj H, Franks T, Rosay M, Pawsey S, Reiter C, Bandara P, Oschkinat H, Tordo P, Engelke F, and Bechinger B, Developing DNP/Solid-State NMR Spectroscopy of Oriented Membranes, *Appl Magn Reson* **2012**, 43, 91–106.

[73] Kiesewetter M K, Corzilius B, Smith A A, Griffin R G, and Swager T M, Dynamic nuclear polarization with a water-soluble rigid biradical, *J Am Chem Soc* **2012**, 134, 4537–40.

[74] Thurber K R, Yau W M, and Tycko R, Low-temperature dynamic nuclear polarization at 9.4 T with a 30 mW microwave source, *J Magn Reson* **2010**, 204, 303–13.

[75] Haze O, Corzilius B, Smith A a, Griffin R G, and Swager T M, Water-soluble narrow-line radicals for dynamic nuclear polarization, *J Am Chem Soc* **2012**, 134, 14287–90.

[76] Magerstädt M, Gansow O A, Brechbiel M W, Colcher D, Baltzer L, Knop R H, Girton M E, and Naegele M, Gd(DOTA): An alternative to Gd(DTPA) as aT1,2 relaxation agent for NMR imaging or spectroscopy, *Magn Reson Med* **1986**, 3, 808–812.

[77] Lumata L, Kovacs Z, Sherry A D, Malloy C, Hill S, van Tol J, Yu L, Song L, and Merritt M E, Electron spin resonance studies of trityl OX063 at a concentration optimal for DNP, *Phys Chem Chem Phys* **2013**, 15, 9800–7.

[78] Maly T, Cui D, Griffin R G, and Miller A F, 1H dynamic nuclear polarization based on an endogenous radical, *J Phys Chem B* **2012**, 116, 7055–65.

[79] Sauvée C, Rosay M, Casano G, Aussenac F, Weber R T, Ouari O, and Tordo P, Highly Efficient, water-soluble polarizing agents for dynamic nuclear polarization at high frequency, *Angew Chem Int Ed Engl* **2013**.

[80] Lange S, Linden A H, Akbey U, Franks W T, Loening N M, van Rossum B J, and Oschkinat H, The effect of biradical concentration on the performance of DNP-MAS-NMR, *J Magn Reson* **2012**, 216, 209–12.

[81] Rossini A J, Zagdoun A, Lelli M, Gajan D, Rascón F, Rosay M, Maas W E, Copéret C, Lesage A, and Emsley L, One hundred fold overall sensitivity enhancements for Silicon-29 NMR spectroscopy of surfaces by dynamic nuclear polarization with CPMG acquisition, *Chem Sci* **2012**, 3, 108.

[82] Takahashi H, Fernández-de Alba C, Lee D, Maurel V, Gambarelli S, Bardet M, Hediger S, Barra A L, and De Paëpe G, Optimization of an absolute sensitivity in a glassy matrix during DNP-enhanced multidimensional solid-state NMR experiments, *J Magn Reson* **2013**, 239C, 91–99.

[83] Renault M, Tommassen-van Boxtel R, Bos M P, Post J A, Tommassen J, and Baldus M, Cellular solid-state nuclear magnetic resonance spectroscopy, *Proc Natl Acad Sci U S A* **2012**, 109,

4863–8.

[84] Rosay M, Lansing J C, Haddad K C, Bachovchin W W, Herzfeld J, Temkin R J, and Griffin R G, High-frequency dynamic nuclear polarization in MAS spectra of membrane and soluble proteins, *J Am Chem Soc* **2003**, 125, 13626–7.

[85] Bajaj V S, Hornstein M K, Kreischer K E, Sirigiri J R, Woskov P P, Mak-Jurkauskas M L, Herzfeld J, Temkin R J, and Griffin R G, 250GHz CW gyrotron oscillator for dynamic nuclear polarization in biological solid state NMR, *J Magn Reson* **2007**, 189, 251–79.

[86] Barnes A B, Mak-Jurkauskas M L, Matsuki Y, Bajaj V S, van der Wel P C a, Derocher R, Bryant J, Sirigiri J R, Temkin R J, Lugtenburg J, Herzfeld J, and Griffin R G, Cryogenic sample exchange NMR probe for magic angle spinning dynamic nuclear polarization, *J Magn Reson* **2009**, 198, 261–70.

[87] Barnes A, Corzilius B, Mak-Jurkauskas M, Andreas L, Bajaj V, Matsuki Y, Belenky M, Lugtenburg J, Sirigiri J, Temkin R, Herzfeld J, and Griffin R, Resolution and polarization distribution in cryogenic DNP/MAS experiments, *Phys Chem Chem Phys* **2010**, 12, 5861–5867.

[88] Debelouchina G T G, Bayro M J, van der Wel P C a, Caporini M a, Barnes A B, Rosay M, Maas W E, and Griffin R G, Dynamic nuclear polarization-enhanced solid-state NMR spectroscopy of GNNQQNY nanocrystals and amyloid fibrils, *Phys Chem Chem Phys* **2010**, 12, 5741–5751.

[89] Debelouchina G T, Bayro M J, Fitzpatrick A W, Ladizhansky V, Colvin M T, Caporini M A, Jaroniec C P, Bajaj V S, Rosay M, Macphee C E, Vendruscolo M, Maas W E, Dobson C M, and Griffin R G, Higher order amyloid fibril structure by MAS NMR and DNP spectroscopy, *J Am Chem Soc* **2013**, 135, 19237–47.

[90] Koers E J, López-Deber M P, Weingarth M, Nand D, Hickman D T, Mlaki Ndao D, Reis P, Granet A, Pfeifer A, Muhs A, and Baldus M, Dynamic nuclear polarization NMR spectroscopy: revealing multiple conformations in lipid-anchored peptide vaccines, *Angew Chemie Int Ed* **2013**, 52, 10905–10908.

[91] Reggie L, Lopez J J, Collinson I, Glaubitz C, and Lorch M, Dynamic nuclear polarization-enhanced solid-state NMR of a 13C-labeled signal peptide bound to lipid-reconstituted Sec translocon, *J Am Chem Soc* **2011**, 133, 19084–6.

[92] Andreas L B, Barnes A B, Corzilius B, Chou J J, Miller E a, Caporini M, Rosay M, and Griffin R G, Dynamic nuclear polarization study of inhibitor binding to the M2(18-60) proton transporter from influenza A, *Biochemistry* **2013**, 52, 2774–82.

[93] Jacso T, Franks W T, Rose H, Fink U, Broecker J, Keller S, Oschkinat H, and Reif B, Characterization of membrane proteins in isolated native cellular membranes by dynamic nuclear polarization solid-state NMR spectroscopy without purification and reconstitution, *Angew Chem Int Ed Engl* **2012**, 51, 432–5.

[94] Linden A H, Lange S, Franks W T, Specker E, Rossum B j V, and Hartmut Oschkinat, Neurotoxin II bound to acetylcholine receptors in native membranes, *J Am Chem Soc* **2011**, 133, 19266–19269.

[95] Zagdoun A, Casano G, Ouari O, Schwarzwälder M, Rossini A J, Aussenac F, Yulikov M, Jeschke G, Copéret C, Lesage A, Tordo P, and Emsley L, Large molecular weight nitroxide biradicals providing efficient dynamic nuclear polarization at temperatures up to 200 K, *J Am Chem Soc* **2013**, 135, 12790–7.

[96] Ravera E, Corzilius B, Michaelis V K, Luchinat C, Griffin R G, and Bertini I, DNP-enhanced MAS NMR of bovine serum albumin sediments and solutions, *J Phys Chem B* **2014**.

2

NMR-BASED STRUCTURAL BIOLOGY ENHANCED BY DYNAMIC NUCLEAR POLARIZATION AT HIGH MAGNETIC FIELD

Submitted manuscript

Eline J. Koers[1], Elwin A. W. van der Cruijsen[1], Melanie Rosay[2], Markus Weingarth[1], Alexander Prokofyev[1,3], Claire Sauvée[4], Olivier Ouari[4], Olaf Pongs[3], Paul Tordo[4], Werner E. Maas[2], Marc Baldus[1]

[1]Bijvoet Center for Biomolecular Research, Utrecht University, Padualaan 8, 3584 CH Utrecht, The Netherlands,
[2]Bruker BioSpin Corporation, 15 Fortune Drive, Billerica MA 01821, USA,
[3]Saarland University, Faculty of Medicine, Department of Physiology, Building 59, 66421 Homburg, Germany,

[4]Aix-Marseille Université, CNRS, ICR UMR 7273, 13397 Marseille, France.

2.1 INTRODUCTION

Dynamic nuclear polarization (DNP, Ref.[1]), a process in which nuclear spins are polarized via microwave irradiation of a nearby electron spin, is finding widespread applications in NMR spectroscopy[2,3] and Magnetic Resonance Imaging (MRI).[4,5] In solid-state NMR (ssNMR), the combined application of low-temperature LT DNP, Magic Angle Spinning (MAS, Ref[6]) and the use of exogenous paramagnetic polarizing agents has been employed as a signal enhancement method with increasing applications in material[7] and life science[8]. For example, LT DNP under MAS has been used to study membrane-associated peptides[9,10] as well as intermediate[11] and ligand-bound membrane protein states.[12–14] In addition, DNP-MAS has been successfully applied on cellular preparations[15–17] and can be used to examine large macromolecular complexes.[18]

On the other hand, paramagnetic agents are widely employed to enhance contrast and resolution in MRI applications.[19] The same principles have made paramagnetic relaxation effects (PREs) invaluable tools to refine molecular structures in biomolecular applications of solution[20,21] and, more recently, solid-state NMR.[22,23] In the latter case, elegant approaches have also been proposed to reduce spectroscopic repetition rates[24] and it is well known that the modulation of longitudinal relaxation rates by PREs favorably influences spectroscopic aspects of low temperature LT DNP studies.

While progress has been made in building DNP systems at high fields,[25,26] most commercially available DNP NMR spectrometers have been operating at a ^1H resonance frequency of 400 MHz (and 263 GHz DNP) where spectroscopic studies, at least in part, can be hampered by the comparatively low spectral resolution. Here, we investigate the use of

MAS DNP instrumentation operating at 800 MHz/527 GHz for biomolecular solid-state NMR. Since ssNMR has become a powerful method for applications in membrane- and cell embedded molecular systems, we utilized in our studies uniformly $\left[^{13}C,^{15}N\right]$ and $\left[^{2}H,^{13}C,^{15}N\right]$ labeled variants of the membrane embedded potassium channel KcsA, for which crystallographic information[27,28] as well as ssNMR data are available.[29–31] As in the general class of K^+ channels, KcsA comprises two coupled gates that are located at either end of the channel pore and that are called the activation and inactivation (a.k.a. selectivity filter, SF) gate. Channel inactivation leads to a closing of the inactivation gate and an opening of the activation gate.[32–34]

Starting with the closed conductive channel state that has been well characterized by X-ray and ssNMR, we examined the influence of transversal PREs and conformational heterogeneity upon LT DNP spectra obtained at 800 MHz/ 527 GHz at the residue-specific level. Our NMR studies were assisted by single channel measurements and MD calculations. Furthermore we compared spectral resolution and DNP enhancements to results obtained at 400 MHz, providing insight into site-specific origin for ssNMR line broadening and signal enhancement under LT DNP conditions. For many ion channel residues, we observed an increase in spectral resolution. These findings provided the basis to employ high-field DNP to examine how variations in ion channel structure correlate to the channel state before and after inactivation.

2.2 MATERIALS AND METHODS

Sample preparation

We prepared proteoliposomal samples containing uniformly (13C,15N) labelled KcsA in the closed conductive and open inactivated state as described before.[30,31,35] As in ref[36], $\left[^{2}H,^{13}C,^{15}N\right]$ labeled KcsA was expressed and back ex-

changed and reconstituted in asolectin. For DNP-based ssNMR experiments, we washed liposomal KcsA samples with 50 μL DNP solution containing TOTAPOL[37] (5 mM as well as 10 mM) or AMUPol[38] (25 mM) in 1:2:2 (v/v/v) glycerol-d8, D_2O, and H_2O. Samples were then centrifuged at 125,000 g for approximately 30 min and the supernatant was removed. This procedure was done twice. The remaining pellet was then transferred from the Eppendorf tube to a 3.2 mm sapphire rotor by means of a funnel and a 5-10 s centrifugation in a bench top centrifuge.

Solid-state NMR and DNP experiments

ssNMR and DNP experiments were conducted using 3.2 mm triple-resonance ^{1}H,^{13}C,^{15}N magic-angle-spinning (MAS) probe heads at static magnetic fields ranging from 9.4 to 18.8 T corresponding to proton/electron resonance frequencies of 400 MHz/ 263 GHz44, 700 MHz or 800 MHz/ 527 GHz (Bruker BioSpin). Data were recorded at 100 K (LT) and at 273 K (referred as ambient temperature, AT) employing MAS rates between 8 and 15 kHz. Pulse schemes reflected standard homonuclear proton-driven spin diffusion (PDSD) and double-quantum filtered $(^{13}C,^{13}C)$ using SPC5 recoupling.[39] NCA experiments typically utilized SPECIFIC-CP transfer.[40]

Molecular dynamics simulations

Atomistic MD simulations were carried out using the GROMACS simulations package version 4.5.3 with the GROMOS53a6 force field.[41] The starting structure was derived from crystal structure 3EFF, truncated to residues 22 to 115. The channel was embedded in a POPG bilayer in an aqueous solution of 150 mM KCl. All simulations were carried out under constant pressure. The chemical shift analysis presented in figure 2.4 is based on a 10 ns simulation, while chemical shifts where predicted every 200 ps using SPARTA+.[42]

Single Channel Measurements

Single channel recordings of KcsA were performed on a planar lipid bilayer setup (Compact, Ionovation GmbH). Lipid bilayers were formed by painting the lipids dissolved in n-decane over a 200 μm hole in a Teflon-septum that separated two chambers (cis and trans). KcsA proteoliposomes (1–5 μL) were added to the cis chamber. Single channel currents were recorded in symmetrical 150 mMKCl solution. The cis side was buffered to pH 7.0 by 10 mM HEPES and trans side was buffered to pH 4.0 by 10 mM succinic acid. All measurements were performed at room temperature. Data were sampled at 10 kHz and filtered at 1 kHz.

2.3 RESULTS AND DISCUSSION

Paramagnetic relaxation effects

In order to probe paramagnetic relaxation effects in our DNP samples, we firstly studied membrane-embedded U-$\left[^{13}C,^{15}N\right]$ KcsA at AT before (figure 2.1a, black) and after addition of 5 mM TOTAPOL and 20% glycerol (figure 2.1a, green). Note that this situation (with water-soluble radicals) is different from using covalently attached radicals (see, e.g. Ref[43]). The addition of the biradical left large parts of the spectra unaffected (i.e. no reduction of signal intensity and chemical shift changes) with the exception of, for example, backbone resonances of Pro 63, Thr 61 or Thr 85 or side-chain cross peaks of Val 84 (figure 2.1a). PRE-induced signal is exclusively found in the solvent-exposed regions as can be deduced from the attenuation plotted on a three-dimensional membrane embedded model of KcsA in the closed conductive state (figure 2.1b, left).

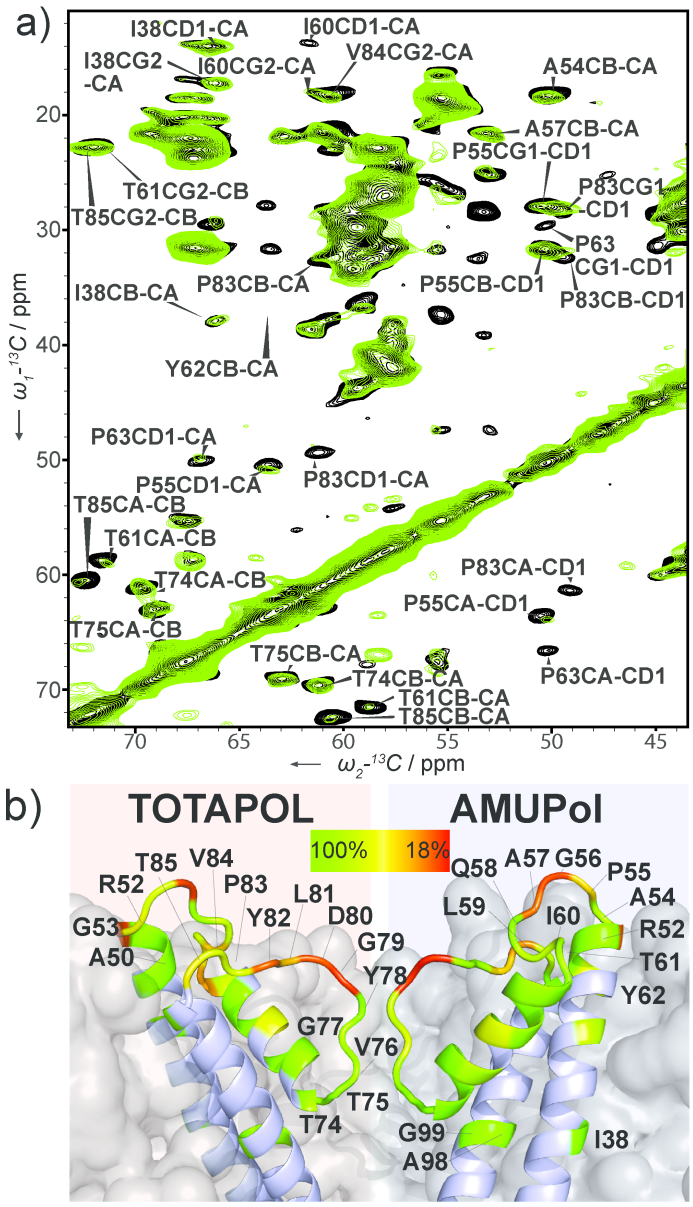

Figure 2.1: a) (^{13}C,^{13}C) PDSD data obtained at AT conditions before (black) or after addition of 5 mM TOTAPOL (green). In b), the residue-specific signal attenuation due to the addition of 5 mM TOTAPOL and 25 mM AMUPol is shown. The scale bar represents signal scaling after addition of biradical ranging from 1 (green) to 0.18 (red).

Within the selectivity filter (SF, residues 74-79) that represents the inactivation gate,[30] we observed a strong decrease in PREs when moving from the water-exposed entry (Gly 79) towards the center of the channel (Thr 74). For many solvent-exposed residues signal intensities were reduced by more than a factor 5 (figure 2.1b, left, red). Variations of solvent PREs[44] on the protein-solvent interface could be explained by similar mechanisms as found for the radical TEMPOL in earlier solution-state NMR experiments.[45–47] Hence, our results suggest that PREs at AT are restricted to a few Angstrom below the solvent exposed channel parts caused by radicals residing in the solvent or close to the solvent-exposed protein surface and not in the membrane. The presence of glycerol, did not lead to additional line broadening at AT conditions (see chapter 3).

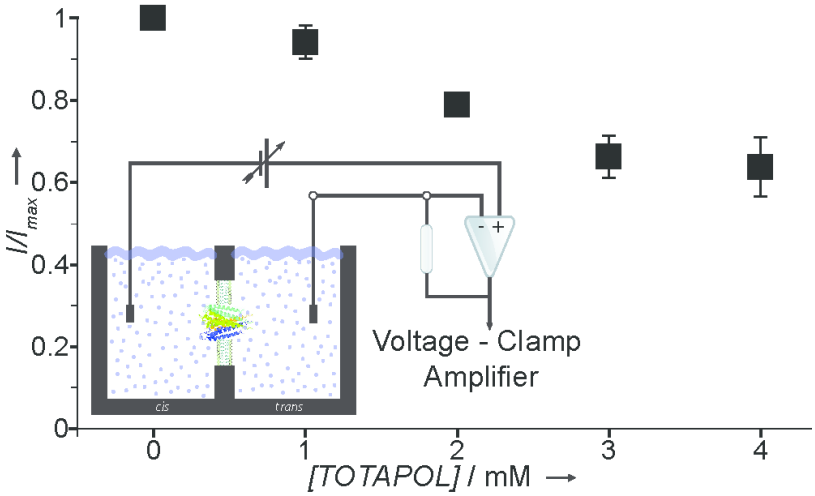

Figure 2.2: Single channel current of KcsA in planar lipid bilayers at increasing levels of TOTAPOL

Since strong PREs were found at the extracellular channel pore entrance, we further investigated the possibility of TOTAPOL binding to KcsA. Electrophysiological experiments (figure 2.2) suggest that concentrations as low as 4 mM TOTAPOL affect single channel properties of KcsA by reducing

amplitudes of the single channel current by as much as 40% at which point a plateau is reached, excluding the possibility of channel blockage by the radical. Instead, these results suggest, together with the lack of chemical shift changes (figure 2.1a), a partial occlusion of the channel entry with increasing concentrations of the biradical without perturbing the structure of the channel itself. Weak, transient binding cannot be excluded.

Next we conducted experiments using 25 mM AMUPol which revealed a similar overall relaxation profile (figure 2.1b, right), albeit with slightly weaker effects at the channel entry. These results suggest that PREs at AT are slightly larger for KcsA samples prepared with 5 mM TOTAPOL than in samples containing 25 mM AMUPol. Taking into account the five times lower TOTAPOL concentration, this observation likely reflects the influence of different molecular sizes of the two biradicals considered. Due to the additional hydrophilic tail of AMUPol and the size of the molecule, the radical center of AMUPol would be, on average, further distant to the protein - lipid surface than in the case of the more hydrophobic TOTAPOL.

Intrinsic line width at low temperature

Our previous analysis identifies PREs as an important source of T_2 relaxation that provides direct insight into the solvent-exposed molecular region (figure 2.1b). In addition, molecular motion should give rise to structural disorder at lower temperatures. Such effects have, for example, been exploited in the context of studying peptide and protein folding by ssNMR.[48,49] More recently, the dynamics of globular proteins[50] and the impact of solvent dynamics for LT ssNMR experiments have been investigated.[51] In the following, we hence considered contributions of both PREs and structural disorder for LT DNP data obtained at 800 MHz/ 527 GHz un-

der variable biradical concentration and compared our results to experiments at 400 MHz LT DNP conditions.

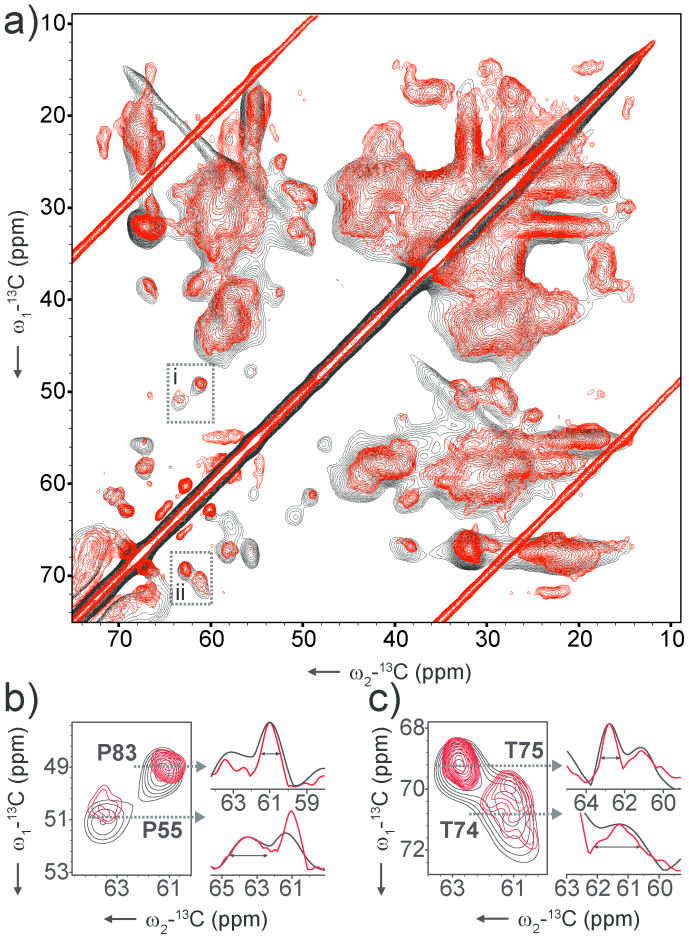

Figure 2.3: 400 MHz and 800 MHz. DNP 2D PDSD spectra recorded at 400 MHz (black) and 800 MHz (red) are overlayed. Proline CD1-CA (b) and Threonine CB-CA (c) regions are shown on the right, together with 1D projections of the CA peaks in the direct dimension. Note: 400 MHz DNP 2D PDSD spectrum contains a folded in sideband.

Figure 2.3 compares results of a standard 2D $\left({}^{13}C,{}^{13}C\right)$ PDSD experiment obtained on U-$\left[{}^{13}C,{}^{15}N\right]$ KcsA in asolectin bilayers at 400 MHz (black) and 800 MHz (red) under DNP conditions using TOTAPOL as polarizing agent. At the lat-

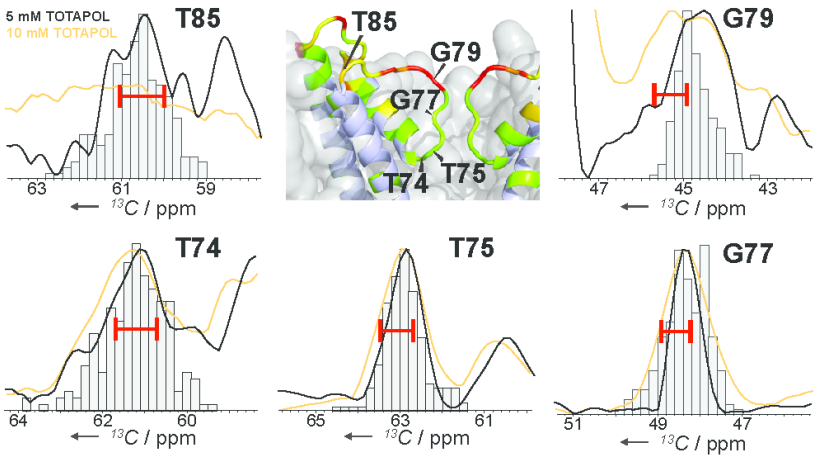

Figure 2.4: Projections of resolved peaks stemming from selectivity filter residues. 1D projections using 5 mM TOTAPOL (black) and 10 mM TOTAPOL (orange) are overlayed with the chemical shift distribution predicted by MD (see experimental details). For reference, the line width measured at 700 MHz AT, without addition of TOTAPOL is given by red bars. Results from Gly 79, Gly 77, Thr 74 and Thr 75 were taken from an NCA spectrum and Thr 85 was determined from a (^{13}C,^{13}C) PDSD spectrum. The inset structure is a zoom-in from figure 2.1b (solvent PREs at AT).

ter field strength, we also compared data for a TOTAPOL concentration of 5 mM (figure 2.4, black) and 10 mM (figure 2.4, orange) and focused on residues around the selectivity filter. In order to obtain complementary insight into the role of residue-specific channel motion we conducted molecular dynamics (MD) simulations and computed the chemical-shift distribution (figure 2.4, histograms) from our MD trajectories as shown before.[48,52] We observed a remarkable correlation between line widths determined experimentally and predicted from MD runs for the residues Gly 77, Thr 74 and Thr 75 (figure 2.4). Note that this analysis suggests that structural disorder in the selectivity filter is restricted to Thr 74 that exhibits a significantly larger line width than Thr75 and Gly 77 (vide infra) and only mildly improves in resolution when moving from 400 to 800 MHz (figure 2.3c). The other two residues investigated, i.e., Thr 85 and Gly 79, exhibit greater line width than predicted by the MD simulation data (figure 2.4). These residues where among the most attenuated ones at AT (fig-

ure 2.1) suggesting that broadening is due to paramagnetic relaxation. This view is further supported by investigating the effect of increasing the concentration of TOTAPOL from 5 to 10 mM. In this case, broadening for Thr 85 and Gly 79 further strongly increases while PREs for Thr 74, Thr 75 and Gly 77 remained limited (figure 2.4). Notably, residues that seem to be dominated by PREs (P55, P83) still exhibit an improvement in spectral resolution at higher field (figure 2.3b). Taken together our analysis confirms that line broadening effects at low temperatures can be explained by two phenomena: conformational heterogeneity and paramagnetic relaxation effects.

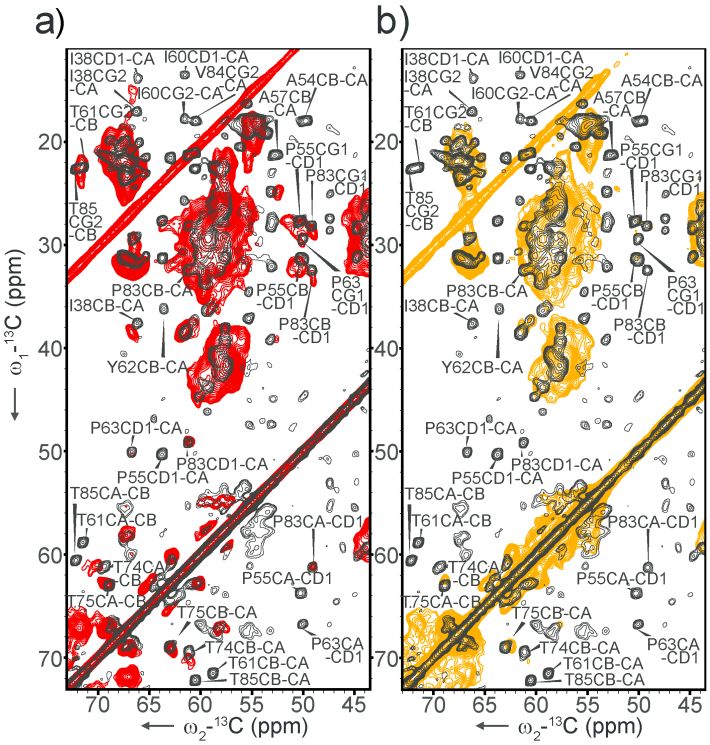

Figure 2.5: Overlay of 13C-13C PDSD at 700 MHz, 273 K without radicals (black) and 800 MHz LT, 5 mM TOTAPOL with (a, red) and without microwaves (b, orange).

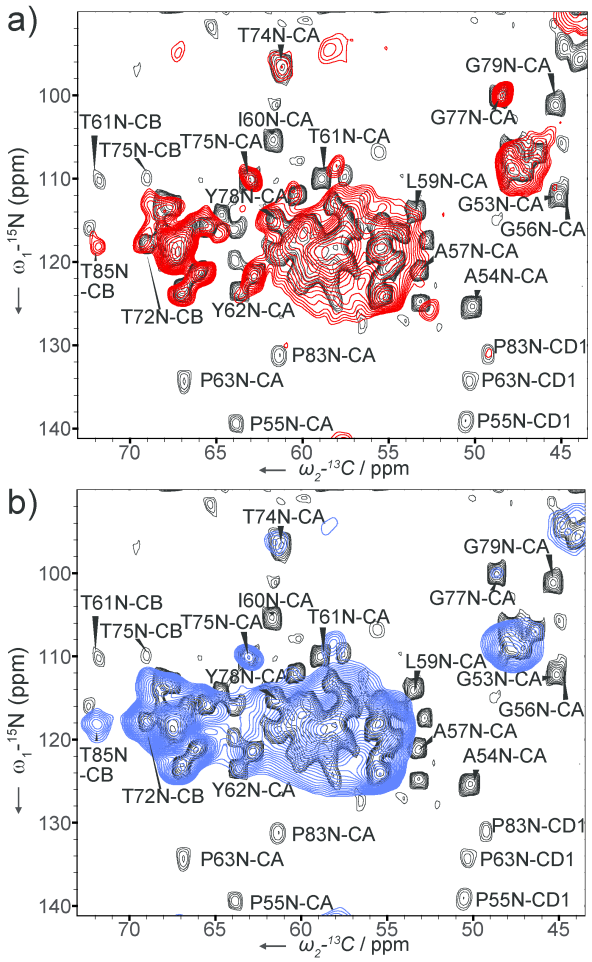

Figure 2.6: Comparison of KcsA data obtained at AT and LT DNP conditions. The results of 2D NCA experiments obtained at 700 MHz at AT conditions and without biradical (black) are compared to data acquired under DNP conditions at 800 MHz/527 GHz using 5 mM TOTAPOL (a, red) or 25 mM AMUPol (b, blue).

Comparison to high field data at AT

To further verify our conclusions regarding the intrinsic line width under 800 MHz DNP conditions, we compared our LT DNP data (figures 2.5 and 2.6, colored) to results obtained at AT conditions in the absence of the two biradicals of interest

(figure 2.5 and 2.6, black). The latter data were obtained at higher field strength (700 MHz). Using previously assigned large fractions of KcsA variants,[29,31] we analyzed 2D PDSD experiments at LT (figure 2.5) as well LT NCA data under DNP conditions using 5 mM TOTAPOL (figure 2.6a) and 25 mM AMUPol (figure 2.6b). In both sets of experiments we observed PRE modulated signal intensities for residues located at the channel-water interface. For example, Thr 61 and Thr 85 exhibited weaker signal intensities than Thr 74 and Thr 75. Note that these findings were made irrespective of the biradical type. Additional correlations in the region 70 to 65 ppm originate from co-purified lipids which are mobile under AT conditions.[53]

On the other hand, the apparent line width of many residues seen at LT DNP in the presence (figure 2.5a) or absence (figure 2.5b, orange) of microwave irradiation compared favorably to data obtained at high temperatures. For example, LT DNP correlations seen for Thr 74 or Pro 83 are virtually identical to data seen at AT 700 MHz conditions. In the case of Gly 79, we previously had detected increased channel dynamics.[54] The observed weak intensity at LT conditions can be explained by a combination of increased dynamics (vide infra) and PREs.

Residue specific and overall enhancements

Firstly, we determined global enhancement factors at 800 MHz/ 527 GHz conditions in one-dimensional ^{13}C CP experiments for both protonated and deuterated variants of membrane-embedded KcsA. We observed factors of 2.8 and up to 8.3 for uniformly labeled [^{1}H,^{13}C,^{15}N] KcsA with 5 mM TOTAPOL and 25 mM AMUPol, respectively. Similar values were obtained for one-dimensional ^{15}N CP experiments. Compared to equivalent experiments conducted at 400 MHz, the 5 mM TOTAPOL sample hence showed an approximately fourfold decrease in DNP enhancement at 800 MHz/ 527 GHz. We

observed a similar reduction in enhancement when analyzing AMUPol preparations at both 800 MHz and 400 MHz. When comparing LT-DNP ssNMR data (figure 2.6) to AT ssNMR experiments (figure 2.6) on [^{1}H,^{13}C,^{15}N] KcsA, only the addition of 25 mM AMUPol resulted in a sizable increase in signal to noise per hour by a factor of 6.9. Deuteration and ^{1}H back exchange for $\left[^{2}H,^{13}C,^{15}N\right]$ KcsA further increased DNP enhancements from 8.3 to 13.2 (figure 2.7d) which is in line with earlier work.[55,56]

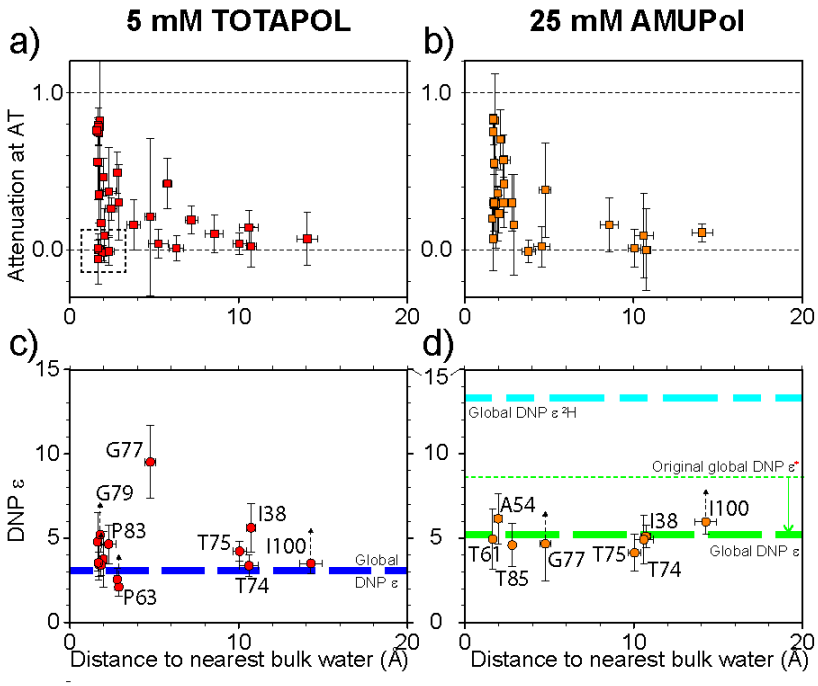

Figure 2.7: Residue specific solvent PRE attenuation at AT (a,b) and DNP enhancements (c,d) as a function of the distance to the nearest bulk water. Dashed arrows are shown for error bars lacking upper boundaries. The boxed area in c contains residues Tyr 45, Ala 50, Glu 51, Arg 52, Trp 87 and Tyr 78. All, but Tyr 78 are part of the protein-lipid-water interface.

Clearly, the enhancements seen at 800 MHz are lower than for data obtained at 400 MHz conditions. However, DNP enhancement factors reported in the literature[10,12–15,57,58] for membrane proteins at 400 MHz and 100 K vary considerably

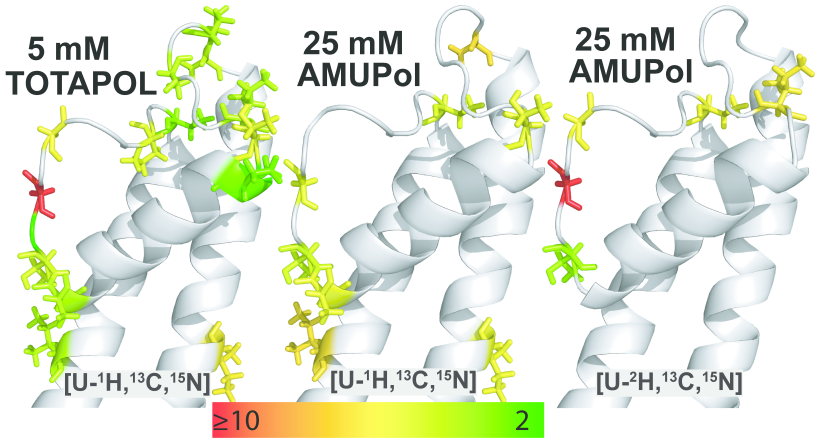

Figure 2.8: Residue-specific LT DNP enhancements in a close up region around the selectivity filter with (left) TOTAPOL, (middel) AMUPol and (right) AMUPol with proton back-exchanged [U-2H,13C,15N]. Scale bar refers to relative DNP enhancements ranging from 2 (green) to ≥10 (red).

in range from 8-32. These observations point to an important influence of the details of the sample preparation upon the LT DNP performance.

The favorable spectral resolution at 800 MHz and the observed signal modulation due to PREs and motional effects prompted us to determine residue-specific DNP enhancements at 800 MHz/ 527GHz. In figure 2.7, this analysis is presented for our $\left[^{1}H,^{13}C,^{15}N\right]$ KcsA samples. To visualize the effect of the distance of the AMUPol or TOTAPOL radical to the nearest position possible to the channel, we plotted PREs obtained at AT and residue-specific DNP enhancements against the distance to the nearest bulk water taken from the MD simulations (Fig 2.7). As expected from the Solomon-Bloembergen equations,[59,60] residues located closer to the surface exhibited stronger signal attenuation. Especially at the lower biradical concentration, residue-specific variations are however, substantial and most likely relate to local shielding effects by lipid-protein interactions for residues such as Tyr 45, Ala 50-Arg 52 or Trp 87 (dashed box in figure 2.7c) which are all located at the protein-lipid interface (see figure 2.1b,

left). Moreover, a uniform biradical distribution may only be established a concentrations higher than 5 mM TOTAPOL.

Both effects may also explain the larger fluctuations in residue-specific DNP enhancements (figure 2.7a,b) with maximum enhancements seen for Gly 77, Ile 38, Thr 75 and Pro 83 in the 5 mM TOTAPOL sample. The most dramatic difference is found for Gly 77. Both in the 5 mM TOTAPOL sample and the $\left[^{2}H,^{13}C,^{15}N\right]$ 25 mM AMUPol sample (figure 2.8) this residue exhibits the highest residue specific enhancement relative to the global values seen in 1D data (figure 2.7a). We note that for the deuterated case, spectra without microwave irradiation suffered from limited signal to noise and an analysis such as shown in figure 2.7 was restricted to a smaller number of protein residues around the channel pore segment. In this protein region, variations in DNP enhance-ments are small compared to the PRE's seen at AT which would be consistent with the dominant influence of spin diffusion.[61]

Strong variations were only observed for Gly 77 that is not only located at the center of the selectivity filter and thereby distant from both the solvent or cavity water but is also surrounded by nearby potassium ions in crystal structures (vide infra).[33]

Residue-specific disorder before and after channel inactivation

Channel inactivation in KcsA is controlled by structural changes at the selectivity filter that represents the inactivation gate and a large hinged motion around the inner helix bundle (the activation gate). In addition, KcsA single-channel recordings show kinetically complex behaviors that are commonly referred to as modal gating. A structural understanding of such local fluctuations is still limited.[62] With our 800 MHz DNP setup, we studied the channel in the closed-conductive (figures 2.4-2.7 and zoom in:2.9a-c) and open-inactivated (zoom in: 2.9d-g) state to be able to compare conformations of the selectivity filter in both states. In the closed-

conductive state, we analyzed 2D CC PDSD (figure 2.9c) and NC spectra (figure 2.9b) both at AT (black) and LT-DNP (red) conditions.

We observed that the peak of residue Thr 74 at the lower part of the selectivity filter (indicated in red in figure 2.9a) is broadened by a higher degree of structural heterogeneity (see also figure 2.4) compared to residues such as Thr 75 and Gly 77 that are located towards the center of the selectivity filter (figure 2.9a, blue). Our results obtained on the closed-conductive state of KcsA hence suggested that residue-specific channel dynamics lead to local disorder under LT DNP conditions.

We then compared our findings of figure 2.9a-c to the channel conformation after inactivation that can be induced by lowering pH and by reducing K^+ concentrations below 20 mM (figures 2.9e-g).[31,32] Spectra recorded at AT conditions are shown in black and LT-DNP in green. In line with our earlier studies on the closely related KcsA-Kv1.3 channel,[30,32] we observed chemical shift changes in the selectivity filter. Compared to the AT data (black, figure 2.9e-g), we now however detected signal attenuation for Thr 75 at LT DNP conditions (figure 2.9g, green) that was clearly visible before inactivation (figure 2.9c), i.e., in the closed conductive state. Interestingly, Thr 74 now is readily apparent in the open inactivated state. In contrast to the change in dynamics at the lower part of the SF, the upper part of the SF showed no change in dynamics. We can conclude by the clear appearance of residue Gly 77 before (figure 2.9b) and after inactivation (figure 2.9f) that in both states this residue showed no disorder. Notably, that the same residue exhibited the strongest DNP enhancements (figure 2.7 and 2.8). We note that SF residues towards the extracellular side could not be examined due to PREs, e.g. residue Gly 79 of the SF remains attenuated (figure 2.9b and 2.1b).

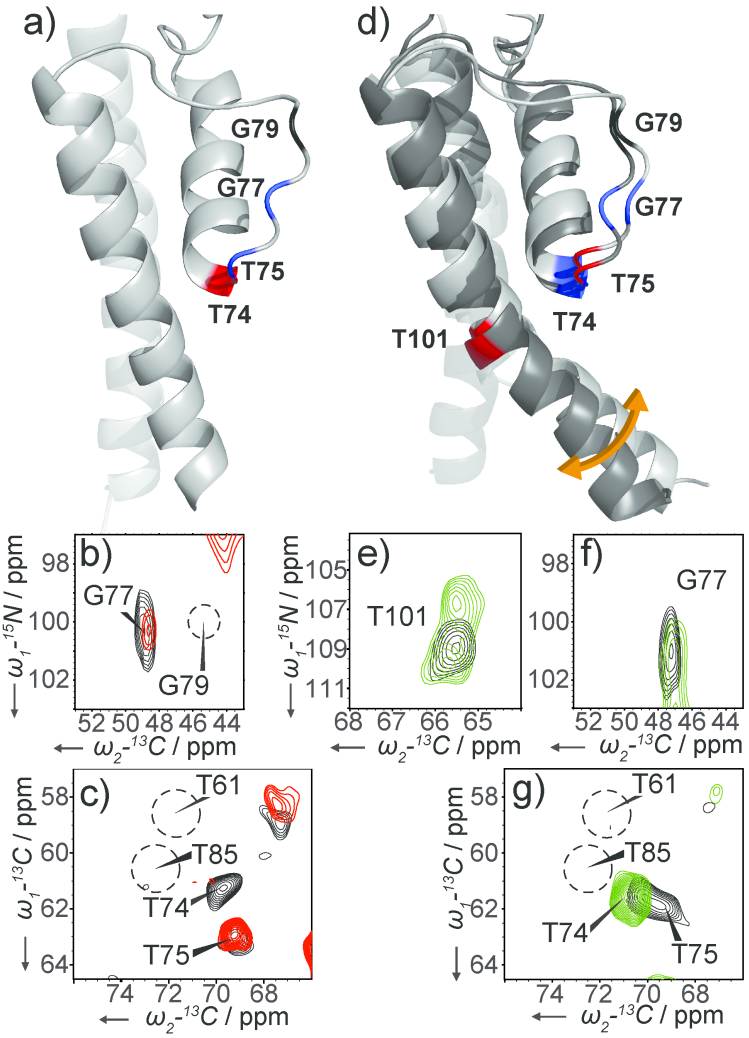

Figure 2.9: Comparison of AT (black) and LT-DNP (red/green) ssNMR before (a-c) and after inactivation (d-g). a) and d) structures are taken from ref[31] and[33]. Channel residues that are apparent in the LT spectra are given in blue on the KcsA structure. Residues that disappear or exhibit strong line broadening at LT are indicated in red. In d, two channel conformations (refering to an activation gate opening of 23 and 32 Angstrom, respectively), that are most compatible with the ssNMR data are overlayed. b) and c) represent zoom-ins from figure 2.6 and figure 2.5a respectively.

In the open-inactivated state under LT DNP conditions, we also observed peak doubling at Thr 101 (figure 2.9e, green) which is situated at the gating hinge of the activation gate.

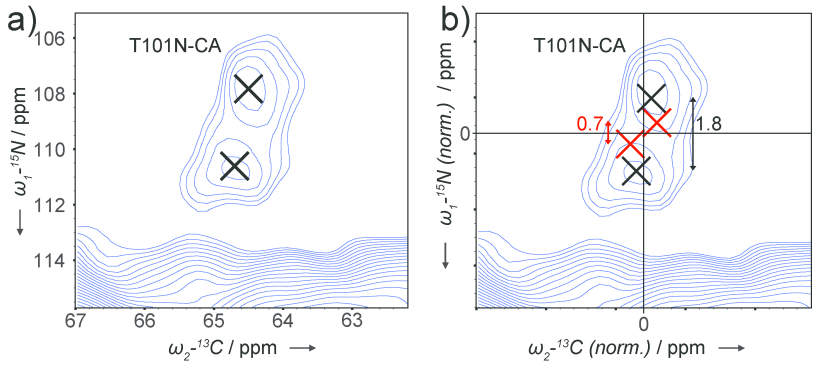

Figure 2.10: Peaks doubling of residue T101: a) peak position and b) relative peak position according to chemical shift back predictions (red) from the crystal structures.

This residue exhibits a well characterized ssNMR chemical shift change[30,32] as a result of opening of the activation gate (figure 2.9d). Note that these observations were insensitive to changes to stronger acidic pH in our proteoliposomal preparations. To understand the nature of the peak doubling observed at Thr 101, we investigated whether changes in activation gate opening as seen in KcsA mutant crystals would lead to chemical-shift variations in our ssNMR spectra. Crystal structures of constitutively open KcsA mutants had revealed various degrees of activation gate opening ranging from 23 to 32 Angstrom.[33] Indeed, when comparing ^{13}Ca, Cb and ^{15}N chemical shift predictions for open mutants forms between 23 Angstrom and 32 Angstrom, the size and trend in chemical shift variations were in remarkable agreement with our experimental results (figure 2.10). Assuming that the ssNMR signal intensity reports on the relative population of these opening events, our ssNMR would be most compatible with the dominant contribution of two channel conformations: one species that only exhibits a limited opening (23 Angstrom) and a second population that displays are fully open activation gate (32 Angstrom) in our ssNMR spectra. These results would be consistent with structural fluctuations of the activation gate even

under strongly acidic pH conditions where the activation gate is fully open.[63]

2.4 CONCLUSION

Dynamic Nuclear Polarization has become a powerful method to enhance spectroscopic sensitivities in the context of NMR and MRI. On the other hand, the availability of standard high-field NMR instruments has greatly enhanced the possibility to study complex (bio)molecular systems where spectral resolution is critical. We have shown that high field DNP significantly enhances the prospects to conduct in-depth structural investigations of complex molecules such as membrane proteins in different functional states.

We have demonstrated that these conditions can not only enhance spectral resolution but also offer the possibility to utilize the intrinsic paramagnetic properties of the polarizing agents as direct structural probes. In the case of the membrane embedded KcsA channel, our results helped to pinpoint the water accessible pore of the channel in membranes. The most solvent-exposed surface shell exhibits strong PREs under the conditions used in our experiments. We suspect that similar processes are also present in the context of material science applications.

The comparison of DNP data to results obtained at ambient temperatures furthermore allowed us to obtain insight into the role of ion channel plasticity before and after inactivation. This flexibility could be closely related to modal gating that represents an effective regulatory mechanism by which ion channels control the extent and time course of ionic fluxes. Our experiments identified specific selectivity filter residues that exhibit conformational flexibility before (Thr 74) and after inactivation (Thr 75, Thr 101). These observations underline that both gates are coupled[32,33] and support emerging views[63] that small structural fluctuations of the filter backbone can have drastic effects on gating changes. As demon-

strated here, the corresponding structural ensembles that represent different functional states become visible under high field DNP conditions.

Compared to earlier DNP studies, that were mostly conducted at 400 MHz, we find reduced overall signal enhancements at 800 MHz DNP conditions. This reduction is higher than discussed in the literature[64] but it is in line with recent studies of AMUPol at lower magnetic fields.[38] As discussed before, the actual signal enhancements may also depend on the details of the sample conditions. For further studies on this subject, the membrane-embedded KcsA channel for which ssNMR resonance assignments as well as structural data are available[29,31] may represent a valuable experimental reference. For example, Gly 77 that is located at the center of the selectivity filter did not show conformational flexibility in the two functional states considered and exhibited the largest residue-specific DNP enhancements.

In parallel, further optimizations of the instrumental details including the use of lower temperatures[26] or of pulsed DNP setups[65] may greatly improve DNP enhancements at high magnetic field. Moreover, our results using AMUPol indicate that further modifications of the polarizing agent (see, e.g., Ref.[66]) or of the proton density of the target molecule itself[55,56,66,67] may additionally enhance the potential of DNP-supported structural biology. Note that in such studies reference data obtained using conventional NMR setups that we here used to examine the high-field DNP performance and the details of the PRE mechanism would not be required. These considerations provide additional opportunities for in-depth studies of the conformational landscape that describes the workings of complex (bio)molecules using high field DNP technology.

2.5 REFERENCES

[1] Overhauser A W, Polarization of nuclei in metals, *Phys Rev* **1953**, 92, 411–415.

[2] Hall D A, Maus D C, Gerfen G J, Inati S J, Becerra L R, Dahlquist F W, and Griffin R G, Polarization-enhanced NMR spectroscopy of biomolecules in frozen solution, *Science* **1997**, 276, 930–932.

[3] Ardenkjaer-Larsen J H, Fridlund B, Gram A, Hansson G, Hansson L, Lerche M H, Servin R, Thaning M, and Golman K, Increase in signal-to-noise ratio of > 10,000 times in liquid-state NMR, *Proc Natl Acad Sci U S A* **2003**, 100, 10158–63.

[4] Gallagher F A, Kettunen M I, Day S E, Hu D E, Ardenkjaer-Larsen J H, Zandt R i t, Jensen P R, Karlsson M, Golman K, Lerche M H, and Brindle K M, Magnetic resonance imaging of pH in vivo using hyperpolarized 13C-labelled bicarbonate, *Nature* **2008**, 453, 940–3.

[5] Cassidy M C, Chan H R, Ross B D, Bhattacharya P K, and Marcus C M, In vivo magnetic resonance imaging of hyperpolarized silicon particles, *Nat Nanotechnol* **2013**, 8, 363–8.

[6] Andrew E R, Bradbury A, and Eades R G, Nuclear magnetic resonance spectra from a crystal rotated at high speed, *Nature* **1958**, 182, 1659–1659.

[7] Rossini A J, Zagdoun A, Lelli M, Lesage A, Copéret C, and Emsley L, Dynamic nuclear polarization surface enhanced NMR spectroscopy., *Acc Chem Res* **2013**, 46, 1942–51.

[8] Ni Q Z, Daviso E, Can T V, Markhasin E, Jawla S K, Swager T M, Temkin R J, Herzfeld J, and Griffin R G, High frequency dynamic nuclear polarization **2013**.

[9] Salnikov E, Rosay M, Pawsey S, Ouari O, Tordo P, and Bechinger B, Solid-state NMR spectroscopy of oriented membrane polypeptides at 100 K with signal enhancement by dynamic nuclear polarization, *J Am Chem Soc* **2010**, 132, 5940–5941.

[10] Koers E J, López-Deber M P, Weingarth M, Nand D, Hickman D T, Mlaki Ndao D, Reis P, Granet A, Pfeifer A, Muhs A, and Baldus M, Dynamic nuclear polarization NMR spectroscopy: revealing multiple conformations in lipid-anchored peptide vaccines, *Angew Chemie Int Ed* **2013**, 52, 10905–10908.

[11] Bajaj V S, Mak-Jurkauskas M L, Belenky M, Herzfeld J, and Griffin R G, Functional and shunt states of bacteriorhodopsin resolved by 250 GHz dynamic nuclear polarization-enhanced solid-state NMR, *Proc Natl Acad Sci U S A* **2009**, 106, 9244–9249.

[12] Linden A H, Lange S, Franks W T, Specker E, Rossum B j V, and Hartmut Oschkinat, Neurotoxin II bound to acetylcholine receptors in native membranes, *J Am Chem Soc* **2011**, 133, 19266–19269.

[13] Reggie L, Lopez J J, Collinson I, Glaubitz C, and Lorch M, Dynamic nuclear polarization-enhanced solid-state NMR of a 13C-labeled signal peptide bound to lipid-reconstituted Sec translocon, *J Am Chem Soc* **2011**, 133, 19084–6.

[14] Andreas L B, Barnes A B, Corzilius B, Chou J J, Miller E a, Caporini M, Rosay M, and Griffin R G, Dynamic nuclear polarization study of inhibitor binding to the M2(18-60) proton transporter from influenza A, *Biochemistry* **2013**, 52, 2774–82.

[15] Renault M, Pawsey S, Bos M P, Koers E J, Nand D, Tommassen-van Boxtel R, Rosay M, Tommassen J, Maas W E, and Baldus M, Solid-state NMR spectroscopy on cellular preparations enhanced by dynamic nuclear polarization, *Angew Chemie Int Ed* **2012**, 51, 2998–3001.

[16] Takahashi H, Ayala I, Bardet M, De Paëpe G, Simorre J P, and Hediger S, Solid-state NMR on bacterial cells: selective cell wall signal enhancement and resolution improvement using dynamic nuclear polarization, *J Am Chem Soc* **2013**, 135, 5105–5110.

[17] Wang T, Park Y B, Caporini M A, Rosay M, Zhong L, Cosgrove D J, and Hong M, Sensitivity-enhanced solid-state NMR detection of expansin's target in plant cell walls, *Proc Natl Acad Sci U S A* **2013**, 110, 16444–9.

[18] Gelis I, Vitzthum V, Dhimole N, Caporini M A, Schedlbauer A, Carnevale D, Connell S R, Fucini P, and Bodenhausen G, Solid-state NMR enhanced by dynamic nuclear polarization as a novel tool for ribosome structural biology, *J Biomol NMR* **2013**, 56, 85–93.

[19] Lauterbur P C, Image formation by induced local interactions. Examples employing nuclear magnetic resonance, *Nature* **1973**, 190–191.

[20] Otting G, Protein NMR using paramagnetic ions, *Annu Rev Biophys* **2010**, 39, 387–405.

[21] Bertini I, Luchinat C, Parigi G, and Pierattelli R, NMR spectroscopy of paramagnetic metalloproteins, *Chembiochem* **2005**, 6, 1536–49.

[22] Buffy J J, Hong T, Yamaguchi S, Waring A J, Lehrer R I, and Hong M, Solid-state NMR investigation of the depth of insertion of protegrin-1 in lipid bilayers using paramagnetic Mn2+, *Biophys J* **2003**, 85, 2363–73.

[23] Nadaud P S, Helmus J J, Höfer N, and Jaroniec C P, Long-range structural restraints in spin-labeled proteins probed by solid-state nuclear magnetic resonance spectroscopy, *J Am Chem Soc* **2007**, 129, 7502–7503.

[24] Wickramasinghe N P, Parthasarathy S, Jones C R, Bhardwaj C, Long F, Kotecha M, Mehboob S, Fung L W M, Past J, Samoson A, and Ishii Y, Nanomole-scale protein solid-state NMR by breaking intrinsic 1HT1 boundaries., *Nat Methods* **2009**, 6, 215–8.

[25] Matsuki Y, Takahashi H, Ueda K, Idehara T, Ogawa I, Toda M, Akutsu H, and Fujiwara T, Dynamic nuclear polarization experiments at 14.1 T for solid-state NMR, *Phys Chem Chem Phys* **2010**, 12, 5799–803.

[26] Barnes A B, Markhasin E, Daviso E, Michaelis V K, Nanni E A, Jawla S K, Mena E L, DeRocher R, Thakkar A, Woskov P P, Herzfeld J, Temkin R J, and Griffin R G, Dynamic nuclear polarization at 700MHz/460GHz, *J Magn Reson* **2012**, 224, 1–7.

[27] Zhou Y, Morais-Cabral J H, Kaufman A, and MacKinnon R, Chemistry of ion coordination and hydration revealed by a K+ channel-Fab complex at 2.0 A resolution, *Nature* **2001**, 414, 43–8.

[28] Uysal S, Vásquez V, Tereshko V, Esaki K, Fellouse F A, Sidhu S S, Koide S, Perozo E, and Kossiakoff A, Crystal structure of full-length KcsA in its closed conformation, *Proc Natl Acad Sci U S A* **2009**, 106, 6644–9.

[29] Schneider R, Ader C, Lange A, Giller K, Hornig S, Pongs O, Becker S, and Baldus M, Solid-state NMR spectroscopy applied to a chimeric potassium channel in lipid bilayers, *J Am Chem Soc* **2008**, 130, 7427–35.

[30] Ader C, Schneider R, Hornig S, Velisetty P, Wilson E M, Lange A, Giller K, Ohmert I, Martin-Eauclaire M F, Trauner D, Becker S, Pongs O, and Baldus M, A structural link between inactivation and block of a K+ channel, *Nat Struct Mol Biol* **2008**, 15, 605–12.

[31] van der Cruijsen E A W, Nand D, Weingarth M, Prokofyev A, Hornig S, Cukkemane A A, Bonvin A M J J, Becker S, Hulse R E, Perozo E, Pongs O, and Baldus M, Importance of lipid-pore loop interface for potassium channel structure and function, *Proc Natl Acad Sci U S A* **2013**, 110, 13008–13.

[32] Ader C, Schneider R, Hornig S, Velisetty P, Vardanyan V, Giller K, Ohmert I, Becker S, Pongs O, and Baldus M, Coupling of activation and inactivation gate in a K+-channel: potassium and ligand sensitivity, *EMBO J* **2009**, 28, 2825–34.

[33] Cuello L G, Jogini V, Cortes D M, and Perozo E, Structural mechanism of C-type inactivation in K(+) channels, *Nature* **2010**, 466, 203–8.

[34] Ader C, Schneider R, Seidel K, Etzkorn M, Becker S, and Baldus M, Structural rearrangements of membrane proteins probed by water-edited solid-state NMR spectroscopy, *J Am Chem Soc* **2009**, 131, 170–6.

[35] Bhate M P, Wylie B J, Tian L, and McDermott A E, Conformational dynamics in the selectivity filter of KcsA in response to potassium ion concentration, *J Mol Biol* **2010**, 401, 155–66.

[36] Weingarth M, van der Cruijsen E A W, Ostmeyer J, Lievestro S, Roux B, and Baldus M, Quantitative analysis of the water occupancy around the selectivity filter of a K(+) channel in different gating modes, *J Am Chem Soc* **2014**, 136, 2000–7.

[37] Song C, Hu K N, Joo C G, Swager T M, and Griffin R G, TOTAPOL: A biradical polarizing agent for dynamic nuclear polarization experiments in aqueous media, *J Am Chem Soc* **2006**, 128, 11385–11390.

[38] Sauvée C, Rosay M, Casano G, Aussenac F, Weber R T, Ouari O, and Tordo P, Highly Efficient, water-soluble polarizing agents for dynamic nuclear polarization at high frequency, *Angew Chem Int Ed Engl* **2013**.

[39] Hohwy M, Rienstra C M, Jaroniec C P, and Griffin R G, Fivefold symmetric homonuclear dipolar recoupling in rotating solids: Application to double quantum spectroscopy, *J Chem Phys* **1999**, 110, 7983–7992.

[40] Baldus M, Petkova A T, Herzfeld J, and Griffin R G, Cross polarization in the tilted frame: assignment and spectral simplification in heteronuclear spin systems, *Mol Phys* **1998**, 95, 1197–1207.

[41] Soares T A, Hünenberger P H, Kastenholz M A, Kräutler V, Lenz T, Lins R D, Oostenbrink C, and van Gunsteren W F, An

improved nucleic acid parameter set for the GROMOS force field, *J Comput Chem* **2005**, 26, 725–37.

[42] Shen Y and Bax A, SPARTA+: a modest improvement in empirical NMR chemical shift prediction by means of an artificial neural network, *J Biomol NMR* **2010**, 48, 13–22.

[43] Sengupta I, Nadaud P S, Helmus J J, Schwieters C D, and Jaroniec C P, Protein fold determined by paramagnetic magic-angle spinning solid-state NMR spectroscopy, *Nat Chem* **2012**, 4, 410–417.

[44] Hocking H G, Zangger K, and Madl T, Studying the structure and dynamics of biomolecules by using soluble paramagnetic probes, *ChemPhysChem* **2013**, 14, 3082–94.

[45] Esposito G, Lesk A M, Molinari H, Motta A, Niccolai N, and Pastore A, Probing protein structure by solvent perturbation of nuclear magnetic resonance spectra, *J Mol Biol* **1992**, 224, 659–670.

[46] Pintacuda G and Otting G, Identification of Protein Surfaces by NMR Measurements with a Paramagnetic Gd(III) Chelate, *J Am Chem Soc* **2002**, 124, 372–373.

[47] Bernini A, Spiga O, Venditti V, Prischi F, Bracci L, Tong A P L, Wong W T, and Niccolai N, NMR studies of lysozyme surface accessibility by using different paramagnetic relaxation probes, *J Am Chem Soc* **2006**, 128, 9290–1.

[48] Heise H, Luca S, de Groot B L, Grubmüller H, and Baldus M, Probing conformational disorder in neurotensin by two-dimensional solid-state NMR and comparison to molecular dynamics simulations, *Biophys J* **2005**, 89, 2113–20.

[49] Havlin R H and Tycko R, Probing site-specific conformational distributions in protein folding with solid-state NMR, *Proc Natl Acad Sci U S A* **2005**, 102, 3284–9.

[50] Linden A H, Franks W T, Akbey U, Lange S, van Rossum B J, and Oschkinat H, Cryogenic temperature effects and resolution upon slow cooling of protein preparations in solid state NMR, *J Biomol NMR* **2011**, 51, 283–92.

[51] Siemer A B, Huang K Y, and McDermott A E, Protein linewidth and solvent dynamics in frozen solution NMR, *PLoS One* **2012**, 7, e47242.

[52] Zachariae U, Schneider R, Velisetty P, Lange A, Seeliger D, Wacker S J, Karimi-Nejad Y, Vriend G, Becker S, Pongs O, Baldus M, and de Groot B L, The molecular mechanism of toxin-induced conformational changes in a potassium channel: rela-

tion to C-type inactivation, *Structure* **2008**, 16, 747–54.

[53] Weingarth M, Prokofyev A, van der Cruijsen E A W, Nand D, Bonvin A M J J, Pongs O, and Baldus M, Structural determinants of specific lipid binding to potassium channels, *J Am Chem Soc* **2013**, 135, 3983–8.

[54] Ader C, Pongs O, Becker S, and Baldus M, Protein dynamics detected in a membrane-embedded potassium channel using two-dimensional solid-state NMR spectroscopy, *Biochim Biophys Acta* **2010**, 1798, 286–90.

[55] Kagawa A, Murokawa Y, Takeda K, and Kitagawa M, Optimization of 1H spin density for dynamic nuclear polarization using photo-excited triplet electron spins, *J Magn Reson* **2009**, 197, 9–13.

[56] Akbey U, Franks W T, Linden A, Lange S, Griffin R G, van Rossum B J, and Oschkinat H, Dynamic nuclear polarization of deuterated proteins, *Angew Chemie Int Ed* **2010**, 49, 7803–6.

[57] Salnikov E S, Ouari O, Koers E, Sarrouj H, Franks T, Rosay M, Pawsey S, Reiter C, Bandara P, Oschkinat H, Tordo P, Engelke F, and Bechinger B, Developing DNP/Solid-State NMR Spectroscopy of Oriented Membranes, *Appl Magn Reson* **2012**, 43, 91–106.

[58] Jacso T, Franks W T, Rose H, Fink U, Broecker J, Keller S, Oschkinat H, and Reif B, Characterization of membrane proteins in isolated native cellular membranes by dynamic nuclear polarization solid-state NMR spectroscopy without purification and reconstitution, *Angew Chem Int Ed Engl* **2012**, 51, 432–5.

[59] Solomon I, Relaxation processes in a system of two spins, *Phys Rev* **1955**, 99, 559–565.

[60] Bloembergen N and Morgan L O, Proton relaxation times in paramagnetic solutions. Effects of electron spin relaxation, *J Chem Phys* **1961**, 34, 842.

[61] van der Wel P C A, Hu K N, Lewandowski J, and Griffin R G, Dynamic nuclear polarization of amyloidogenic peptide nanocrystals: GNNQQNY, a core segment of the yeast prion protein Sup35p, *J Am Chem Soc* **2006**, 128, 10840–10846.

[62] Chakrapani S, Cordero-Morales J F, Jogini V, Pan A C, Cortes D M, Roux B, and Perozo E, On the structural basis of modal gating behavior in K(+) channels, *Nat Struct Mol Biol* **2011**, 18, 67–74.

[63] Chakrapani S, Cordero-Morales J F, and Perozo E, A quantitative description of KcsA gating II: single-channel currents, *J*

Gen Physiol **2007**, 130, 479–96.

[64] Hu K N, Debelouchina G T, Smith A A, and Griffin R G, Quantum mechanical theory of dynamic nuclear polarization in solid dielectrics, *J Chem Phys* **2011**, 134, 125105.

[65] Smith A A, Corzilius B, Bryant J A, DeRocher R, Woskov P P, Temkin R J, and Griffin R G, A 140 GHz pulsed EPR/212 MHz NMR spectrometer for DNP studies, *J Magn Reson* **2012**, 223, 170–9.

[66] Zagdoun A, Casano G, Ouari O, Schwarzwälder M, Rossini A J, Aussenac F, Yulikov M, Jeschke G, Copéret C, Lesage A, Tordo P, and Emsley L, Large molecular weight nitroxide biradicals providing efficient dynamic nuclear polarization at temperatures up to 200 K, *J Am Chem Soc* **2013**, 135, 12790–7.

[67] Maly T, Cui D, Griffin R G, and Miller A F, 1H dynamic nuclear polarization based on an endogenous radical, *J Phys Chem B* **2012**, 116, 7055–65.

3

BIOMOLECULAR DNP- SUPPORTED NMR SPECTROSCOPY USING SITE-DIRECTED SPIN LABELING

Submitted manuscript

Elwin A.W. van der Cruijsen[1], Eline J. Koers[1], Raymond E. Hulse[2], Eduardo Perozo[2], Marc Baldus[1]

[1]Bijvoet Center For Biomolecular Research, Utrecht University Padualaan 8, 3584 CH Utrecht, The Netherlands

[2]Department of Biochemistry and Molecular Biology, The University of Chicago, 929 E57th Street, Chicago, Illinois 60637, USA

3.1 INTRODUCTION

Molecular probes that combine the benefits of enhanced spectroscopic sensitivity with site-specific localization have significantly expanded the chemical repertoire to track molecular structure and function in applications ranging from cell biology[1,2] to material science.[3] In the field of magnetic resonance, dynamic polarization (DNP) has been show to greatly enhance spectroscopic sensitivity in solid[4] and solution-state[5] NMR. Usually, such studies involve the addition of soluble paramagnetic compounds to enhance NMR signals via DNP at low temperatures (LTs). In the following, we demonstrate that sizable DNP enhancements can be achieved by directly labeling DNP-active molecular units to the target molecule of interest. Previous efforts in this direction examined endogeneous radicals (flavomonucleotide[6]) or involved attachment of a biradical (TOTAPOL[7]) C-terminally to a decapeptide.[8] Here, we aim at a general route to study (membrane) proteins using localized DNP. For this purpose, we employed site-directed spin labeling using the well-established MTSL (S-(2,2,5,5-tetramethyl-2,5-dihydro-1H-pyrrol-3-yl)methylmethanesulfonothio-ate) approach that provides the basis for structural studies in EPR.[9,10] In NMR, the addition of site-specific spin labels leads to paramagnetic relaxation effects (PREs) and pseudocontact shifts that are known to affect spectral resolution and report on molecular 3D structure.[11]

In our studies, we investigated the membrane-embedded bacterial potassium KcsA, which has been well characterized by EPR[12] and solid-state NMR.[13] Since KcsA is a homotetramer with no natural cysteines, we examined in detail the effect of a single cysteine mutation at two different channel locations. We focused on the mutations V84C and G116C that are well characterized by EPR.[12,14] Residue 84 (figure 3.1) is

part of the turret between the selectivity filter (SF) and the transmembrane-helix 2 (TM2), while G116 is located between the lipid bilayer and the activation gate.

3.2 MATERIALS AND METHODS

Proteolipsomal samples containing uniformly $[^{13}C,^{15}N]$ labelled KcsA G116C and V84C were prepared and tagged with MTSSL and MTS as described before.[12,14] For DNP-based ssNMR experiments, we washed liposomal KcsA samples 2x with 50 µL DNP solution containing 1:2:2 (v/v/v) glycerol-d8, D2O, and H2O. ssNMR (AT at 273 K) and LT-DNP (100 K) experiments were conducted using 3.2 mm triple-resonance $(^{1}H,^{13}C,^{15}N)$ magic-angle-spinning (MAS) probe heads at static magnetic fields of 9.4 to 18.8 T corresponding to proton/electron resonance frequencies between 400 MHz/ 263 GHz, 700 and 800 MHz/ 527 GHz (Bruker BioSpin).

3.3 RESULTS

Using published ssNMR assignments[13,15] we firstly verified by ssNMR experiments at 273 K that paramagnetic tagging at increasing concentrations was site specific (figure3.2 and 3.3). Indeed, NCA spectra recorded for both preparations confirmed PREs (figure 3.1) in a distance range of roughly 8 Å around the mutation site in line with theoretical expectations.[11,16] Note that tagging at position 116 significantly increased spectral resolution since signal contributions of large α-helical transmembrane segments were quenched by PREs (figure 3.3). On the other hand, the same spectrum readily contained signals of the turret region and the inactivation gate that are more distant from the radical site. Interestingly we observed small changes for residues that establish a link to the lipid bilayer and form a coupled network during channel inactivation.[13]

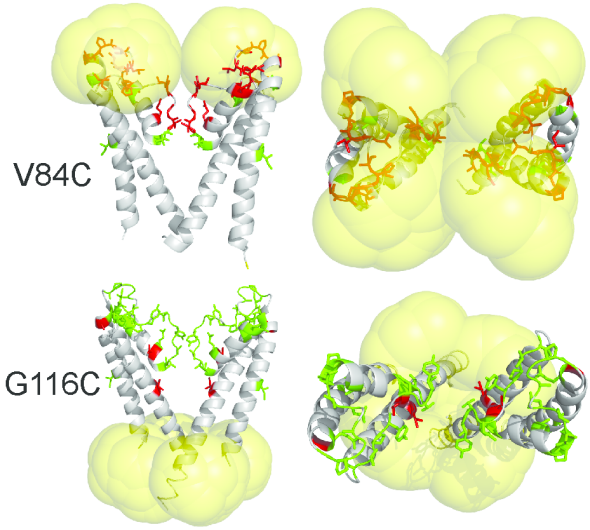

Figure 3.1: a) Rotamers plotted on a dimer structure of KcsA assuming a 2 site and 4 site MTSL labelling (yellow spheres) for V84C (top) and G116C (bottom) in side- and topview. Residues exhibiting no (green) or sizable (red) PREs are indicated.

So far, the highest DNP enhancements have been obtained using the Cross Effect (CE) that depends on the electron-electron dipole coupling strength.[17] Taking into account the tetrameric channel arrangement and known MTSL rotamer properties, we modelled[18,19] the electron-electron distance distribution for both considered positions (figure 3.4). We obtained a broad distribution of inter-electron distances with an average e^- - e^- distance of 25.6 Å (Pos 84) and 20.8 Å (Pos 116) in a closed-conductive model of KcsA. The corresponding distances in DNP biradicals such as TOTAPOL or AMUPol[20] are shorter but well within the overall distribution shown in figure 3.4. To investigate the effect of increasing levels of paramagnetic tagging upon spectral resolution and DNP enhancement, we conducted 2D LT-DNP experiments at 400 MHz and 800 MHz conditions.

We varied the ratio of MTSL and MTS, the diamagnetic N-acetylated spin label analogue of MTSL in the range of 25%,

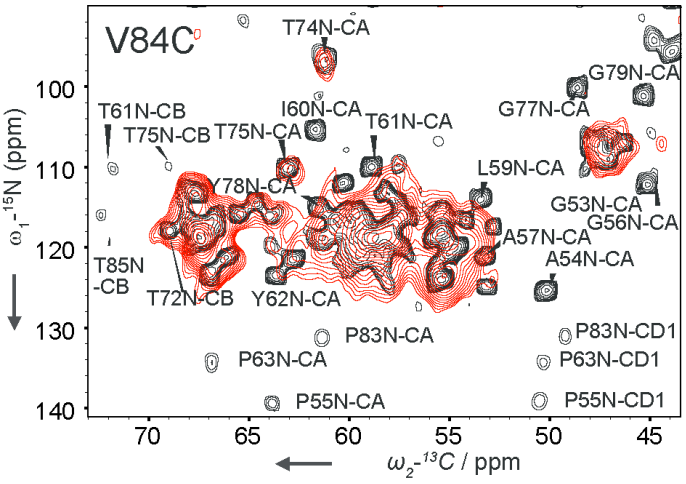

Figure 3.2: Comparison of NCA spectra of WT KcsA (black) with NMR results obtained on paramagnetically labelled V84C in red at 273 K sample temperature.

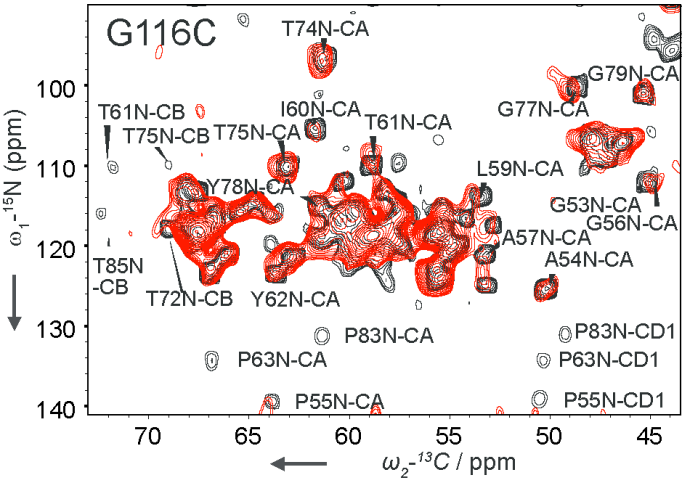

Figure 3.3: Comparison of NCA spectra of WT KcsA (black) with NMR results obtained on paramagnetically labelled G116C in red at 273 K sample temperature.

50%, 75 and 100% and compared our results to the high-temperature data. In both cases, we found good agreement in the overall correlation pattern in NCA experiments (figure 3.5,3.6). As we have investigated (see chapter 2) for soluble biradicals, the signal loss at LT conditions can be explained

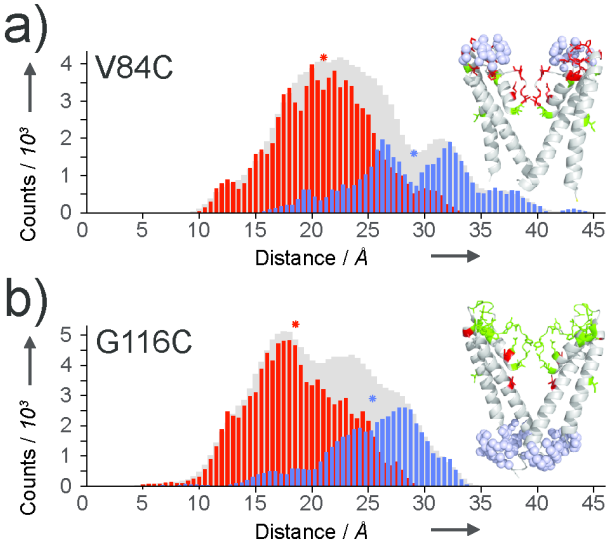

Figure 3.4: Predicted distance distribution between MTSL radical rotamers of KcsA V84C (a) and G116C (b) for adjacent (red) and diagonal (blue) e- positions and the combinations of both grey. Stars depict the average distance. b) 800 MHz LT-DNP 2D NCAs recorded at 100 K show similar patterns as at 273 K.

by the presence of local dynamics (such as in the case of Thr 74) and an overall increase in PREs due to the longer electron T_1 relaxation time. In the case of the V84C mutant, these effects largely quench signals of the turret and SF region and the remaining signals can be explained by the transmembrane α-helical segments (figure 3.5). In contrast, DNP studies on G116C allowed us to identify residues of the selectivity filter (Thr 74, Thr 75, figure 3.6). Interestingly, many turret residues of G116C, e.g., Ala 54 or Gly 56 exhibit broadening at LT conditions which is unlikely to be induced by PREs. Instead, additional ssNMR experiments at higher temperatures (manuscript in preparation) suggest the presence of turret motions that lead to structural disorder and thus signal loss for several turret residues at LT conditions. Nevertheless, changing the position of the tag influences the overall correlation pattern confirming signal modulation by the location of the spin labels.

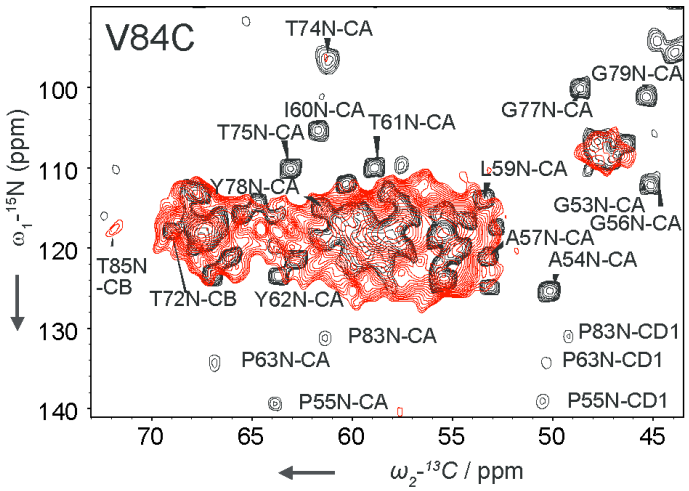

Figure 3.5: 2D NCAs of KcsA V84C recorded at 800 MHz LT-DNP (100 K, red) and of WT KcsA recorded at 700 MHz (273 K, black).

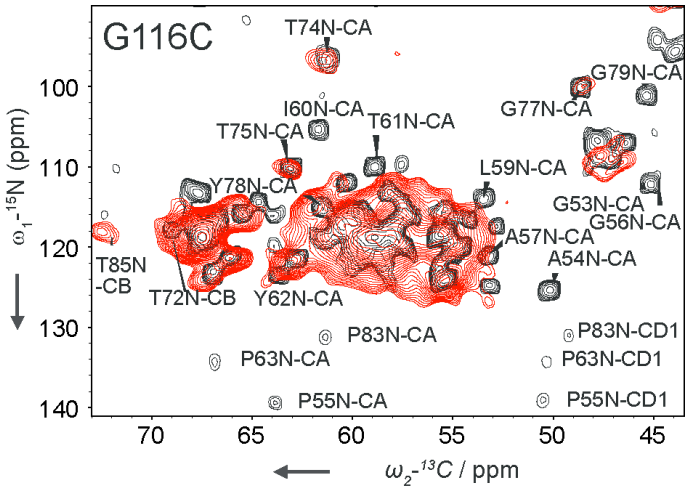

Figure 3.6: 2D NCAs of KcsA G116C recorded at 800 MHz LT-DNP (100 K, red) and of WT KcsA recorded at 700 MHz (273 K, black)

When varying the radical concentration from 25 to 100 % (figure 3.7), we observed a clear correlation between the over-

all signal enhancement and experimental DNP build-up times 1/TDNP. Absolute enhancements shown in figure 3.7 were obtained from set of KcsA samples that were simultaneously solubilized, labeled and reconstituted as described in Ref.[12] Additional experiments suggest that these values may in part be influenced by variations in preparation procedure, for example leading to unspecific binding of MTSL to membranes. In line with our studies using soluble biradicals (chapter 2) we observed a four-fold decrease when comparing DNP enhancements at 400 MHz and 800 MHz.

Based on the shorter average interspin distance of G116C, we expected a higher DNP enhancement for the G116C mutant than the V84C mutant. Indeed, we observed a 2.5 times higher signal enhancements for G116C compared to the same MTSL loading for V84C confirming the presence of CE-DNP. In fact, the DNP enhancements using 100 % tagging at G116C (ε = 14.5 at 400 MHz/ 263 GHz) improve sensitivity by a factor 12 compared to conventional (AT) ssNMR and were higher than seen in preparations using WT KcsA and TOTAPOL in solution.

Assuming 100% labeling efficiency, we estimated a global radical concentration of 19 mM for the 100% MTSL tagged sample. A comparable 10 mM TOTAPOL concentration in solution yielded a DNP enhancement of 13 at 400 MHz for WT KcsA. Minimizing the H2O-content in our proteoliposomal preparations did not reduce the enhancement, indicating the proton-driven spin diffusion via the solvent is not important for the observed polarization enhancement. Also, initial experiments using diluted KcsA samples suggest that the observed enhancements are largely determined by intramolecular electron-electron interactions.

Figure 3.7 suggests that higher DNP enhancements should be possible, for example by deuteration of the target protein.[6] Also, the use of nitroxide radicals with a longer T1e/T2e,[20,21] including AMUPol[20] or the optimization of the radical geometry might further increase the use of DNP by

site-directed spin labeling. On the other hand, DNP enhancements may report on overall structural changes, such as in the case of KcsA, where structural changes related to inactivation can lead to weaker electron-electron dipolar couplings.[12]

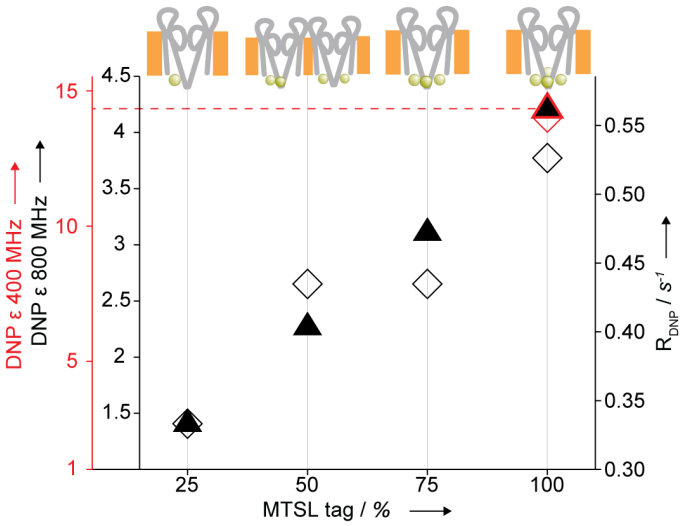

Figure 3.7: DNP enhancements seen in 1D NCA experiments (▲, 800 MHz; ▲ 400 MHz) and the inverse polarization DNP build-up time RDNP (◇ ,800MHz;◇ ,400MHz) at LT for KcsA G116C. Cartoons (top) depict the dominant MTSL labeling arrangements expected for the various amounts of labeling..

3.4 CONCLUSIONS

In summary, we have demonstrated that significant DNP enhancements can be achieved by creating local electron clusters. Unlike local NMR enhancements methods such as photo-CIDNP,[22] these enhancements are visible outside a core shell where PREs are active and can lead to spectral simplification in LT-DNP ssNMR data sets. Outside this shell, we did not observe sizable variations in DNP enhancements. These findings are in excellent agreement with earlier work on complex biomolecules suggesting that DNP enhancements induced by local electron clusters are dictated by spin diffusion processes and can be constant over at least tens of nanometers.[23,24]

NMR studies using DNP by site specific labelling should hence be readily possible for other oligomeric proteins such as regularly observed in the case of membrane proteins or present during the process of folding and aggregation. Future applications could utilize other chemical routes, for example involving unnatural amino acids[25] or the addition of functionalized nanoparticles recently shown in the case of MRI.[26] DNP using chemical tagging may also provide an attractive route in cases where solubility is of critical influence or when a water soluble radical leads to undesirable PREs at the solvent-protein interface.[16] Finally, DNP using spin labeled components offers a means to introduce molecular specificity into DNP studies, for example by placing the DNP agents on specific molecular components such as ligands, lipids or nucleotides. Such strategies may enhance the DNP-based investigation of large biomolecules such as ribosomes[27] or cellular preparations[28] for which the general use of DNP has already been demonstrated.

3.5 REFERENCES

[1] Giepmans B N G, Adams S R, Ellisman M H, and Tsien R Y, The fluorescent toolbox for assessing protein location and function, *Science* **2006**, 312, 217–24.

[2] Reiner A and Isacoff E Y, The Brain Prize 2013: the optogenetics revolution, *Trends Neurosci* **2013**, 36, 557–60.

[3] Buurmans I L C, Ruiz-Martínez J, Knowles W V, van der Beek D, Bergwerff J A, Vogt E T C, and Weckhuysen B M, Catalytic activity in individual cracking catalyst particles imaged throughout different life stages by selective staining, *Nat Chem* **2011**, 3, 862–7.

[4] Griffin R G and Prisner T F, High field dynamic nuclear polarization–the renaissance, *Phys Chem Chem Phys* **2010**, 12, 5737–40.

[5] Ardenkjaer-Larsen J H, Fridlund B, Gram A, Hansson G, Hansson L, Lerche M H, Servin R, Thaning M, and Golman K, Increase in signal-to-noise ratio of > 10,000 times in liquid-state NMR, *Proc Natl Acad Sci U S A* **2003**, 100, 10158–63.

[6] Maly T, Cui D, Griffin R G, and Miller A F, 1H dynamic nuclear polarization based on an endogenous radical, *J Phys Chem B* **2012**, 116, 7055–65.

[7] Song C, Hu K N, Joo C G, Swager T M, and Griffin R G, TOTAPOL: A biradical polarizing agent for dynamic nuclear polarization experiments in aqueous media, *J Am Chem Soc* **2006**, 128, 11385–11390.

[8] Vitzthum V, Borcard F, Jannin S, Morin M, Miéville P, Caporini M a, Sienkiewicz A, Gerber-Lemaire S, and Bodenhausen G, Fractional spin-labeling of polymers for enhancing NMR sensitivity by solvent-free dynamic nuclear polarization, *Chemphyschem* **2011**, 12, 2929–32.

[9] Hubbell W L, Cafiso D S, and Altenbach C, Identifying conformational changes with site-directed spin labeling, *Nat Struct Biol* **2000**, 7, 735–9.

[10] Klare J P and Steinhoff H J, Spin labeling EPR, *Photosynth Res* **2009**, 102, 377–90.

[11] Otting G, Protein NMR using paramagnetic ions, *Annu Rev Biophys* **2010**, 39, 387–405.

[12] Perozo E, Cortes D M, and Cuello L G, Three-dimensional architecture and gating mechanism of a K+ channel studied by EPR spectroscopy, *Nat Struct Biol* **1998**, 5, 459–69.

[13] van der Cruijsen E A W, Nand D, Weingarth M, Prokofyev A, Hornig S, Cukkemane A A, Bonvin A M J J, Becker S, Hulse R E, Perozo E, Pongs O, and Baldus M, Importance of lipid-pore loop interface for potassium channel structure and function, *Proc Natl Acad Sci U S A* **2013**, 110, 13008–13.

[14] Perozo E, Cortes D M, and Cuello L G, Structural rearrangements underlying K+-channel activation gating, *Science* **1999**, 285, 73–8.

[15] Schneider R, Ader C, Lange A, Giller K, Hornig S, Pongs O, Becker S, and Baldus M, Solid-state NMR spectroscopy applied to a chimeric potassium channel in lipid bilayers, *J Am Chem Soc* **2008**, 130, 7427–35.

[16] Koers E J, van der Cruijsen E A W, Rosay M, Weingarth M, Prokofyev, Alexander Sauvée C, Ouari O, Pongs O, Tordo P, Maas W E, and Baldus M, NMR-based structural biology enhanced by dynamic nuclear polarization at high magnetic field, *nd* .

[17] Hu K N, Song C, Yu H H, Swager T M, and Griffin R G, High-frequency dynamic nuclear polarization using biradicals: a multifrequency EPR lineshape analysis, *J Chem Phys* **2008**, 128, 052302.

[18] Polyhach Y, Bordignon E, and Jeschke G, Rotamer libraries of spin labelled cysteines for protein studies, *Phys Chem Chem Phys* **2011**, 13, 2356–66.

[19] Dalmas O, Hyde H C, Hulse R E, and Perozo E, Symmetry-constrained analysis of pulsed double electron-electron resonance (DEER) spectroscopy reveals the dynamic nature of the KcsA activation gate, *J Am Chem Soc* **2012**, 134, 16360–9.

[20] Sauvée C, Rosay M, Casano G, Aussenac F, Weber R T, Ouari O, and Tordo P, Highly Efficient, water-soluble polarizing agents for dynamic nuclear polarization at high frequency, *Angew Chem Int Ed Engl* **2013**.

[21] Zagdoun A, Casano G, Ouari O, Schwarzwälder M, Rossini A J, Aussenac F, Yulikov M, Jeschke G, Copéret C, Lesage A, Tordo P, and Emsley L, Large molecular weight nitroxide biradicals providing efficient dynamic nuclear polarization at temperatures up to 200 K, *J Am Chem Soc* **2013**, 135, 12790–7.

[22] Kaptein R, Dijkstra K, and Nicolay K, Laser photo-CIDNP as a surface probe for proteins in solution, *Nature* **1978**, 274, 293–294.

[23] van der Wel P C A, Hu K N, Lewandowski J, and Griffin R G, Dynamic nuclear polarization of amyloidogenic peptide nanocrystals: GNNQQNY, a core segment of the yeast prion protein Sup35p, *J Am Chem Soc* **2006**, 128, 10840–10846.

[24] Barnes A, Corzilius B, Mak-Jurkauskas M, Andreas L, Bajaj V, Matsuki Y, Belenky M, Lugtenburg J, Sirigiri J, Temkin R, Herzfeld J, and Griffin R, Resolution and polarization distribution in cryogenic DNP/MAS experiments, *Phys Chem Chem Phys* **2010**, 12, 5861–5867.

[25] Fleissner M R, Brustad E M, Kálai T, Altenbach C, Cascio D, Peters F B, Hideg K, Peuker S, Schultz P G, and Hubbell W L, Site-directed spin labeling of a genetically encoded unnatural amino acid, *Proc Natl Acad Sci U S A* **2009**, 106, 21637–42.

[26] Cassidy M C, Chan H R, Ross B D, Bhattacharya P K, and Marcus C M, In vivo magnetic resonance imaging of hyperpolarized silicon particles, *Nat Nanotechnol* **2013**, 8, 363–8.

[27] Gelis I, Vitzthum V, Dhimole N, Caporini M A, Schedlbauer A, Carnevale D, Connell S R, Fucini P, and Bodenhausen G, Solid-state NMR enhanced by dynamic nuclear polarization as a novel tool for ribosome structural biology, *J Biomol NMR* **2013**, 56, 85–93.

[28] Renault M, Pawsey S, Bos M P, Koers E J, Nand D, Tommassen-van Boxtel R, Rosay M, Tommassen J, Maas W E, and Baldus M, Solid-state NMR spectroscopy on cellular preparations enhanced by dynamic nuclear polarization, *Angew Chemie Int Ed* **2012**, 51, 2998–3001.

4

DYNAMIC NUCLEAR POLARIZATION NMR REVEALS MULTIPLE CONFORMATIONS IN LIPID-ANCHORED PEPTIDE VACCINES

Published in Angew Chem Int Ed 2013 52:10905–10908.

Eline J. Koers[1], Maria Pilar López-Deber[2], Markus Weingarth[1], Deepak Nand[1], David T. Hickman[2], Dorin Mlaki Ndao[2], Pedro Reis[2], Anne Granet[2], Andrea Pfeifer[2], Andreas Muhs[2], Marc Baldus[1]

[1]Bijvoet Center For Biomolecular Research, Utrecht University Padualaan 8, 3584 CH Utrecht, The Netherlands

[2]AC Immune SA PSE-B, EPFL CH-1015 Lausanne, Switzerland

4.1 INTRODUCTION

Many pharmacological properties of conventional drugs can be improved using drug delivery systems, composed primarily of polymers or lipids.[1] Liposomes have become versatile delivery systems for induction of antibody and T-lymphocyte responses to associated subunit antigens.[2] The resulting immune response depends on the structural and physicochemical properties of liposomal vaccines. Biophysical methods including circular dichroism (CD) or Attenuated Total Reflectance Infrared spectroscopy (ATR-IR) have been used to investigate liposomal vaccines or other drug delivery systems (see, e.g., Ref.[3]). Solid-state NMR (ssNMR) allows for the atomic study of liposomes or peptides and proteins associated with them.[4,5] However, the requirement of high polypeptide concentrations may not be compatible with the formulation of liposomal vaccines.

We investigated the use of DNP-ssNMR (Dynamic Nuclear Polarization, Ref.[6–11]) to study liposomal vaccines designed to target Alzheimer's disease. Previous work[3,12] has shown that tetrapalmitoylated β-amyloid 1–15 peptide (Palm1–15) embedded into liposomes along with monophosphoryl lipid A (MPLA) can elicit an immune response that restores the cognitive impairment of APP (Amyloid Precursor Protein) transgenic mice. Biophysical and one-dimensional ssNMR experiments on Palm1–15 uniformly labeled with $^{13}C/^{15}N$ at Ala 2, Ser 8, and Gly 9 (Palm1–15 (ASG), figure 4.1) suggested that the peptide adopts an extended backbone conformation that may be influenced by the lipid environment.[3] However, further in-depth structural ssNMR studies were precluded by limited spectroscopic sensitivity.

4.2 MATERIALS AND METHODS

Liposomal Palm1-15 was prepared as described before.[3] For the NMR measurements, 666 µl of the liposomes were spun down (100,000 g, 1 hr) to a volume of approximately 25 µL. The pellet was washed with 50 µL of 5 mM TOTAPOL (DyNuPol, MA) in 2:6:2 glycerol-d8/D2O/H2O. Liposomes were pelleted for 1-3 hrs at 100,000 g, followed by the removal of the supernatant. The washing procedure was repeated twice.

NMR experiments were performed using a 400 MHz/263 GHz DNP system (Bruker Biospin). The sample was cooled to approximately 100 K in a 3.2 mm sapphire rotor spinning at 8 kHz. DNP enhancements were measured by overlaying HC CP/MAS spectra recorded with and without microwave irradiation. (2Q/1Q) experiments were performed using the SPC5 sequence[13] with a 1 ms double-quantum excitation time. CGMD simulations[14] were conducted for each lipid composition using eighteen Palm 1-15 copies over 25 µs.

4.3 RESULTS AND DISCUSSION

For our DNP studies, we treated liposomes containing Palm1-15 with DMPC/DMPG/Cholesterol/MPLA (9:1:7:0.06 molar ratio) (figure 4.1a,c) or DMTAP/Cholesterol/MPLA (10:7:0.06) (figure 4.1b,d) with the polarizing reagent TOTAPOL[15] and glycerol-d8. These preparations exhibited strong signal enhancements in 1D CP and Additional experiments suggested that low concentrations of TOTAPOL provide a good compromise between signal enhancement and paramagnetic relaxation enabling us to conduct two-dimensional (2Q,1Q) experiments (figure 4.2,4.3). Because of the low peptide concentration ((1:200) peptide/lipid ratio), the resulting ssNMR spectra contained signals of ^{13}C–labeled peptide residues as well as correlations originating from natural abundance lipids. Compared to the labeled peptide, lipid signals should be attenu-

ated by at least a factor 10,000, suggesting that the effective lipid to peptide ratio is higher than 500:1 strongly limiting the use of conventional ssNMR methods.[3] We could readily distinguish peptide and lipid signals due to their distinct chemical-shift pattern. For the three labeled residues (Ala 2, Ser 8 and Gly 9) we observed two signal sets for the DMPC/DMPG/Chol sample (figure 4.2).

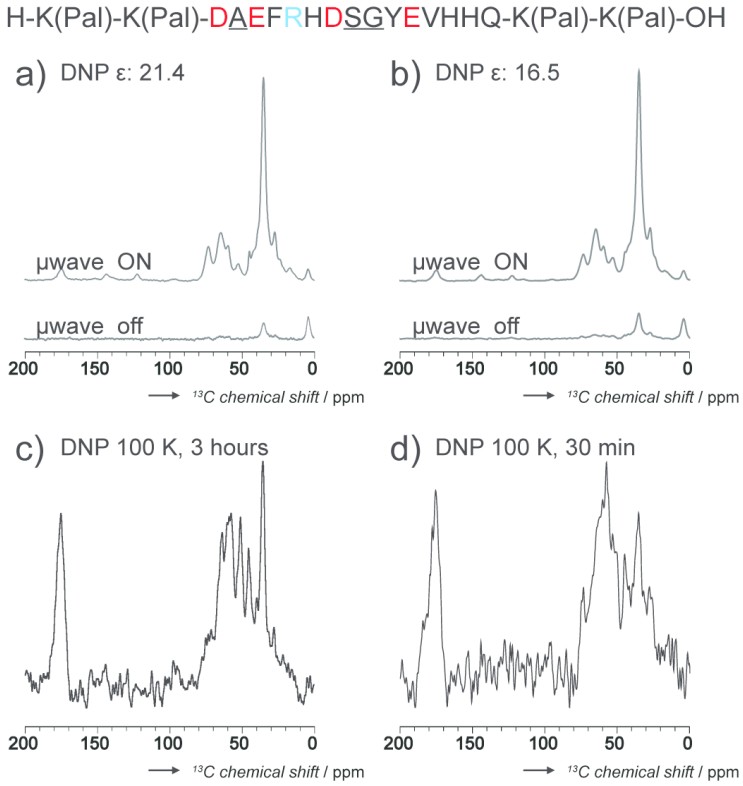

Figure 4.1: Top: Sequence of Palm1-15(ASG) with $^{13}C/^{15}N$ labelled residues underlined and charged residues (at pH 7) coloured. 1D NMR spectra of liposomal Palm1-15 in DMPC/DMPG/Chol (a,c) or DMTAP/Chol (b,d). CP-MAS at 100 K are depicted in a) and b); the 1D 2QF spectra with 1 ms excitation time in c) and d).; All samples were washed in 5 mM TOTAPOL in (2:6:2) glycerol-d8/D_2O/H_2O. Signal enhancements are given relative to the case with microwave irradiation off.

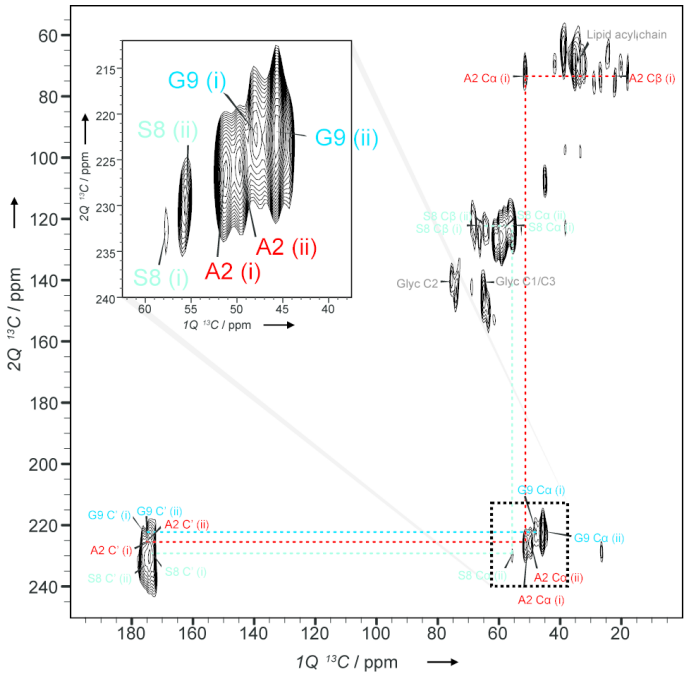

Figure 4.2: 13C (2Q/1Q) 2D experiments on liposomal Palm1-15 (ASG). Liposomes consisted of DMPC/DMPG/Chol.

In the DMTAP/Chol case, four sets of ssNMR correlations could be identified (figure 4.3). As shown before[16], we subsequently computed secondary chemical shifts $\Delta\delta$ that represent established parameters to infer polypeptide conformation in solution and solid-state NMR.[17,18] In figure 4.4a, $\Delta\delta$ were determined for Cα resonances for both lipid compositions. In the DMPC/DMPG/Chol case (figure 4.4a, top graph), the more dominant correlations (denoted by ii) for Ala 2 and Ser 8 are strongly negative. This is consistent with an extended backbone conformation. In this arrangement, $\Delta\delta$ values for Gly 9 residues are close to random coil values[19] in line with the more dominant signals (ii) in figure 4.4a. A second weaker population (i) exhibited secondary chemical shifts close to random coil arrangements. In the case of the cationic DMTAP/Chol (figure 4.4a, bottom graph), we also observed secondary chemical shifts that were compatible with extended

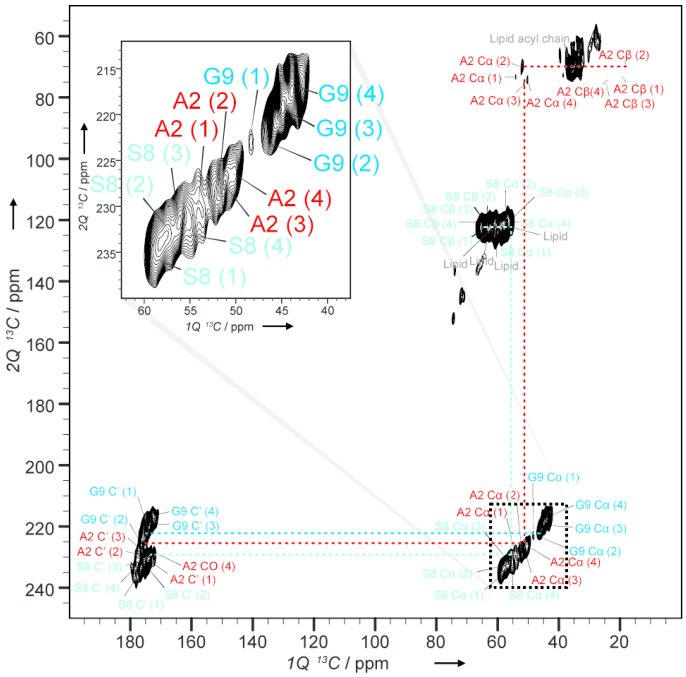

Figure 4.3: 13C (2Q/1Q) 2D experiments on liposomal Palm1-15 (ASG). Liposomes consisted of DMTAP/Chol.

conformations (denoted by species 3 and 4). However, their spectroscopic intensities were comparable to additional signals that exhibited small or even positive $\Delta\delta$ values and are denoted as populations 1 and 2 (figure 4.3 and 4.4a). Note that in the absence of sequential assignments, the numbering of the populations may not correspond to the same peptide unit.

ATR-IR experiments (figure 4.4b) confirmed the presence of additional peptide folds in liposomal Palm1-15. Curve fitting procedures suggest a prominent β-sheet conformation (72% in total) in the case of DMPC/DMPG/Chol (figure 4.4b, red line) in qualitative agreement with 60:40 intensity ratio between populations (ii) and (i) seen in ssNMR. In line with our earlier findings[3], the use of cationic DMTAP/Chol leads to a

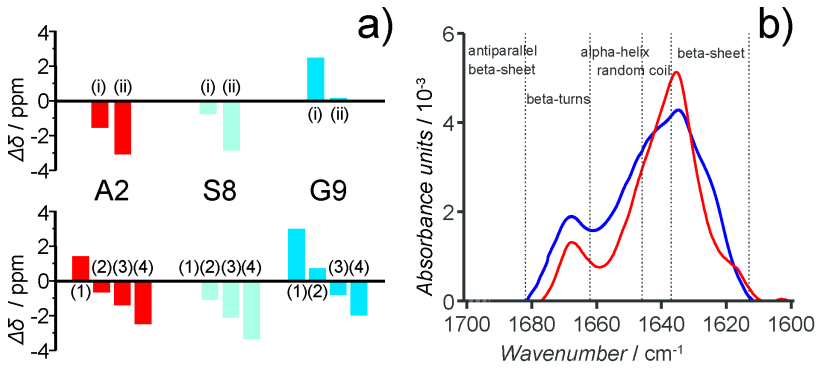

Figure 4.4: NMR difference chemical shifts Δδ=δCα-δCα(rc) for liposomal Palm1-15 vaccine in DMPC/DMPG/Chol (a, top) and in DMTAP/Chol (a, bottom) derived from 2Q1Q experiments; b) ATR-IR amide I band of liposomal Palm1-15 spectra in anionic liposomes (DMPCG/DMPGC/cholChol, red) and cationic liposomes (DMTAP/Chol, blue).

significant reduction of β-sheet conformation and an increase in conformations with other peptide folds (blue line, figure 4.4b).

For further investigation, we resorted to mesoscopic coarse-grained molecular dynamics (CGMD) simulations. Peptides in the aqueous phase partitioned at the membrane surface within less than a microsecond. Here, extended peptide conformations formed in line with our ssNMR data obtained on the free peptide that suggest the β-strand formation is more pronounced at the membrane compared to the free case. We observed spontaneous aggregation of peptides into β-sheet-like aggregates in both lipid mixtures. Further analysis of the surface-bound peptides revealed significantly broader density profiles of the peptide backbone in DMTAP/Chol in comparison to DMPC/DMPG/Chol (figure 4.5a,b).

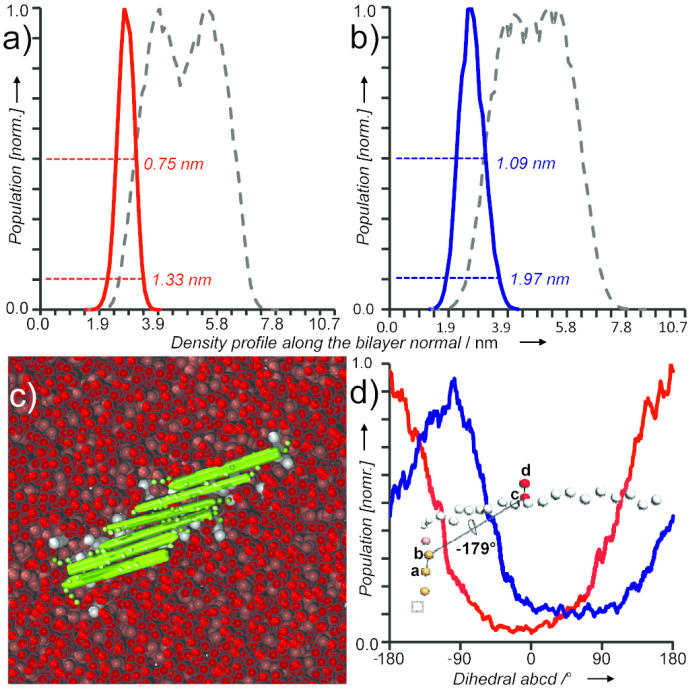

Figure 4.5: Density profile of the peptide backbone in a) a 9:1:7 DMPC/DMPG/Chol and b) a 10:7 DMTAP/cholesterol mixture. Continuous and dashed lines stand for peptide and membrane profiles, respectively. c) Example of an ordered hexameric β-sheet of Palm 1-15 in DMPC/DMPG/Chol after 25 μs of simulation. DMPC/DMPG lipids and cholesterol are colored in light and dark red, respectively. Palmitoyl anchors and peptide backbones are given as gray and green beads, respectively. d) While negatively charged side chains such as Asp 7 predominately orient along the bilayer normal in DMPC/DMPG/Chol (red), side chains in DMTAP/Chol orient almost parallel to the surface (blue). Dihedral angles were averaged over all peptides and 25 μs of simulation.

In DMPC/DMPG/Chol, peptide backbones can approach each other with limited steric or electrostatic hindrance (figure 4.5c), because negatively charged side chains predominately orient orthogonal to the membrane surface (figure 4.5d). In cationic DMTAP lipids, anionic side chains orient almost parallel to the bilayer surface, suggesting that membrane charge modulates peptide aggregation behaviour.[3] Note that another modulator of peptide aggregation may be the reduced thickness and head group size of DMTAP lipids, which led to

a slight positive curvature of the peptide-containing leaflet in the simulations.

4.4 CONCLUSION

Taken together our results show that DNP-enhanced bio-ssNMR provides a powerful method to structurally study surface-associated biomolecules at low molecular concentrations. In the case of Palm1-15, our studies indicate that the active vaccine contains antigen moieties for which β-strands are, at least in part, triggered by peptide-peptide interactions that subsequently associate from dimers to larger oligomers to the membrane. Our work suggests that larger β-sheets only form in the DMPC/DMPG/Chol case and that additional conformations which are particularly relevant for the DMTAP case may reduce in vivo target specificity. These findings open the way for rational structure-based design of liposome-bound peptide immunogens with defined conformations to generate optimized vaccines against a range of protein misfolding diseases. Future studies may involve cellular settings in which DNP-ssNMR studies have been demonstrated.[20,21] Moreover, DNP-supported ssNMR studies may help to elucidate the role of lipid surfaces for protein aggregation, toxicity and pore formation in general or the aid the study of Amyloid folding intermediates.

4.5 References

[1] Allen T and Cullis P, Drug delivery systems: entering the mainstream, *Science* **2004**, 303, 1818–1822.

[2] Watson D S, Endsley A N, and Huang L, Design considerations for liposomal vaccines: influence of formulation parameters on antibody and cell-mediated immune responses to liposome associated antigens, *Vaccine* **2012**, 30, 2256–72.

[3] Hickman D T, López-Deber M P, Ndao D M, Silva A B, Nand D, Pihlgren M, Giriens V, Madani R, St-Pierre A, Karastaneva H, Nagel-Steger L, Willbold D, Riesner D, Nicolau C, Baldus M, Pfeifer A, and Muhs A, Sequence-independent control of peptide conformation in liposomal vaccines for targeting protein misfolding diseases, *J Biol Chem* **2011**, 286, 13966–13976.

[4] Ader C, Schneider R, Seidel K, Etzkorn M, and Baldus M, Magic-angle-spinning NMR spectroscopy applied to small molecules and peptides in lipid bilayers, *Biochem Soc Trans* **2007**, 35, 991–5.

[5] Bechinger B and Salnikov E S, The membrane interactions of antimicrobial peptides revealed by solid-state NMR spectroscopy, *Chem Phys Lipids* **2012**, 165, 282–301.

[6] Griffin R G, Clear signals from surfaces, *Nature* **2012**, 468, 381–382.

[7] Bajaj V S, Mak-Jurkauskas M L, Belenky M, Herzfeld J, and Griffin R G, Functional and shunt states of bacteriorhodopsin resolved by 250 GHz dynamic nuclear polarization-enhanced solid-state NMR, *Proc Natl Acad Sci U S A* **2009**, 106, 9244–9249.

[8] Lesage A, Lelli M, Gajan D, Caporini M a, Vitzthum V, Miéville P, Alauzun J, Roussey A, Thieuleux C, Mehdi A, Bodenhausen G, Copéret C, and Emsley L, Surface enhanced NMR spectroscopy by dynamic nuclear polarization, *J Am Chem Soc* **2010**, 132, 15459–61.

[9] Linden A H, Franks W T, Akbey U, Lange S, van Rossum B J, and Oschkinat H, Cryogenic temperature effects and resolution upon slow cooling of protein preparations in solid state NMR, *J Biomol NMR* **2011**, 51, 283–92.

[10] Reggie L, Lopez J J, Collinson I, Glaubitz C, and Lorch M, Dynamic nuclear polarization-enhanced solid-state NMR of a 13C-labeled signal peptide bound to lipid-reconstituted Sec translo-

con, *J Am Chem Soc* **2011**, 133, 19084–6.

[11] Salnikov E, Rosay M, Pawsey S, Ouari O, Tordo P, and Bechinger B, Solid-state NMR spectroscopy of oriented membrane polypeptides at 100 K with signal enhancement by dynamic nuclear polarization, *J Am Chem Soc* **2010**, 132, 5940–5941.

[12] Muhs A, Hickman D T, Pihlgren M, Chuard N, Giriens V, Meerschman C, van der Auwera I, van Leuven F, Sugawara M, Weingertner M C, Bechinger B, Greferath R, Kolonko N, Nagel-Steger L, Riesner D, Brady R O, Pfeifer A, and Nicolau C, Liposomal vaccines with conformation-specific amyloid peptide antigens define immune response and efficacy in APP transgenic mice, *Proc Natl Acad Sci U S A* **2007**, 104, 9810–5.

[13] Hohwy M, Rienstra C M, Jaroniec C P, and Griffin R G, Fivefold symmetric homonuclear dipolar recoupling in rotating solids: Application to double quantum spectroscopy, *J Chem Phys* **1999**, 110, 7983–7992.

[14] Marrink S J, Risselada H J, Yefimov S, Tieleman D P, and de Vries A H, The MARTINI force field: coarse grained model for biomolecular simulations, *J Phys Chem B* **2007**, 111, 7812–24.

[15] Song C, Hu K N, Joo C G, Swager T M, and Griffin R G, TOTAPOL: A biradical polarizing agent for dynamic nuclear polarization experiments in aqueous media, *J Am Chem Soc* **2006**, 128, 11385–11390.

[16] Luca S, White J F, Sohal A K, Filippov D V, van Boom J H, Grisshammer R, and Baldus M, The conformation of neurotensin bound to its G protein-coupled receptor, *Proc Natl Acad Sci U S A* **2003**, 100, 10706–11.

[17] Wishart D S and Sykes B D, The 13C chemical-shift index: a simple method for the identification of protein secondary structure using 13C chemical-shift data., *J Biomol NMR* **1994**, 4, 171–80.

[18] Luca S, Filippov D V, van Boom J H, Oschkinat H, de Groot H J, and Baldus M, Secondary chemical shifts in immobilized peptides and proteins: a qualitative basis for structure refinement under magic angle spinning, *J Biomol NMR* **2001**, 20, 325–31.

[19] Wang Y and Jardetzky O, Probability-based protein secondary structure identification using combined NMR chemical-shift data, *Protein Sci* **2002**, 11, 852–861.

[20] Renault M, Tommassen-van Boxtel R, Bos M P, Post J A, Tommassen J, and Baldus M, Cellular solid-state nuclear magnetic

resonance spectroscopy, *Proc Natl Acad Sci U S A* **2012**, 109, 4863–8.

[21] Renault M, Pawsey S, Bos M P, Koers E J, Nand D, Tommassen-van Boxtel R, Rosay M, Tommassen J, Maas W E, and Baldus M, Solid-state NMR spectroscopy on cellular preparations enhanced by dynamic nuclear polarization, *Angew Chemie Int Ed* **2012**, 51, 2998–3001.

5

DYNAMIC NUCLEAR POLARIZATION STUDIES OF DIATOM BIOSILICA

Manuscript in preparation

Anne Jantschke[1], Eline J Koers[2], Eike Brunner[1], Marc Baldus[2]

[1]Bioanalytical Chemistry, TU Dresden Bergstraße 66, 01069 Dresden , Germany

[2]Bijvoet Center For Biomolecular Research, Utrecht University Padualaan 8, 3584 CH Utrecht, The Netherlands

5.1 INTRODUCTION

Biosilica formed by diatoms is a particularly interesting silica/organic hybrid material. The cell walls of these unicellular algae consist of amorphous biosilica with a species-specific micro- and nano-patterning and contain a certain amount of organic molecules (typically 1 – 15 wt. %). Some of these biomolecules are assumed to be involved in the structure formation process. Extended research interest is therefore focused on the isolation and analysis of biosilica-associated or embedded biomolecules. Long-chain polyamines (LCPAs),[1,2] special peptide classes such as the silaffins,[3,4] the silacidins,[5] and cingulins[6] have been identified. Polysaccharides were also observed and may take part in valve formation of several diatom species.[7–11]

Solid-state NMR (ssNMR) spectroscopy is a well-established and powerful method for the characterization of various types of materials as well as complex biomolecules. It is also increasingly used to understand the structure of organic/ inorganic hybrid materials such as biominerals.[12,13] Special interest is devoted to the characterization of surface functionalities and the organic/ inorganic interfaces. The small concentration of surface/ interface species in combination with the low natural abundance of NMR active nuclei, strongly limit the achievable spectroscopic signal per unit time. Multidimensional ssNMR experiments are hence impractical and call for the use of DNP, that, as described in the previous chapters, strongly enhances the sensitivity of ssNMR spectroscopy. During the past decade, this technique has developed into an increasingly used method with applications in high-magnetic fields.[14,15] The combination of ssNMR with DNP offers the possibility to selectively enhance the surface species in hybrid materials like functionalized silica[16,17] or alumina.[18] The materials are wetted in a

suitable solvent containing a DNP polarizing agent such as TOTAPOL[19] by incipient wetness impregnation. The resulting sample allows for polarization transfer from the highly polarized electron spins to nearby ^{1}H nuclei of the solvent and, subsequently, via CP-MAS to ^{13}C, ^{15}N or ^{29}Si nuclei of the organic functional groups at the surface.[16–18,20]

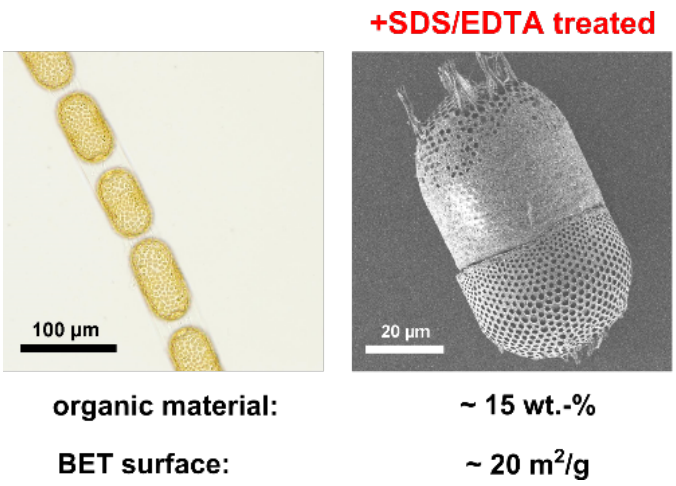

Figure 5.1: Biosilica as silica/ organic hybrid material. Left panel: bright field microscopic image of Stephanopyxis turris (living cell). Right panel: SEM image of biosilica of *S. turris* treated with SDS/EDTA.

In this chapter, we propose a model for the location of biomolecules associated with diatom biosilica based on the application of dynamic nuclear polarization (DNP).

5.2 MATERIALS AND METHODS

Diatom cultivation, harvesting and isolation of biosilica

Stephanopyxis turris has been isolated from the North Sea in June 2004. Cultivation was performed in a 20 L polycarbonate vessel (Nalgene) with artificial seawater (ASW) medium prepared according to the protocol of the North East Pacific Culture Collection.[21] After adding 50 mL of a pre-culture to 20 L

of sterile filtered (0.2 lm, Kleenpak) ASW medium, growing *S. turris* takes about 3 to 4 weeks. A RUMED 1301 light thermostat (18 °C, 12 h/12 h day/night cycle, ca. 1000 lux) was used to provide constant growing conditions. We determined the silicic acid concentration of the medium via the molybdenum blue method[22–24] to control the growing state. In the end stadium (concentration of silicic acid < 20 µM) the rising pH was adjusted to 8.0–8.2 with 2.5 M HCl. As soon as the silicic acid concentration reached zero values, the cells were harvested by consecutive filtration of the culture medium with a 11 µm nylon mesh (Stockhausen Sieb- und Filtererzeugnisse) and subsequent centrifugation (1000 RCF). The resulting pellets were frozen with liquid nitrogen and stored at -20 °C.

For ^{13}C, and ^{15}N-labeling the protocol was modified by using either $NaH^{13}CO_3$ (Chemotrade Leipzig, 99 atom-% 13C) or $Na^{15}NO_3$ (Campro Scientific Berlin, 98 atom-% 15N). For ^{29}Si-labeling the protocol was adapted by using $Na_2{}^{29}SiO_3$ which was synthesized from isotope labelled SiO_2 and Na_2CO_3 in a solid state reaction.[25]

Subsequently, we performed the cell wall extraction following the protocol described by Kröger *et al.*[26] based on treatment with a buffer containing EDTA (0.1 M) and SDS (2 %) at pH 8 in order to remove physically bound organic material from the cell walls. Typically, cells were suspended in 20 mL buffer solution and heated to 95 °C for 10 minutes. This treatment was repeated three times. Finally, the biosilica was washed at least three times with Milli-Q water. In all steps the biosilica was separated from the supernatants via centrifugation (Heraeus biofuge primo, swinging bucket rotor, 1000 RCF). After extraction, the samples were freeze dried.

NMR Sample Preparation via incipient wetness

3.2 mm sapphire rotors were filled with biosilica (ca. 10 mg of wet material), wetted just prior to loading the rotor in the NMR spectrometer. Wetting of the biosilica was carried out

using the method of incipient wetness impregnation with the radical solution at room temperature. The radical stock solution was prepared by dissolving TOTAPOL or AMUPol in D_2O/H_2O 90:10 resulting in a concentration of 10 mM. The solution was stored at -20°C. About 8-9 mg of biosilica was wetted with 33 µl liquid containing the biradical solution and an additional D_2O/H_2O mixture (90:10) giving final concentrations of 10 µM and 25 µM TOTAPOL. The sample was then immediately transferred to the NMR probe which was cooled to 100 K.

DNP measurements

DNP experiments were conducted using a triple-resonance (^1H,^{13}C,^{15}N) magic-angle-spinning (MAS) probe head at a static magnetic field of 9.4 T corresponding to proton/electron resonance frequencies of 400 MHz/ 263 GHz (Bruker BioSpin)[15]. Data were recorded at 100 K employing a MAS rate of 8 kHz. Pulse schemes reflected standard homonuclear proton-driven spin diffusion (PDSD) and double-quantum filtered (^{13}C,^{13}C) using SPC5 recoupling[27]. NC correlation experiments typically utilized SPECIFIC-CP transfer.[28]

5.3 RESULTS

After extraction from the cells, biosilica (figure 5.1) consists of bulk amorphous silica and the aforementioned strongly silica-associated biomolecules. These molecules are either deeply embedded in the silica or tightly attached to the surface of the siliceous cell walls. DNP ssNMR offers the possibility to selectively enhance organic material located near the surface. In order to accomplish this goal, we have cultivated the diatom species Stephanopyxis turris with triple-labelling (^{13}C, ^{15}N and ^{29}Si). The isotope-labelled diatom biosilica was extracted by treatment with SDS/EDTA[26] (about 15 wt.-% of the organic material is left).[12] 1D experiments (direct exci-

tation and CP-MAS) for ^{13}C, ^{15}N and ^{29}Si were performed to monitor the presence of organic material and determine the DNP enhancement factors (table 5.1). The $^{1}H - ^{13}C$ CP-MAS ssNMR spectrum of *S. turris* biosilica (see figure 5.2a) represents a superposition of signals stemming from different organic macromolecules (peptides, polyamines and polysaccharides).[10,12] Compared to the CP data, the ^{13}C spectrum after direct excitation (figure 5.2b) contains prominent signals around 76 (C2-C6) and 101 ppm (C1 position) indicating the dominant influence of polysaccharides. Deviations between the ssNMR spectra obtained using CP or direct excitation schemes are also detected in the case of ^{15}N nuclei. The $^{1}H - ^{15}N$ CP-MAS ssNMR spectrum (figure 5.2c) shows two signal regions corresponding to frequencies typically observed of peptide backbone nitrogens (120 ppm) and expected for long-chain polyamines as well as lysine-side chains around 45 ppm. Note that in the directly excited ^{15}N spectrum (figure 5.2d), NMR signals stemming from peptide backbone amides are dominant.

Table 5.1: Enhancement factors (ε) for biosilica extracted with SDS/EDTA from direct excitation($\pi/2$) and cross polarization (CP-MAS, via ^{1}H) experiments

	($\pi/2$)	CP-MAS	species	δ (ppm)
^{13}C	7.5	4.4	C=O	178
	6-8	-	C=C	132
	1-2	-	C_1sugars	103
	2.5	3.5	CO/CN	75
	8	-	CO-CN	54
	14-15	-	alkyl	32
^{15}N	20	7	peptide	120
	-	2-3	amine	45
^{29}Si	2	1.6	Q^3/Q^4	-100/-110

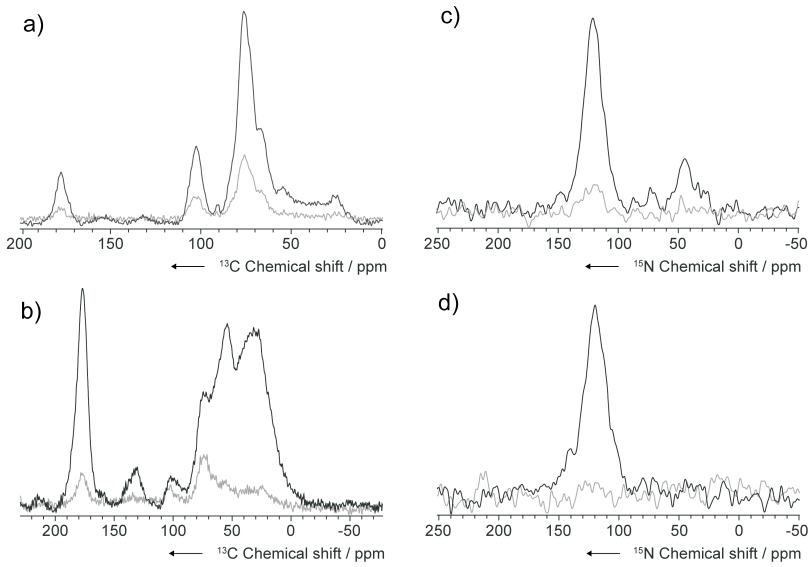

Figure 5.2: LT (low temperature) spectra of *S. turris* biosilica with 10 mM TOTAPOL measured at 400 MHz with microwaves (black) or without (grey). a) $^{1}H-^{13}C$ CP-MAS, ε = 3.5-4.4. b) ^{13}C direct excitation, ε = 1-15. c) $^{1}H-^{15}N$ CP-MAS, ε = 2-7 d)^{15}N direct excitation, ε = 20.

In general, we observed that DNP enhancement factors for ^{13}C and ^{15}N located at the organic material are 2 to 10 times larger than for ^{29}Si (see Table 5.1). Remarkably, a selective enhancement for individual signals can be observed in both direct excitation spectra (figure 5.2b,d). In particular, NMR signals stemming from peptide backbones or sidechains are most strongly enhanced by DNP both in the ^{13}C and the ^{15}N spectra.

To obtain more enhancement for the application of 2D ssNMR spectroscopy, a second (^{13}C, ^{15}N , ^{29}Si) labeled biosilica sample was prepared for measurements using 10 mM AMUPol[29] as a radical. 1D experiments (direct excitation and CP-MAS) were performed to monitor the new DNP enhancement factors. These measurements showed similar variations between the different species and overall higher enhancements (factor ~4) compared to the results previously obtained for biosilica wetted with TOTAPOL.

Subsections of a $^{15}N - ^{13}C$ correlation spectrum obtained with this preparation are shown in figure 5.3. Strong amine signals can be found in the 30-50 ppm region (figure 5.3a). The chemical shifts coincide with a structure proposed by Sumper *et al.*[2] which includes an alkyl (^{13}C, 24 ppm) and a primary amine with a distinct ^{15}N chemical shift (33 ppm) from the other (tertiary) amines (~45 ppm).

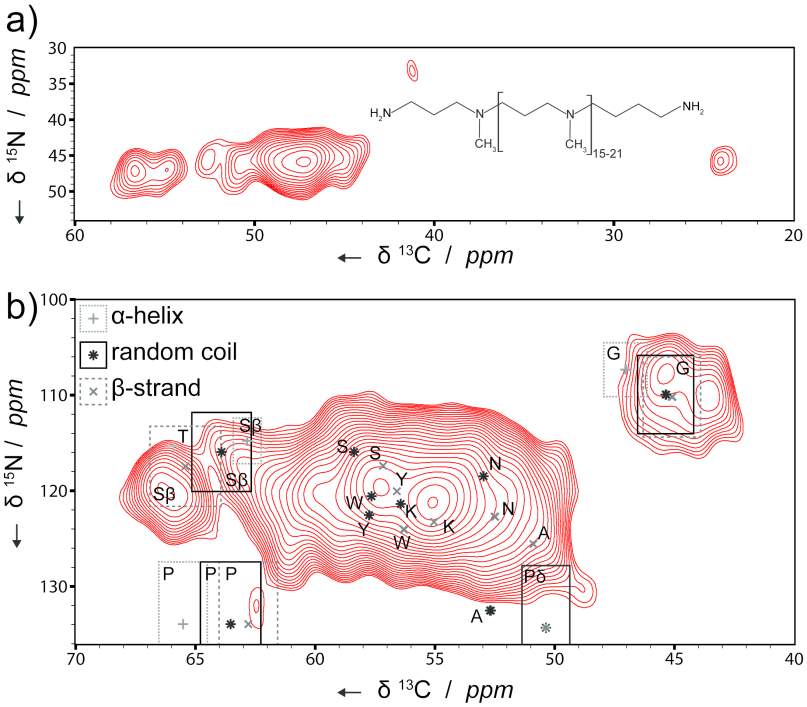

Figure 5.3: 2D ^{13}C-^{15}N correlation experiment using AMUPol measured at 400 MHz DNP LT conditions. a) Polyamine region with the polyamine structure found by Sumper et al.[2] b) Peptide region with chemical shift predictions[30] for different secondary structures. Boxes indicate the standard deviation of the predictions.

In the peptide backbone (N-CA) region of the $^{15}N - ^{13}C$ correlation spectrum (figure 5.3b), various signals are detected. Silaffins[3,4,31,32] represent in most diatoms the main fraction of peptides associated with diatom biosilica. All silaffins are rich in serine and lysine and are highly post-translationally modified. Sequencing analysis of cingulins[6] showed silaffin-

like regions (KXXK domains, X = S or G) which alternate with tryptophan- and/or tyrosine-rich segments. A variety of different and intense ^{13}C signals overlap in the region of 50-62 ppm and can be assigned to serine, lysine as well as a variety of other amino acids. Individual and characteristic signals can be observed for the Cα of proline (62 ppm), arginine (43 ppm – 85 ppm (^{15}N), not shown) and glycine (43.5 and 45 ppm). To gain further information we overlayed chemical shift predictions for different secondary structures. The most intense signals can be well explained using a KSWYGNA sequence. This is in good agreement with sequencing results obtained for all silaffins studied so far.[6] Additionally, signals stemming from serine Cβ (66 ppm) and proline Cα (62 ppm) in the $^{15}N -^{13} C$ correlation spectrum are consistent with the presence of β-strand conformations. In line with this notion, two signals are present in the glycine region corresponding to β-sheet/random coil folds (45 ppm) and polypeptide segments in pronounced β-strand extended conformations (43.5 ppm). Notably, the spectral resolution of the NCA experiment is still limiting and preliminary ^{15}N-edited (^{13}C,$^{13} C$) 2D experiments have been conducted to alleviate these problems. We note that the ^{13}C correlations around 66pm could also be explained by α-helical Thr Cα correlations, albeit with less agreement to the experimentally observed ^{15}N chemical shifts.

Nevertheless, we can already conclude that peptides, when associated with the biosilica, adopt, on the level of secondary structure, mostly random coil and β-strand folds. This observation is in line with in vitro experiments using recombinant silaffin proteins, rSilC, at liquid–solid and air–solid interfaces. These polypeptides showed a partial transition from random coil into β-sheet state upon removal of water.[33,34] Clearly, additional DNP experiments should be conducted to further refine the structural properties of the polypeptides species present in our samples. To this end, preliminary 2D experiments were conducted using the 800 MHz DNP setup which suggest that spectral resolution may be favourable at higher

magnetic field, albeit at lower overall DNP enhancements (see chapter 2).

In conclusion, the results presented above for the first time provide in-situ insight into the secondary structure elements of the peptides associated with the intact biosilica.

Interestingly, we observed weaker direct ^{13}C and ^{15}N DNP enhancements (see table 5.1) for polysaccharides (^{13}C shifts around 103 ppm) and polyamines (^{15}N shifts around 45 ppm). In principle two reasons can be considered for this lower enhancement: Firstly, the molecules may be located inside the diffusion barrier (see chapter 1) and their signal is therefore quenched by paramagnetic effects due to nearby DNP biradicals. The size of this diffusion barrier has been estimated to be in the range of 3-17 Å.[35–40] Secondly, nuclear (^{1}H or ^{15}N) spin diffusion is inefficient to transfer polarization to these molecules from the DNP agents, i.e., they are embedded deep within the silica matrix. Indeed, long-chain polyamines are known to mediate the silica precipitation in diatoms and are therefore supposed to be in close association with the amorphous silica material.[1,2,41,42] Their precise location is unknown. Remarkably, the signal corresponding to polyamines cannot be observed in the directly excited ^{15}N spectra without and with DNP (figure 5.2d). The polyamine signal is hardly seen even in the $^{1}H - ^{15}N$ CP-MAS spectrum measured without DNP (figure 5.2c, grey). This suggests the polyamines represent a minor fraction of the organic material associated with the biosilica. We speculate that the polyamines occupy a location shielded from the radicals, far enough to not be directly polarized, but connected to the surface through a hydrogen dipolar coupled network delivering polarization from this surface. Polyamines are thus relatively close to the surface and not surrounded by silica only. Although the enhancement is lower than the one measured on the proteins, the relative intensity gain with DNP is higher for the polyamines. This can be explained by quenching of the protein signal by paramagnetic relaxation due to its closer proximity to the radicals.

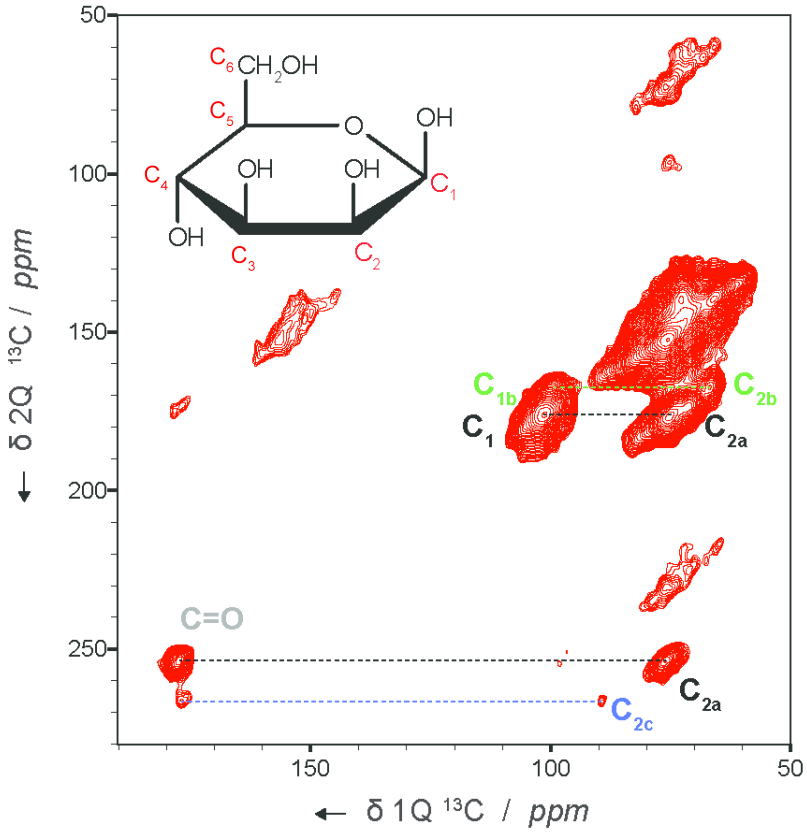

Figure 5.4: 2Q1Q spectrum of *S. turris* biosilica with TOTAPOL measured at 400 MHz DNP LT conditions using 2.5 ms excitation-reconversion time.

In diatoms, saccharides mainly occur in the form of extracellular polymeric substances (EPS)[7,9–11,43,44] which are removed by treatment with SDS/EDTA.[26] The remaining saccharides are strongly associated with the biosilica surface or could be attached to silica-bound peptides. It has been shown that TOTAPOL has an affinity for saccharides like glucose.[45] For these reasons we assume that the polysaccharides could be quenched by the radicals when located at the surface.

In addition to ^{15}N,^{13}C correlation experiments, we performed (^{13}C,^{13}C) double quantum – single quantum - exper-

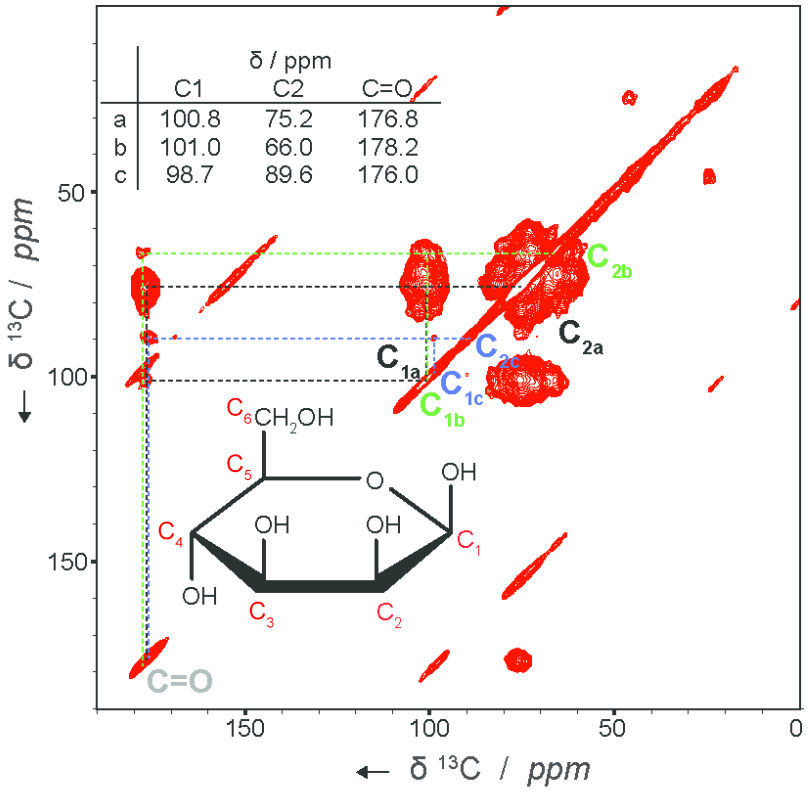

Figure 5.5: 1D PDSD spectrum of *S. turris* biosilica with AMUPol measured at 400 MHz DNP LT conditions using 20 ms mixing.

iments (2Q,1Q data shown in figure 5.4) and proton-driven spin diffusion experiments (PDSD, depicted in figure 5.5) to obtain $^{13}C-^{13}C$ correlations. These $^{1}H-^{13}C$ CP-based spectra are dominated by signals stemming from polysaccharides. In (2Q,1Q) data and PDSD experiments at short mixing times (20 ms), correlations between C1 and C2 and the carbonyl position of three different species a-c were observed. Note, that these three different correlations may represent the most abundant and, at the same time, resolved correlations among a variety of different sugars in these biological environments.[11]

This leads us to the conclusion that the carbonyls are located close to the saccharide rings. GC-MS analysis[11] of the hy-

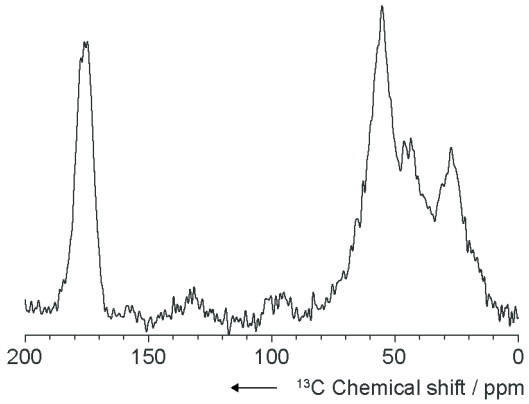

Figure 5.6: 1D NCC spectrum of *S. turris* biosilica with AMUPol measured at 400 MHz DNP LT conditions using 30 ms z-mixing.

drolysed polysaccharides of SDS/EDTA treated biosilica of *S. turris* revealed mannose and mannose-6-phosphate as a main fraction and glucosamine and glucuronic acid as carbonyl bearing. Taking these results into account, the 2D DNP data indicate the presence of either an enrichment in glucuronic acid or N-acetylglucosamine. The absence of a methyl-carbonyl correlation in the PDSD and 2Q1Q spectrum suggests that N-acetylglucosamine is not the main saccharide component.

In principle, the carbonyl bearing compound could be linked via the C1 oxygen atom or via nitrogen to an amino acid side-chain of a peptide. To study this, we compared data from the 2D $^{15}N-^{13}C$ correlation experiment (figure 5.3) with a 1D ^{15}N edited ^{13}C experiment in which after the N-C transfer a proton-driven mixing of 30 ms was used (figure 5.6). For N-linked sugars, a signal corresponding to the C1 position should occur in the $^{15}N-^{13}C$ correlation spectrum and a signal corresponding to the C2 position in the 1D NCC. Since there are no correlations with the C1/C2 position of the polysaccharides, we can conclude that N-linked sugars are not present at high concentration. Furthermore, a significant amount of N-acetylglucosamine can be excluded as well. Therefore, we can conclude that the main carbonyl bearing component is an oxygen-linked glucuronic acid. The data do

not reveal whether the glucuronic acid is linked to a peptide or a polysaccharide like mannan, which was suggested previously.[7,9–11,43,44]

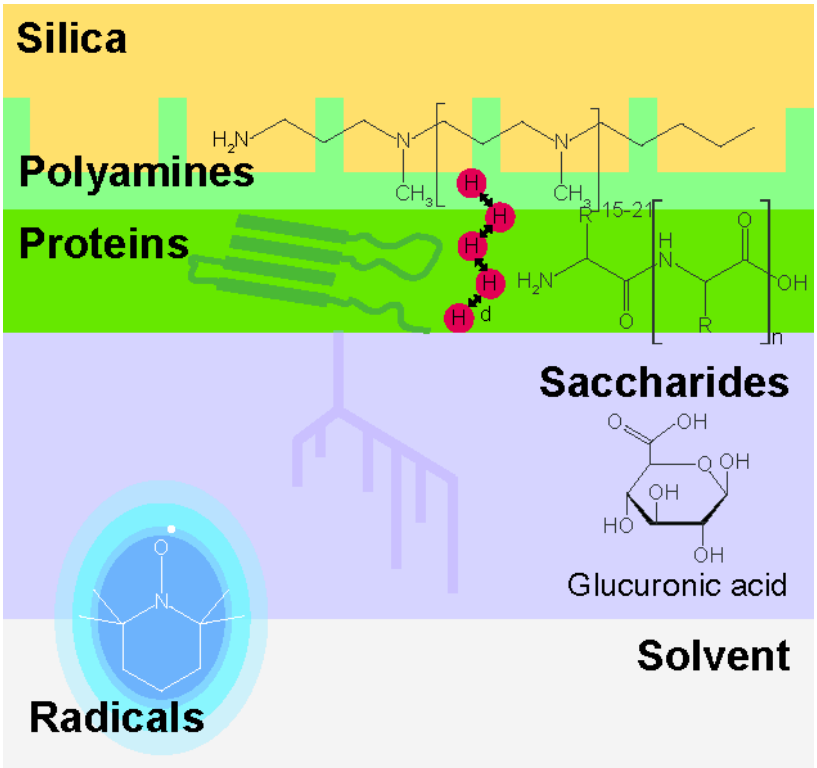

Figure 5.7: Proposed model regarding the location of organic material of *S. turris* biosilica. The polyamines, a small fraction of the nitrogenous compounds present, are protected from paramagnetic quenching due to protrusion into the silica or because of the presence of the protein layer. Protonated peptide groups also establish a dipolar network that supports polarization transfer via DNP transfer to polyamines. Saccharides are either linked to the proteins or other saccharides and are the predominant carbonaceous compound in the biosilica. The saccharides show cross peaks with carbonyl groups. Biradicals are either located in solvent or situated close to the surface in a saccharide environment (violet).

5.4 CONCLUSIONS

In summary, we have demonstrated the application of DNP ssNMR to investigate diatom biosilica. Enhancement factors

could be measured for various nuclei in direct excitation and CP-MAS. Peptide signals were strongly enhanced whereas polysaccharides and polyamines exhibit weaker DNP enhancements. Most likely, the peptides are situated on the biosilica surface thus shielding the polyamines (figure 7). We anticipate that NMR signals of polysaccharides are partially quenched by the DNP radicals. In addition to their location, we could also for the first time obtain direct insight into the backbone fold of peptides associated with diatom biosilica. Our preliminary analysis suggests a mixture of random coil and β-conformations that may help to establish compactness as well as intermolecular network formation. In addition, we could confirm the polyamine structure determined by Sumper *et al.*[2] The prominent signals can be assigned to the N-methyl-propyleneimine repetitive unit in the LCPAs. 2D $^{13}C - ^{13}C$ correlations (2Q1Q, PDSD) and a 1D NCC showed an oxygen-linked saccharide as a main fraction of the polysaccharide material. N-linked saccharides as well as N-acetylglucosamine could be excluded.

5.5 REFERENCES

[1] Kröger N, Deutzmann R, Bergsdorf C, and Sumper M, Species-specific polyamines from diatoms control silica morphology, *Proc Natl Acad Sci U S A* **2000**, 97, 14133–8.

[2] Sumper M, Brunner E, and Lehmann G, Biomineralization in diatoms: characterization of novel polyamines associated with silica, *FEBS Lett* **2005**, 579, 3765–9.

[3] Kröger N, Deutzmann R, and Sumper M, Polycationic peptides from diatom biosilica that direct silica nanosphere formation, *Science* **1999**, 286, 1129–32.

[4] Poulsen N and Kröger N, Silica morphogenesis by alternative processing of silaffins in the diatom Thalassiosira pseudonana, *J Biol Chem* **2004**, 279, 42993–9.

[5] Wenzl S, Hett R, Richthammer P, and Sumper M, Silacidins: highly acidic phosphopeptides from diatom shells assist in silica precipitation in vitro, *Angew Chem Int Ed Engl* **2008**, 47, 1729–32.

[6] Scheffel A, Poulsen N, Shian S, and Kröger N, Nanopatterned protein microrings from a diatom that direct silica morphogenesis, *Proc Natl Acad Sci U S A* **2011**, 108, 3175–80.

[7] Hecky R E, Mopper K, Kilham P, and Degens E T, The amino acid and sugar composition of diatom cell-walls, *Mar Biol* **1973**, 19, 323–331.

[8] Volcani B, *Silicon and siliceous structures in biological systems*, Springer New York, New York, NY, **1981**.

[9] Wustman B A, Gretz M R, and Hoagland K D, Extracellular matrix assembly in diatoms (Bacillariophyceae) (I. A model of adhesives based on chemical characterization and localization of polysaccharides from the marine diatom Achnanthes longipes and other diatoms), *Plant Physiol* **1997**, 113, 1059–1069.

[10] McConville M J, Wetherbee R, and Bacic A, Subcellular location and composition of the wall and secreted extracellular sulphated polysaccharides/proteoglycans of the diatom Stauroneis amphioxys Gregory, *Protoplasma* **1999**, 206, 188–200.

[11] Hedrich R, Machill S, and Brunner E, Biomineralization in diatoms-phosphorylated saccharides are part of Stephanopyxis turris biosilica, *Carbohydr Res* **2013**, 365, 52–60.

[12] Gröger C, Lutz K, and Brunner E, NMR studies of biomineralisation, *Prog Nucl Magn Reson Spectrosc* **2009**, 54, 54–68.

[13] Hu Y Y, Rawal A, and Schmidt-Rohr K, Strongly bound citrate stabilizes the apatite nanocrystals in bone, *Proc Natl Acad Sci U S A* **2010**, 107, 22425–9.

[14] Becerra L, Gerfen G, Temkin R, Singel D, and Griffin R, Dynamic nuclear polarization with a cyclotron resonance maser at 5 T, *Phys Rev Lett* **1993**, 71, 3561–3564.

[15] Rosay M, Tometich L, Pawsey S, Bader R, Schauwecker R, Blank M, Borchard P M, Cauffman S R, Felch K L, Weber R T, Temkin R J, Griffin R G, and Maas W E, Solid-state dynamic nuclear polarization at 263 GHz: spectrometer design and experimental results, *Phys Chem Chem Phys* **2010**, 12, 5850–60.

[16] Lesage A, Lelli M, Gajan D, Caporini M a, Vitzthum V, Miéville P, Alauzun J, Roussey A, Thieuleux C, Mehdi A, Bodenhausen G, Copéret C, and Emsley L, Surface enhanced NMR spectroscopy by dynamic nuclear polarization, *J Am Chem Soc* **2010**, 132, 15459–61.

[17] Lelli M, Gajan D, Lesage A, Caporini M A, Vitzthum V, Miéville P, Héroguel F, Rascón F, Roussey A, Thieuleux C, Boualleg M, Veyre L, Bodenhausen G, Copéret C, and Emsley L, Fast characterization of functionalized silica materials by silicon-29 surface-enhanced NMR spectroscopy using dynamic nuclear polarization, *J Am Chem Soc* **2011**, 133, 2104–7.

[18] Vitzthum V, Miéville P, Carnevale D, Caporini M A, Gajan D, Copéret C, Lelli M, Zagdoun A, Rossini A J, Lesage A, Emsley L, and Bodenhausen G, Dynamic nuclear polarization of quadrupolar nuclei using cross polarization from protons: surface-enhanced aluminium-27 NMR, *Chem Commun (Camb)* **2012**, 48, 1988–90.

[19] Song C, Hu K N, Joo C G, Swager T M, and Griffin R G, TOTAPOL: A biradical polarizing agent for dynamic nuclear polarization experiments in aqueous media, *J Am Chem Soc* **2006**, 128, 11385–11390.

[20] Rossini A J, Zagdoun A, Lelli M, Canivet J, Aguado S, Ouari O, Tordo P, Rosay M, Maas W E, Copéret C, Farrusseng D, Emsley L, and Lesage A, Dynamic nuclear polarization enhanced solid-state NMR spectroscopy of functionalized metal-organic frameworks, *Angew Chem Int Ed Engl* **2012**, 51, 123–7.

[21] Harrison P J, Waters R E, and Taylor F J R, A broad spectrum of artificial sea water medium for coastal and open ocean phy-

toplankton, *J Phycol* **1980**, 16, 28–35.
[22] Iler R K, *The chemistry of silica: solubility, polymerization, colloid and surface properties and biochemistry of silica*, Wiley, New York, NY, **1979**.
[23] Mullin J and Riley J, The colorimetric determination of silicate with special reference to sea and natural waters, *Anal Chim Acta* **1955**, 12, 162–176.
[24] Coradin T, Eglin D, and Livage J, The silicomolybdic acid spectrophotometric method and its application to silicate/biopolymer interaction studies, *Spectrosc An Int J* **2004**, 18, 567–576.
[25] Brauer G, *Handbuch der präparativen anorganischen Chemie : in drei Bänden*, Ferdinand Enke Verlag, Stuttgart, **1975**.
[26] Kröger N, Bergsdorf C, and Sumper M, A new calcium binding glycoprotein family constitutes a major diatom cell wall component, *EMBO J* **1994**, 13, 4676–83.
[27] Hohwy M, Rienstra C M, Jaroniec C P, and Griffin R G, Fivefold symmetric homonuclear dipolar recoupling in rotating solids: Application to double quantum spectroscopy, *J Chem Phys* **1999**, 110, 7983–7992.
[28] Baldus M, Petkova A T, Herzfeld J, and Griffin R G, Cross polarization in the tilted frame: assignment and spectral simplification in heteronuclear spin systems, *Mol Phys* **1998**, 95, 1197–1207.
[29] Sauvée C, Rosay M, Casano G, Aussenac F, Weber R T, Ouari O, and Tordo P, Highly Efficient, water-soluble polarizing agents for dynamic nuclear polarization at high frequency, *Angew Chem Int Ed Engl* **2013**.
[30] Wang Y and Jardetzky O, Probability-based protein secondary structure identification using combined NMR chemical-shift data, *Protein Sci* **2002**, 11, 852–861.
[31] Kröger N, Lorenz S, Brunner E, and Sumper M, Self-assembly of highly phosphorylated silaffins and their function in biosilica morphogenesis, *Science* **2002**, 298, 584–6.
[32] Richthammer P, Börmel M, Brunner E, and van Pée K H, Biomineralization in diatoms: the role of silacidins, *Chembiochem* **2011**, 12, 1362–6.
[33] Kharlampieva E, Slocik J M, Singamaneni S, Poulsen N, Kröger N, Naik R R, and Tsukruk V V, Protein-enabled synthesis of Monodisperse titania nanoparticles on and within polyelectrolyte matrices, *Adv Funct Mater* **2009**, 19, 2303–2311.

[34] Kharlampieva E, Jung C M, Kozlovskaya V, and Tsukruk V V, Secondary structure of silaffin at interfaces and titania formation, *J Mater Chem* **2010**, 20, 5242.
[35] Bloembergen N, On the interaction of nuclear spins in a crystalline lattice, *Physica* **1949**, 15, 386–426.
[36] Blumberg W, Nuclear Spin-Lattice Relaxation Caused by Paramagnetic Impurities, *Phys Rev* **1960**, 119, 79–84.
[37] Goldman M, Impurity-Controlled Nuclear Relaxation, *Phys Rev* **1965**, 138, A1675–A1681.
[38] Schmugge T and Jeffries C, High Dynamic Polarization of Protons, *Phys Rev* **1965**, 138, A1785–A1801.
[39] Wolfe J, Direct observation of a nuclear spin diffusion barrier, *Phys Rev Lett* **1973**, 31, 907–910.
[40] Ramanathan C, Dynamic nuclear polarization and spin diffusion in nonconducting solids, *Appl Magn Reson* **2008**, 34, 409–421.
[41] Sumper M, Lorenz S, and Brunner E, Biomimetic control of size in the polyamine-directed formation of silica nanospheres, *Angew Chem Int Ed Engl* **2003**, 42, 5192–5.
[42] Sumper M, Biomimetic Patterning of Silica by Long-Chain Polyamines, *Angew Chemie* **2004**, 116, 2301–2304.
[43] Brunner E, Richthammer P, Ehrlich H, Paasch S, Simon P, Ueberlein S, and van Pée K H, Chitin-based organic networks: an integral part of cell wall biosilica in the diatom Thalassiosira pseudonana, *Angew Chem Int Ed Engl* **2009**, 48, 9724–7.
[44] Tesson B and Hildebrand M, Characterization and localization of insoluble organic matrices associated with diatom cell walls: insight into their roles during cell wall formation, *PLoS One* **2013**, 8, e61675.
[45] Takahashi H, Ayala I, Bardet M, De Paëpe G, Simorre J P, and Hediger S, Solid-state NMR on bacterial cells: selective cell wall signal enhancement and resolution improvement using dynamic nuclear polarization, *J Am Chem Soc* **2013**, 135, 5105–5110.

6

CONCLUSIONS AND PERSPECTIVES

6.1 CONCLUSIONS

While DNP has a history that goes back 60 years, high-field DNP is a young and rapidly developing field. Applications of DNP on proteins have been published from 1997[1] on, but stayed of limited use until a few years ago. The possibilities have not been fully explored. Two applications in the field of medicine and biomaterials have been presented in this thesis. Further, methodological developments using spin labels covalently attached to proteins are described. The thesis also contains the first data recorded at 800 MHz / 527 GHz system, its performance in terms of enhancement and resolution, and new insight in the structure of the membrane protein KcsA.

DNP as a valuable tool for detecting dynamics in membrane proteins

The bacterial K^+ channel KcsA has been investigated with the newly available 800 MHz/ 527 GHz DNP system. Comparison with 400 MHz / 263 GHz spectra, revealed a small line width improvement. Transverse paramagnetic relaxation only played a role for residues close to the protein surface. Residues more deeply buried in the membrane showed only minor or no PRE contribution to the line width. Comparison of line width and shape using MD simulations indicated that the majority of the line width increase can be explained by conformational heterogeneity of the residues in question. The freezing out of motion causes all conformations to be present in the spectra leading to major line broadening and therefore intensity loss. This is nicely demonstrated with residues T74 and T75 which were visible or broadened out in the spectra depending on the state in the gating cycle of KcsA.

Spin labeling of biomolecules provides a radical source for DNP and selective quenching of unwanted signals

Quenching of the protein surface due to paramagnetic relaxation is not always prefered. By using site-directed labeling techniques, the location of the transverse paramagnetic relaxation can be controlled. Due to the tetrameric nature of the protein KcsA, the MTS spin labeling of a single cysteine mutation lead to four radicals close enough to facilitate the CE. We found a sizeable DNP enhancement for the KcsA mutant G116C (14.2 at 400 MHz) and were able to modulate the signals in the spectra by choosing a different labeling site of the protein KcsA.

Structure information from low-concentrated liposomal vaccine acquired with DNP

The liposomal Alzheimer's vaccine Palm1-15 contains the N-terminal part of the protein Aβ. The peptide is retained on the lipid surface by palmitoyl anchors on both sides. Three amino acids were $^{15}N^{13}C$ labeled. Secondary chemical shifts extracted from 2D 2Q1Q correlations revealed more than one conformation for the peptide. The lipid composition of the liposome changed the chemical shift of the amino acids. MD simulations suggest more β-sheet-like oligomer formation of the peptide in the case of the lipid formulation DMPC/DMPG/Cholesterol compared to DMTAP/Cholesterol.

DNP reveals location and structure information of proteins in diatom frustule

Biominerals extracted from the marine unicellular eukaryote *Stephanopyxis turris* were investigated using DNP. Proteins protected from the SDS/EDTA treatment by the silica cell wall, were found. Also, resonances from polyamines were present in the NC-correlation spectra. No signs of protein-sugar links

were found. The secondary structure information extracted from the NMR data suggests that at least a fraction of peptides adopt a β-sheet conformation.

6.2 PERSPECTIVES

The 800 MHz/ 527 GHz DNP data presented here are encouraging for the continuation of the development of high-field DNP. Yet some difficulties have to be overcome in order to make this a mature technique. One major hurdle is the poor performance of currently employed biradicals at such high field. The major reason for this is that, at increasing field, a smaller part of the EPR-line is irradiated. Better performing radicals may have to be developed from narrow-line radicals, as has been suggested by Thurber *et al.*[2] Another way to tackle the problem is to use field or frequency modulation in order to irradiate a larger part of the EPR lineshape. Another major problem is the signal quenching due to transverse paramagnetic relaxation enhancement. This problem can be circumvented by using low radical concentrations. This particular strategy has also been applied several times in this thesis. The drawback is the drop in enhancement compared to higher concentrations of radical. Another solution to this problem has been presented in this thesis: selective labeling of biomolecules with radicals. Considering the efficient transport of polarization in the μm range,[3] spin labeling of a matrix instead of the protein of interest could be a way to shield the parts of interest of the protein from quenching.

Another hurdle is the decrease in spectral resolution. Since this is mostly caused by lack of motion, one way to improve the resolution would be the development of DNP above the glass transition of proteins. The performance of the CE and SE are closely tied to the level of saturation reached by the radicals. Therefore, either radicals with longer relaxation times or stronger microwave sources should be developed for this purpose. AMUPol already provides a significant improvement

over TOTAPOL in terms of performance at higher temperatures. In fact, with the design of AMUPol, it has been shown that purposeful design of radicals towards more favorable relaxation properties can greatly improve the performance of the said radical in DNP.

Most studies so far have focused on method development using model systems and only a handful present new insights into the structure or function of relevant biological systems. Two problems, unfeasible with conventional NMR techniques, have been presented in this thesis that prove the advantage of DNP hopefully contributing to the general use of the technique for the structural biology field. It also opens up the possibility to perform multi-dimensional NMR experiments on non-labeled samples.[4] This greatly increases the applicability of NMR, in for example drug development. While in general, the additional information in the form of more/broader peaks due to conformational heterogeneity, makes the spectra more complex, DNP could still become useful for bigger biological systems. On way to apply DNP to large systems is to use selective (nuclear) labeling techniques and/or paramagnetic quenching of unwanted areas. Another possible route is the manipulation of the ^1H concentration that could be employed to manipulate the localization of the DNP effect through the reduction of the speed of proton driven spin diffusion.

6.3 REFERENCES

[1] Hall D A, Maus D C, Gerfen G J, Inati S J, Becerra L R, Dahlquist F W, and Griffin R G, Polarization-enhanced NMR spectroscopy of biomolecules in frozen solution, *Science* **1997**, 276, 930–932.

[2] Thurber K R and Tycko R, Theory for cross effect dynamic nuclear polarization under magic-angle spinning in solid state nuclear magnetic resonance: the importance of level crossings, *J Chem Phys* **2012**, 137, 084508.

[3] van der Wel P C A, Hu K N, Lewandowski J, and Griffin R G, Dynamic nuclear polarization of amyloidogenic peptide nanocrystals: GNNQQNY, a core segment of the yeast prion protein Sup35p, *J Am Chem Soc* **2006**, 128, 10840–10846.

[4] Takahashi H, Lee D, Dubois L, Bardet M, Hediger S, and De Paëpe G, Rapid natural-abundance 2D 13C-13C correlation spectroscopy using dynamic nuclear polarization enhanced solid-state NMR and matrix-free sample preparation, *Angew Chem Int Ed Engl* **2012**, 51, 11766–9.

SAMENVATTING

Kernspinresonantie is een techniek die zeer precies de chemische structuur van moleculen kan detecteren. Dit gebeurt door de moleculen in een magnetisch veld te plaatsen waardoor de energiestaten van de kernspin (een kwantummechanische eigenschap) worden opgesplitst in een hogere en een lagere energie. Uit de Boltzmann-verdeling volgt dan dat er een populatieverschil ontstaat tussen de beide kernspinstaten (polarisatie). Er is dus een grotere kans dat een kernspin zich in de toestand met de lagere energie bevindt. Door middel van radiogolven worden de populaties van de energiestaten gemanipuleerd, kan polarisatie worden overgedragen naar een naburig atoom en uiteindelijk wordt een elektrisch signaal opgewekt (resonantie) dat vervolgens gedetecteerd kan worden met een gevoelig electronisch circuit. De techniek is in het verleden nuttig gebleken op vele vakgebieden, inclusief structuurbiologie. De belangrijkste tekortkoming is echter de gevoeligheid die beperkt wordt door het relatief kleine energieverschil van de spinstaten. Daardoor is het een vereiste dat de moleculen hooggeconcentreerd zijn. In het geval van de bestudering van eiwitten, betekent het dat deze in relatief grote hoeveelheden moeten worden geproduceerd en gezuiverd.

Dynamische kernspinpolarisatie is een techniek die de gevoeligheid van kernspinresonantie drastisch kan verbeteren. Vergeleken met atoomkernen hebben ongepaarde elektronen een groter energieverschil tussen de twee spinstaten. Door middel van overdracht van de veel grotere polarisatie van ongepaarde elektronen (zogenaamde radicalen) naar de kernspins, kan theoretisch de gevoeligheid van kernspinresonantie worden verbeterd met drie ordegroottes. De techniek werkt slechts op zeer lage temperaturen. Een vereiste is daardoor dat moleculen die gevoelig zijn voor bevriezing beschermd worden tegen ijskristallen. Vaak wordt dit gedaan door mid-

del van de toevoeging van glycerol. In dit proefschrift zijn enkele toepassingen van dynamische kernspinpolarisatie op het gebied van structuurbiologie beschreven.

In hoofdstuk 2 worden de bevindingen beschreven die met de hoog-veld 18.8 T dynamische kernspinpolarisatiespectrometer zijn verkregen van het bacteriële kaliumkanaal KcsA. De invloed van het toegevoegde radicaal op de eigenschappen van het ionenkanaal wordt gemeld. De oorzaken van spectrale lijnverbreding worden besproken en de aanwezigheid van verschillen hierin binnen het eiwit. De verbetering van de lijnbreedte ten opzichte van het 9.4 T systeem wordt belicht. Lokale dynamiek blijkt een zeer grote invloed te hebben op de lijnbreedte en daarmee laten we zien dat dynamische kernspinresonantie een waardevolle techniek is om deze dynamiek te bestuderen. In aansluiting daarop worden in hoofdstuk 3 de experimenten beschreven waar een radicaal aan het eiwit gehecht is door middel van een zwavelbrug. We laten voor het eerst zien dat dit ook tot dynamische kernspinpolarisatie leidt. Deze studie biedt perspectieven op het gebied van methodologische verbeteringen van de techniek.

De structuur van het laaggeconcentreerde kleine eiwit (peptide) in Palm1-15, een liposomaal vaccin tegen Alzheimer, kon worden bestudeerd met behulp van dynamische kernspinpolarisatie en computationele technieken. Verschillende conformaties van het peptide konden worden gedetecteerd. De verhoudingen tussen deze conformaties zijn afhankelijk van het soort lipiden in het vaccin.

Diatomen, een stam van (vaak eencellige) dierlijke algen, hebben behalve een celmembraan ook een skelet van kiezel. Dit exoskelet wordt opgebouwd door middel van ingevangen kiezelzuur. Er is weinig bekend over de verantwoordelijke eiwitten. Met behulp van dynamische kernspinpolarisatie konden deze (spaarzame) eiwitten in het exoskelet worden bestudeerd.

In samenvatting: dynamische kernspinpolarisatie draagt bij tot het vergroten van het toepassingsgebied van kernspinre-

sonantie. Door deze techniek kon de eiwitstructuur van het liposomale vaccin Palm1-15 worden bestudeerd, die slechts in lage concentratie aanwezig is. Ook kon voor het eerst de structuur van de eiwitten in de mantel van diatomen bestudeerd worden. Met het ionenkanaal KcsA werd bewezen dat spinlabeling van het eiwit kan leiden tot grotere signaalverhogingen dan met een oplosbaar radicaal. Voor KcsA werd bepaald dat gebruik van een 800 MHz spectrometer in plaats van een 400 MHz spectrometer een kleine verbetering geeft in de lijnbreedte van een gedeelte van de signalen. Ook is de nabijheid van radicalen een factor. De lijnverbreding is echter voornamelijk afhankelijk van de heterogeniteit van de eiwitconformatie. Dit leidt tot een nieuwe methode om de lokale dynamiek in een eiwit detecteren.

PUBLICATION LIST

JJHB Sattler, ID Gonzalez-Jimenez, L Luo, BA Stears, A Malek, DG Barton, BA Kilos, MP Kaminsky, TWGM. Verhoeven, **EJ Koers**, M Baldus and BM Weckhuysen, *Pt Promoted Ga/Al2O3 as a Highly Active, Selective and Stable Catalyst for the Dehydrogenation of Propane* Angew Chemie Int Ed DOI: 10.1002/anie.201404460R1

EJ Koers, MP López-Deber, M Weingarth, D Nand, DT Hickman, D Mlaki Ndao, P Reis, A Granet, A Pfeifer, A Muhs, and M Baldus, *Dynamic Nuclear Polarization NMR Spectroscopy: Revealing Multiple Conformations in Lipid-Anchored Peptide Vaccines*, Angew Chemie Int Ed, **2013**, 52, pp 10905–10908

M Renault, S Pawsey, MP Bos, **EJ Koers**, D Nand, R Tommassen-van Boxtel, M Rosay, J Tommassen, WE Maas, and M Baldus, *Solid-state NMR spectroscopy on cellular preparations enhanced by dynamic nuclear polarization*, Angew Chemie Int Ed, **2012**, 51 , pp. 2998–3001

E S Salnikov, O Ouari, **E Koer**s, H Sarrouj, T Franks, M Rosay, S Pawsey, C Reiter, P Bandara, H Oschkinat, P Tordo, F Engelke, and B Bechinger, *Developing DNP/Solid-State NMR Spectroscopy of Oriented Membranes*, Appl Magn Reson, **2012**, 43, pp 91–106

D Meyer, P Neumann, **E Koers**, H Sjuts, S Lüdtke, GM Sheldrick, R Ficner, and K Tittmann, *Unexpected tautomeric equilibria of the carbanion-enamine intermediate in pyruvate oxidase highlight unrecognized chemical versatility of thiamin*, Proc Natl Acad Sci, **2012**, 109, pp 10867–10872

ACKNOWLEDGEMENTS

First of all, I would like to thank Marc Baldus for giving me the opportunity to do my PhD on a very exciting topic. Also special thanks for arranging together with Werner Maas a half year internship at Bruker Biospin in order to get familiar with the DNP system.

Secondly, many thanks to the Bruker Biospin DNP team. Melanie Rosay, Shane Pawsey, Leo Tometich, Paddy Saul and Eckhard Bez: thank you for teaching me DNP and making my time in Billerica very pleasant and worthwhile.

I am indebted to several people, including Maria Pilar Lopez-Deber of AC Immune, Basel and Eduardo Perozo and Raymond Hulse (University of Chicago) and Eike Brunner and Anne Jantschke (TU Dresden) for providing samples for DNP measurements.

Also, thanks to the people that inspired or encouraged me to follow the path into science: Theo Jurriens, Hans Morelis, Gert Folkers, Stefan Rüdiger and Kai Tittmann.

Johan, thank you for the great technical support regarding the spectrometers and in specific the DNP setup. I learned many things from you and I also enjoyed discussing technical as well as scientific problems.

Thank you Elwin for providing numerous KcsA samples and also for lending me your "super"sample.

I would like to thank Markus, Klaartje and Hugo for being a helpful resource regarding theoretical or other kind of questions.

Tessa and Lindsay: it was nice to have you as colleagues and I will miss our girl's night out. Thank you Lindsay for the conversations about everything. It was great to share an office with you. Also thanks to officemates Deni and Sasha for bringing their own flair into the office.

Barbara, thanks for your support with finishing my thesis.

Thanks to Mark Daniels, Panos and Koen for throwing borrels every once in a while. I would like to thank the whole NMR spectroscopy group for patiently listening and nodding when I was telling useless facts about some random topic during lunch or borrel.

Mijn dank gaat uit naar familie en vrienden. Speciaal dank aan mijn ouders en Ido die mij gesteund hebben door dik en dun, in ziekte en gezondheid.

CURRICULUM VITAE

Eline Koers was born on the 26th of October 1987 in Kamperveen, the Netherlands. In 2005 she started studying Chemistry in Utrecht starting from focusing on biochemistry and physical chemistry. In September 2009, she continued her studies in the international Molecular Biology Master's Program of the Göttingen Graduate School for Neurosciences, Biophysics, and Molecular Biosciences (GGNB). Her 6-month internship in Prof. Kai Titmann's group resulted in the Master's thesis 'Determination of Carbanion Intermediates in ThDP-dependent Enzymes". She started her PhD in July 2010 in the group of Prof. Dr. Marc Baldus.